Russian Original Vol. 49, No. 5, November, 1980

May, 1981

SATEAZ 49(5) 711-796 (1980)

SOVIET ATOMIC ENERGY

АТОМНАЯ ЭНЕРГИЯ
(ATOMNAYA ÉNERGIYA)

TRANSLATED FROM RUSSIAN

CONSULTANTS BUREAU, NEW YORK

SOVIET ATOMIC ENERGY

Soviet Atomic Energy is a translation of *Atomnaya Energiya*, a publication of the Academy of Sciences of the USSR.

An agreement with the Copyright Agency of the USSR (VAAP) makes available both advance copies of the Russian journal and original glossy photographs and artwork. This serves to decrease the necessary time lag between publication of the original and publication of the translation and helps to improve the quality of the latter. The translation began with the first issue of the Russian journal.

Consultants Bureau journals appear about six months after the publication of the original Russian issue. For bibliographic accuracy, the English issue published by Consultants Bureau carries the same number and date as the original Russian from which it was translated. For example, a Russian issue published in December will appear in a Consultants Bureau English translation about the following June, but the translation issue will carry the December date. When ordering any volume or particular issue of a Consultants Bureau journal, please specify the date and, where applicable, the volume and issue numbers of the original Russian. The material you will receive will be a translation of that Russian volume or issue.

Subscription (2 volumes per year)
Vols. 48 & 49: $335 (domestic); $374 (foreign)
Vols. 50 & 51: $380 (domestic); $423 (foreign)

Single Issue: $50
Single Article: $7.50

Soviet Atomic Energy is abstracted or indexed in *Chemical Abstracts, Chemical Titles, Pollution Abstracts, Science Research Abstracts, Parts A and B, Safety Science Abstracts Journal, Current Contents, Energy Research Abstracts,* and *Engineering Index.*

CONSULTANTS BUREAU, NEW YORK AND LONDON

c/b
233 Spring Street
New York, New York 10013

Published monthly. Second-class postage paid at Jamaica, New York 11431.

SOVIET ATOMIC ENERGY

A translation of *Atomnaya Énergiya*
May, 1981

Volume 49, Number 5 November, 1980

CONTENTS

CONTENTS

(continued)

The Russian press date (podpisano k pechati) of this issue was 10/23/1980. Publication therefore did not occur prior to this date, but must be assumed to have taken place reasonably soon thereafter.

FAST REACTORS WITH AXIAL POSITION OF OXIDE AND METAL FUELS IN THE CORE

M. F. Troyanov, V. G. Ilyunin,
V. I. Matveev, V. M. Murogov,
A. A. Proshkin, V. Ya. Rudneva,
and A. N. Shmelev

UDC 621.039.5

In order to improve the technicoeconomic parameters of fast breeder reactors, one must improve the design of reactors with oxide fuel and search for new technological solutions which are based on, e.g., the use of other heat-transfer media; also promising are fuel varieties such as carbides, nitrides, and metal fuels [1, 2]. The utilization of metal fuel has been contemplated from the very beginning of the development of fast reactors and recently has again attracted the attention of researchers [3]. It is generally accepted that metallic fuel has certain advantages over ceramic fuels, e.g., a) high breeding ratio (BR = 1.7-1.9) and b) possibility of building reactors characterized by insignificant changes of the reactivity during their operating period, which provides advantages in the control aspect and increases the continuous reactor operation without reactor recharging (approximately to 1 yr or more).

It is also known that the technological properties of metallic nuclear fuel (particularly plutonium-containing fuel) at the present time do not allow the same temperature parameters of the steam and water cycle of an atomic power station as do the oxide fuels. This is mainly a consequence of the difficulties of obtaining reliable fuel-element operation at temperatures in excess of 650°C and of the unsatisfactory compatibility of this fuel with steel at temperatures in excess of 550°C [4]. If it were possible to use metal fuel and maintain the parameters of the steam and water cycle characteristic of ceramic fuel at a rather high burnup (~ 5% of the heavy atoms), it would be possible to substantially increase the excess conversion, which, in turn, would improve the technicoeconomic parameters of an atomic power plant equipped with fast reactors. A solution to this problem might be found (along with technological developments of new alloys, etc.) by using certain new core designs of fast reactors which make it possible to efficiently use metal fuel in the core.

For example, the possibility of using natural or slightly enriched uranium with a low (1-2%) pile-up level of fission products in an oxide-fuel reactor has been contemplated. This idea found its embodiment in the so-called heterogeneous design concept of the core of fast reactors [5]. The heterogeneous core facilitates the solution of the problem of radiative stability of the metal fuel, because the required degree of burnup can be considerably reduced. However, on the fuel-element jackets with metal fuel there remain temperature conditions characteristic of the jackets of fuel elements with ceramic fuel. This makes it difficult to employ the heterogeneous core design in a fast reactor.

The present article describes the results of an investigation of another concept, which makes it possible to use metal fuel in the core of a fast reactor under temperature conditions close to previously employed conditions [6].

We consider a reactor in which fuel elements with a metal fuel are situated on the inlet side of the "cold" coolant. The relatively low temperature (400-480°C) of the coolant in this part of the reactor creates conditions favorable for the operation of such fuel elements. In the region in which the coolant is at higher temperatures (500-560°C), fuel elements with an oxide fuel are arranged. When the metal fuel is situated in the "low-temperature region" of the core and the oxide fuel is situated in the "high-temperature" region, the temperature parameters of a pure oxide reactor are preserved, yet at the same time, the total breeding ratio is increased by about 0.15. The increase in the total breeding ratio results basically from the increase in the internal breeding coefficient of the core, which is important not only for the breeding rate of the nuclear fuel but also for optimizing the conditions of operation of a high-power fast reactor, taking into account changes in reactivity during continuous operation.

Translated from Atomnaya Énergiya, Vol. 49, No. 5, pp. 275-278, November, 1980. Original article submitted June 3, 1980.

0038-531X/80/4905-0711 $07.50

The design can be realized in various ways. One can conceive a single fuel element with the fuel filling varying with height, the fuels being enclosed in a single jacket. Another version consists of an assembly with lattices of various fuel elements containing metal or oxide fuel. In this case, the metallic and oxidic fuel elements are separated by an intermediate layer containing the steel shafts of the fuel elements and sodium.

As far as the technology is concerned, the use of a single fuel element with a gas-contact underlayer in analogy to oxide fuel is the simplest version. When separate lattices of oxide and metal fuel elements are employed, the metal fuel elements can have either a sodium underlayer or a gas underlayer. Though the sodium-contact underlayer is technologically more complicated, this type of underlayer makes it possible to increase the fraction of the metal fuel in the core by increasing the relative height of the metal fuel elements. Besides that, in fuel elements with such an underlayer, the temperature of the center of the fuel may be reduced to 650°C and lower if required. When different types of fuel are distributed along the height of the fuel-breeding system, the reactor parameters can be optimized by varying the parameters of the fuel element lattices, the enrichment ratio of the oxide and metal fuels, and the height of the fuel elements.

Figure 1 shows one of the versions of a calculated model of a fast breeder with a composite core. The calculations were made for a BN-1600 reactor with use of the multigroup BNAB-78 nuclear constants [7].

Below we list the initial data used as a basis of the nuclear-physics investigations and the analysis of the breeding parameters of fast reactors with a combination of oxide and metal fuels:

Thermal power (MW) of the reactor	4200
Temperature (°C) of the coolant:	
inlet to the reactor	354
outlet from the reactor	547
Fuel density (g/cm^3) in the core:	
oxide	8.5
metal	13
Maximum burnup (% of heavy atoms) of the fuel:	
oxide	10
metal	15
Volume fractions of the materials in the core:	
fuel	0.45
building materials	0.22
collant	0.33
Height (cm) of the core	100

It was assumed that the isotope composition of the plutonium corresponds to the composition of the plutonium piled up in energy-producing thermal water-moderated water-cooled power reactors. It was assumed that the lower lattice of the fuel elements has a shielding end section in the form of metallic uranium and a core portion with metallic plutonium or uranium fuel. Oxide fuel, PuO_2-UO_2, is mounted in the upper fuel-element lattice; UO_2 is assumed to be present in the shielding end portion. Internal axial interlayers comprising fuel elements with raw material in the form of ceramics or metals can be inserted between the lattices containing the various fuels.

As far as the physics is concerned, this model of the core of a fast reactor is one of the possible core versions with axial heterogeneity. By contrast to the usually considered heterogeneity, more favorable conditions of heat generation are obtained in the case of a metal fuel; this makes it possible to substantially increase the fraction of the power released in the metallic subzone.

Some results of the calculations are listed in Table 1. In a reactor in which oxide and metal fuels are jointly used and which has parameters close to the optimum breeding rate of the fuel, the oxide subzone is characterized by increased enrichment and by a reduced intrinsic breeding coefficient. However, this reduction of the intrinsic breeding rate is more than compensated for and offset by the increased breeding in the metallic subzone of reduced enrichment.

The investigations show that a certain preferable breeding value of the metallic fuel exists in relation to the breeding of the reactor as a whole. When this value in the subzone with the metallic fuel is reduced, the density of the heat liberation is decreased and that means that the height fraction of the fuel-breeding system occupied by the fuel proper is increased. However, when the height of the fuel-breeding system and the total power are maintained, an increase in the height of the less loaded metallic portion makes it necessary to increase the density of heat liberation in the oxide portion of the fuel-breeding system. This process is limited by the limit temperatures of the fuel core of an oxide fuel element. At the same time, when the enrichment in the metal subzone is increased, a relative increase in temperature takes place and the acceptable height of the metal subzone is decreased. This also means a reduction of the breeding rate in the metal subzone.

TABLE 1. Characteristics of a Reactor with Combined Use of Oxide and Metal Fuels

Characteristic	BN-1600 reactor with oxide fuel	Reactor with oxide and metal fuel	
		with single grid of fuel elements	with separate grids of fuel elem.
Fraction of height of core filled by metal fuel	—	0,40	0,45
Radial inhomogeneity coef.	1,21	1,21	1,21
Axial inhomogeneity coef.	1,26	1,28	1,31
Total breeding coef.	1,37	1,53	1,49
Enrichment, %; of oxide fuel ZLE/ZHE*	9,92/11,98	10,20/12,34	10,52/12,84
Enrichment, % ZLE/ZHE, of metal fuel	—	6,19/7,49	6,54/8,00
Specific excess fuel breeding [kg/MW-(el)·y];	0,284	0,410	0,377
Specific reactor charge [kg/MW(el)]	1,99	2,13	2,25
Ratio of rel. rate of fission product pile-up in metal—oxide fuels	—	0,49	0,50
Reactivity loss during 120 days, $\Delta k_{eff}/k_{eff}$	0,0195	0,0085	0,0095
Fraction of total power supplied by metal fuel	—	0,38	0,43
Max. temp. °C of metal fuel	—	730	650
Efficiency factor (net %) of atomic power station	38	38	38
Doubling time (rel. units)	1,00	0,73	0,85

*ZLE and ZHE denote the zones of low and high enrichment, respectively.

The highly enriched subzone with the oxide fuel plays to some extent the role of an "igniting" subzone. The result is that though the burn-up of the fuel in the metal subzone is relatively low (4-5% of the heavy atoms), the fraction of the burning-up initial charge in this zone is relatively large. The corresponding burn-up of the oxide fuel amounts to 8-10% of the heavy atoms in a single irradiation period of about 1.5 yr of the composite fuel-breeding system. We note that an increase in the average degree of burn-up of the metal fuel in excess of 5% of the heavy atoms does not substantially increase the nuclear-fuel breeding rate.

A higher intrinsic breeding rate in the metal subzone at a power fraction of about 40% in it and a rather high burn-up of the initial charge render in the composite core a total breeding rate which is about 1.25 times greater than the breeding rate in an oxide reactor under otherwise equal conditions.

The increase in the internal breeding coefficient of the core in which oxide and metal fuel are used in combination is another important factor. In the core models with oxide and metal fuels under consideration, the breeding coefficient of the core reaches values which are slightly greater than unity. This means, in particular, that the reactivity changes much less than in the oxide core during the reactor operation and, for unchanged power of the control and safety rods, it is possible to substantially increase the time between re-

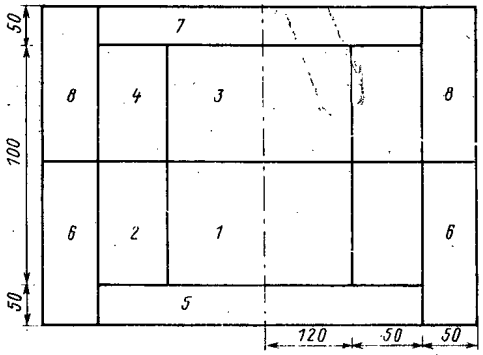

Fig. 1. Calculation model of a reactor with a composite core: 1, 2) metal core of low and high enrichment, respectively; 3, 4) oxide core of low and high enrichment, respectively; 5, 7) lower metal and upper oxide end shields, respectively; 6, 8) metal and oxide portions of the side shield, respectively (dimensions indicated in cm).

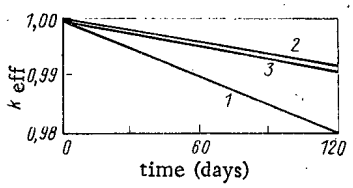

Fig. 2. Change in the reactivity during the operation of a fast reactor using oxide and metal fuels in combination: 1) BN-1600 reactor with oxide fuel; 2) reactor with combined use of oxide $(U + Pu)O_2$ and metal U + Pu fuel (height fraction of the metal subzone reaches 40%); 3) reactor with combined use of oxide $(U + Pu)O_2$ and metallic uranium fuel (height fraction of the metal subzone reaches 50%).

chargings, thus increasing the load coefficient of an atomic power station. This is very important from an economic viewpoint [8]: It improves the reactor exploitation and increases the reliability of reactor operation. Figure 2 shows the time dependence of k_{eff} during reactor operation.

It should be noted that the use of enriched metallic uranium instead of the mixed uranium–plutonium fuel in the "metal" subzone of the core entails a substantial improvement in the reactivity changes between reactor rechargings, as compared with the reactivity changes in the core of a reactor merely having mixed oxide fuels. An intermediate version is possible, i.e., where the metallic fuel contains a certain amount of plutonium in addition to ^{235}U.

In investigations of the work of fast reactors in nuclear power generation (the considerations including reactors of various types), the specific annual production of excess secondary fuel from the fast reactor can be used as an indicator of the optimal breeding conditions attainable with fast reactors [9, 10]:

$$r_b - \omega_{AE} g_b,$$

where r_b denotes the specific annual production of secondary excess fuel in a fast breeder [expressed in kg/MW(el) · yr]; g_b denotes the specific fuel load in the fuel cycle of a fast reactor [expressed in kg/MW(el)]; and ω_{AE} denotes the annual rate of the development of the nuclear power (yr^{-1}) (see Table 2). It follows from the table that fast reactors, in which oxide and metal fuels are used in combination, have an increased specific load and an increased breeding coefficient relative to fast reactors with oxide fuel; this reactor type allows faster rates in the development of the entire nuclear energy generation balanced in regard to fuel. Finally, the

TABLE 2. Specific Production of Excess Fuel from a Fast Reactor System (load coefficient $\varphi = 0.8$)

ω_{AE}	$r_b - \omega_{AE} g_b$, kg / MW(el)·year	
	Reactor with oxide fuel	reactor with a single fuel-element lattice with oxide–metal fuel
0,01	0,258	0,382
0,05	0,151	0,268
0,10	0,018	0,127
0,12	*	0,070
0,14	*	0,013

*AE denotes atomic energy. Conditions of self-sufficiency of fuel are impossible in nuclear energy generation.

combined use of mixed oxide and metal fuels requires additional research on the possible operation of fuel elements in such a core. This may somewhat complicate the design and technology of production of fuel elements in comparison with the conventional oxide fuel. However, any way of increasing the breeding rate implies problems. It cannot be ruled out that our proposed solution might be practicable and, at the same time, efficient in improving the parameters of fast reactors.

The authors thank L. A. Kochetkov, É. A. Stumbur, V. E. Kolesov, V. A. Apsé, A. I. Zinin, and L. V. Tochenii for useful discussions during the execution of the present work.

LITERATURE CITED

1. A. I. Leipunskii et al., Fourth Geneva Conf., USSR Rep. No. 709 [in Russian] (1971).
2. V. V. Orlov et al., in: Trans. Second Symp. of the COMECON, State and Prospects in the Work on Building Atomic Power Stations with Fast Neutron Reactors [in Russian], Vol. 3, Fiz. Énerg. Inst., Obninsk (1975), p. 168.
3. P. Lam and W. Barthold, Trans. Am. Nucl. Soc., 27, 753 (1977).
4. J. Kittel et al., Nucl. Eng. Design, 15, 373 (1971).
5. A. I. Voropaev, At. Tekh. Rubezhom, No. 11, 3 (1979).
6. V. G. Ilyunin et al., in: Trans. Second Symp., op. cit., p. 37.
7. L. P. Abagyan et al., At. Energ., 48, No. 2, 110 (1980).
8. E. V. Kirillov, in: Trans. Second Symp., op. cit., Vol. 1, p. 79.
9. V. V. Orlov, V. N. Sharapov, and A. N. Galanin, in: Experience in the Exploitation of Atomic Power Stations and Ways of the Future Development of Nuclear Energy Generation [in Russian], Vol. 1, Fiz. Énerg. Inst., Obninsk (1974), p. 251.
10. V. G. Ilyunin et al., Preprint Fiz. Énerg. Inst. No. FÉI-1036, Obninsk (1980).

THEORY OF UNSTEADY SLOWING DOWN OF NEUTRONS IN A HEAVY MEDIUM WITH ARBITRARY SCATTERING AND CAPTURE CROSS SECTIONS

S. A. Podosenov and G. Ya. Trukhanov

UDC 539.125.523.5

The unsteady transport of neutrons in various media is of interest for many important problems in the physics of shielding against penetrating radiation, reactor physics, nuclear geophysics, metrology of ionizing radiation, biophysics, etc. Practical requirements have been satisfied in the main by numerical methods. At the same time repeated attempts have been made to solve the appropriate kinetic equation analytically (cf. [1-4] and bibliographies in them), but so far no analytic solution of the kinetic equation has been found in explicit form – even for an infinite homogeneous heavy medium with a source uniformly distributed in space, for arbitrary energy dependences of the scattering and capture cross sections $\Sigma_S(E)$ and $\Sigma_C(E)$. The most important steps in this direction, in our opinion, were taken in [1, 3]. Kazarnovskii [1] found an approximate solution of the appropriate kinetic equation for $\Sigma_C = 0$ and arbitrary $\Sigma_S(v)$ in the form of a power series in $\xi = [\bar{v}(\tau) - v]/v$, where $\bar{v}(\tau)$ is the average neutron velocity at time τ. The solution derived contains two terms of the expansion proportional to ξ^2 and ξ^3. It correctly describes the energy–time distribution of the neutron collision density $\Psi(v, t)$ only near the maximum of the distribution. The awkwardness of the method used makes it difficult to derive the third term of the expansion proportional to ξ^4. Taking account of absorption $\Sigma_C \neq 0$, except for the trivial case $\Sigma_C \sim 1/v$, is possible in principle within the framework of the Kazarnovskii method if $\Sigma_C/\Sigma_S \ll 1$. The corresponding solution will also be valid only near the maximum of the distribution $\Psi(v, t)$. Thus, the Kazarnovskii solution [1] is restricted to the case of a small absorption cross section, does not describe the distribution $\Psi(v, t)$ far from its maximum, and therefore cannot be used as a Green's function.

The Laplace transform $F_\lambda(u)$ of the required function $\Psi(u, t)$, where u is the neutron lethargy, is written down in [3, 4] for arbitrary $\Sigma_S(v)$ and $\Sigma_C(v)$, but the inverse transform is recovered in [3] for only the two simplest cases: for $\Sigma_S(v) \sim 1/v$, $\Sigma_C(v) \sim 1/v$ and $\Sigma_C \sim 1/v$, $\Sigma_S(u)v(u) = (\Sigma_S v)_0 \exp(-ku)$, $k > 0$, which are very rarely encountered in practice. The relations derived are so cumbersome that their use in calculations and estimates is hardly justified. Kozhevnikov [4] studied the general properties of the function $F_\lambda(u)$ and derived an asymptotic expression for the inverse transform $\Psi(u, t)$.

In the present paper we take a new approach to the solution of the unsteady kinetic equation for the transport of neutrons in an infinite heavy homogeneous medium with arbitrary $\Sigma_S(E)$ and $\Sigma_C(E)$. We find an explicit expression for $\Psi(v, t)$ as the sum of a convergent series, including the Kazarnovskii solution as a special case. The formulas derived are convenient to use in calculations.

The neutron collision density in the problem under consideration satisfies the equation [1]

$$\left.\begin{aligned} \frac{L}{v}\frac{\partial\Psi(u,t)}{\partial t} + \Psi(u,t) = \frac{1}{1-\varepsilon}\int\limits_{u-u_M}^{u} e^{-(u-u')}h(u')\,\Psi(u',t)\,du' + \delta(u)\,\delta(t); \\ \frac{1}{L} = \frac{1}{L_s} + \frac{1}{L_c} = \Sigma = \Sigma_s + \Sigma_c; \\ h(u) = \frac{L}{L_s} = 1 - \frac{L}{L_c}, \\ u_M = \ln\frac{1}{\varepsilon};\ \varepsilon = \left(\frac{M-1}{M+1}\right)^2;\ u = \ln\frac{E_0}{E}, \end{aligned}\right\} \quad (1)$$

where the notation for physical quantities is that used in [1].

Translated from Atomnaya Énergiya, Vol. 49, No. 5, pp. 278-283, November, 1980. Original article submitted January 8, 1980.

0038-531X/80/4905-0716$07.50

We restrict ourselves to a consideration of a heavy medium ($M \gg 1$). Then the solution for Ψ can be written in the form [1]

$$\left.\begin{aligned}\Psi = \frac{1}{\tau}\exp\left\{\frac{1}{\eta}\varphi_{-1}(v,\tau)+\varphi_0(v,\tau)+\ldots\right\}\\ \tau=\eta t;\ \ \eta=2/(M+1).\end{aligned}\right\} \tag{2}$$

We introduce the following notation:

$$\varphi_{-1}\equiv P;\ \frac{\partial P}{\partial\tau}\equiv\dot{P};\ \frac{\partial P}{\partial y}\equiv P_y,$$

where $y \equiv \ln v/v_{min}$, and v_{min} is the minimum neutron velocity below which it is necessary to take acount of the effect of neutron thermalization. Substituting Eq. (2) into (1), we obtain

$$\frac{L(y)}{v(y)}\dot{P}+1=h(y)\frac{e^{P_y}-1}{P_y}; \tag{3}$$

$$\left.\begin{aligned}\frac{L}{v}\left(\dot{\varphi}_0-\frac{1}{\tau}\right)=h(y)\frac{e^{P_y}-1}{P_y}+\left[h_y-h\left(2-\varphi_{0y}-\frac{1}{2}P_y\right)\right]I_1+\frac{1}{2}hP_{yy}I_2;\\ I_1=\int_0^1 x\,e^{xP_y}\,dx=\frac{e^{P_y}}{P_y}+\frac{1-e^{P_y}}{(P_y)^2};\\ I_2=\int_0^1 x^2 e^{xP_y}\,dx+e^{P_y}\left[(P_y)^{-1}-2(P_y)^{-2}+2(P_y)^{-3}\right]-2(P_y)^{-3}.\end{aligned}\right\} \tag{4}$$

Equation (4) is a linear inhomogeneous first-order equation for $\varphi_0(y,\tau)$ which can be solved if the solution of Eq. (3) is known.

Equation (3) has the complete integral

$$P=a\tau+\int\Psi_2(y,a)\,dy+b, \tag{5}$$

where $\psi_2(y, a) = P_y$ and can be found from the equation

$$h(y)\frac{e^{\Psi_2}-1}{\Psi_2}-1=\frac{aL(y)}{v_{min}}e^{-y}. \tag{6}$$

Knowing the complete integral (5), it is possible to solve the basic problem of determining the integral surface passing through a given curve. We separate out from the two-parameter family of integral surfaces

$$\Phi(P,\ \tau,\ y,\ a,\ b)=a\tau+\int\Psi_2(y,\ a)\,dy+b-P=0 \tag{7}$$

a one-parameter family. To do this we choose the function $b = b(a)$ in Eq. (7) so that the envelope of the one-parameter family

$$\Phi[P,\ \tau,\ y,\ a,\ b(a)]=0, \tag{8}$$

determined by Eq. (8) and the equation

$$\frac{\partial\Phi}{\partial a}+\frac{\partial\Phi}{\partial b}\frac{db}{da}=0, \tag{9}$$

passes through the given curve, which we write in parametric form:

$$P=P(\xi);\ y=y(\xi);\ \tau=\xi-\xi_0;\ \xi_0=\text{const}. \tag{10}$$

On curve (10) Eqs. (8) and (9) reduce to identities. In principle it would be possible to determine $b(a)$ from system (8)-(10), but this is a rather complicated problem. As shown in [5], $b(a)$ can be found by using the equation

$$\Phi_P P_\xi+\Phi_\tau\tau_\xi+\Phi_y y_\xi=0, \tag{11}$$

instead of Eq. (9). The geometrical meaning of this equation is that the tangent to the curve (10) must lie in a plane tangent to the surface being sought. From Eq. (11)

$$\Psi_2\frac{dy}{d\xi}=\frac{dP}{d\xi}-a.$$

The complete integral (7) along curve (10) has the form

$$a(\xi-\xi_0)+\int \Psi_2 \frac{ay}{d\xi}\,d\xi+b-P(\xi)=0,$$

i.e.

$$a(\xi-\xi_0)+\int\left(\frac{dP}{d\xi}-a\right)d\xi+b-P=0,$$

whence

$$b(a)=\xi_0 a;\ \xi_0=\text{const}. \tag{12}$$

From Eqs. (12), (9), and (7) we find the equation for determining the parameter a as a function of τ and y:

$$\tau+\xi_0+\frac{\partial}{\partial a}\int \Psi_2(y,a)\,dy=0. \tag{13}$$

By using (13) to eliminate a from (5) we obtain in principle the solution of the problem posed (3).

We find the solution of the transcendental equation (6) by using a Burmann–Lagrange series [6, 7]:

$$\left.\begin{aligned}&\Psi_2(y,a)=\sum_{n=1}^{\infty}c_n(g+af)^n h^{-n};\ f\equiv\frac{L(y)}{v_{\min}}e^{-y};\\ &g=1-h=\frac{L}{L_c};\ c_n=\frac{1}{n!}\left\{\frac{d^{n-1}}{dy^{n-1}}\left[\frac{y}{\omega(y)}\right]^n\right\}\Big|_{y=0};\ \omega(y)=(e^y-1-y)/y.\end{aligned}\right\} \tag{14}$$

In particular, we find for the first four terms

$$c_1=2;\ c_2=-\frac{4}{3};\ c_3=\frac{10}{9};\ c_4=-\frac{136}{135}. \tag{15}$$

Transforming from the variables y and τ to v and τ, and assuming that at $\tau=\tau_0$ and $v=v_0$ $P(\tau_0, v_0)=c$, we obtain

$$P(v,\tau)=c+a(\tau-\tau_0)+\int_{v_0}^{v}\sum_{n=1}^{\infty}c_n\frac{L_s^n(x)}{x^{n+1}}\left(a+\frac{x}{L_c(x)}\right)^n dx. \tag{16}$$

In integrating Eq. (16) a is assumed constant, and is eliminated by using the equation

$$\tau-\tau_0+\int_{v_0}^{v}\sum_{n=1}^{\infty}nc_n\frac{L_s^n}{x^{n+1}}\left(a+\frac{x}{L_c}\right)^{n-1}dx=0. \tag{17}$$

Let us consider the case $\Sigma_c=0$, for which

$$\left.\begin{aligned}&-\left[\tau-\tau_0+c_1\int_{v_0}^{v}\frac{L_s(x)}{x^2}\,dx\right]\equiv Z_0=\sum_{n=1}^{\infty}\alpha_n a^n;\\ &\alpha_n=-(n+1)c_{n+1}I^{(n+1)}_{(n+2)}(v);\ I^{(n)}_{(k)}(v)\equiv\int_{v}^{v_0}\frac{L_s^n(x)}{x^k}\,dx.\end{aligned}\right\} \tag{18}$$

By using well-known formulas for the inversion of power series [8], we find the expressions

$$\left.\begin{aligned}&a=\sum_{n=1}^{\infty}\beta_n Z_0^n;\ \beta_1=\frac{1}{\alpha_1};\ \beta_2=-\alpha_2/\alpha_1^3;\\ &\beta_3=\frac{1}{\alpha_1^5}(2\alpha_2^2-\alpha_1\alpha_3);\ \beta_4=\frac{1}{\alpha_1^7}(5\alpha_1\alpha_2\alpha_3-\alpha_1^2\alpha_4-5\alpha_2^3),\end{aligned}\right\} \tag{19}$$

and use them to obtain

$$P(v,\tau)=c+\sum_{k=1}^{\infty}(k-1)c_k I^{(k)}_{(k+1)}(v)\Big(\sum_{n=1}^{\infty}\beta_n Z_0^n\Big)^k. \tag{20}$$

Equation (20) is an integral surface of Eq. (3) for h = 1, L = L_S passing through the curve of the general form (10).

Let us find the equation of the curve along which the distribution function Ψ is maximum; this is equivalent to the equation $P[v_m(\tau), \tau] = c$, where $v_m(\tau)$ is the velocity along this curve. In view of the arbitrary dependence of L_S on v, it follows from Eq. (20) that along this curve the following relation holds:

$$Z_0[v_m(\tau), \tau] = 0 = \tau - \tau_0 - 2\int_{v_m(\tau)}^{v_0} \frac{L_s(x)}{x^2}\,dx. \tag{21}$$

Equation (21) agrees with the result in [1], and to within the factor $\sim(M + 2/3)/(M + 1) \approx 1$, which must be inserted in front of the integral, corresponds to the known formula determining the energy dependence of the slowing down time in age theory [9].

Restricting ourselves to Z_0^4 terms, we obtain at points close to curve (21)

$$P(v, \tau) = -\frac{3}{16}[I_{(3)}^{(2)}(v)]^{-1} Z_0^2 - \frac{15}{256} I_{(4)}^{(3)} [I_{(3)}^{(2)}]^{-3} Z_0^3 + \\ + \left(\frac{3}{8}\right)^4 \left[\frac{136}{135} I_{(5)}^{(4)} - \frac{25}{12}(I_{(4)}^{(3)})^2 (I_{(3)}^{(2)})^{-1}\right] (I_{(3)}^{(2)})^{-4} Z_0^4. \tag{22}$$

In order to compare with the result in [1] we expand the function (22) in terms of the quantity $\varepsilon = [v_m(\tau) - v]/v$ and find

$$P = -\frac{1}{2}\overset{*}{K}(\tau)\,\varepsilon^2 - \frac{1}{3}\overset{*}{L}(\tau)\,\varepsilon^3 + \ldots, \tag{23}$$

where

$$\overset{*}{K}(\tau) = \frac{3}{2}\frac{L_s^2(v_m(\tau))}{v_m^2(\tau)}[I_{(3)}^{(2)}(v_m)]^{-1}; \tag{24}$$

$$\overset{*}{L}(\tau) = -\frac{9}{4}\frac{L_s(v_m)}{v_m}\frac{dL_s(v_m)}{dv_m}[I_{(3)}^{(2)}(v_m)]^{-1} - \frac{9}{4}\frac{L_s^4(v_m)}{v_m^4}[I_{(3)}^{(2)}(v_m)]^{-2} + \frac{45}{32}\frac{L_s^3(v_m)}{v_m^3} I_{(4)}^{(3)}(v_m)\,[I_{(3)}^{(2)}(v_m)]^{-3}. \tag{25}$$

The expressions for K* and L* agree with analogous expressions in [1] for the values

$$c = L_0 = \frac{1}{K_0} = 0.$$

Let us consider the case $\Sigma_c(v) \neq 0$. It is clear from Eq. (17) that the simplest case to calculate is $L_c = \alpha v$, $\alpha = \text{const}$. For this case

$$P'(v, \tau) = P(v, \tau) - \frac{v}{L_c}(\tau - \tau_0), \tag{26}$$

where $P(v, \tau)$ is the solution of Eq. (20) when there is no capture.

For an arbitrary velocity dependence of the capture cross section the quantity $a + x/L_c(x)$ is not constant, and this complicates the computational scheme somewhat.

It follows from Eqs. (17) and (19) that

$$\left.\begin{aligned} -(\tau - \tau_0 + \gamma_1) \equiv Z &= \sum_{k=1}^{\infty} \alpha_k' a^k; \\ \alpha_k' &= (k+1)\,\gamma_{k+1}; \\ \gamma_k &= \int_{v_0}^{v} \sum_{n=k}^{\infty} c_n \binom{n}{k} \frac{L_s^n(x)}{L_c^{n-k}(x)} \frac{1}{x^{1+k}}\,dx; \\ a &= \sum_{n=1}^{\infty} \beta_n' Z^n, \end{aligned}\right\} \tag{27}$$

where β_n' is related to α_n' by Eqs. (19).

Using (16) and (27), we obtain the solution in the form

$$P(v, \tau) = \sum_{k=1}^{\infty}\left[(1-k)\,\gamma_k\left(\sum_{n=1}^{\infty}\beta_n' Z^n\right)^k + c_k\int_{v_0}^{v}\frac{L_s^k(x)}{xL_c^k(x)}\,dx\right]. \tag{28}$$

By using the identity

$$\left.\begin{aligned} a + v/L_c(v) &\equiv \overset{*}{a} + \varepsilon_1; \\ \overset{*}{a} &\equiv a + \frac{\bar{v}(\tau)}{L_c[\bar{v}(\tau)]}; \quad \varepsilon_1 = \frac{v}{L_c(v)} - \frac{\bar{v}(\tau)}{L_c[\bar{v}(\tau)]}, \end{aligned}\right\} \tag{29}$$

and taking account of (16) and (17), Eq. (28) can be written in a form convenient for study:

$$P(v, \tau) = \sum_{k=2}^{\infty}\left(1-k\right)\overset{*}{\gamma}_k\left(\sum_{n=1}^{\infty}\overset{*}{\beta}_n\overset{*}{Z}^n\right)^k - (\tau - \tau_0)\frac{\bar{v}(\tau)}{L_c[\bar{v}(\tau)]} + \int_{v_0}^{v}\sum_{n=1}^{\infty} c_n \frac{L_s^n(x)}{x^{n+1}}\,\varepsilon_1^n(x, \tau)\,dx, \tag{30}$$

$$\left.\begin{aligned} \overset{*}{\gamma}_k &= \int_{v_0}^{v} \sum_{n=k}^{\infty} c_n \frac{L_s^n}{x^{n+1}} \binom{n}{k} \varepsilon_1^{n-k}\, dx, \\ & (k=0,\ 1,\ 0\ldots); \\ \overset{*}{Z} &= -(\tau-\tau_0+\overset{*}{\gamma}_1) = \sum_{k=1}^{\infty} \overset{*}{\alpha}_k \overset{*}{a}^k;\quad \overset{*}{\alpha}_k = (k+1)\overset{*}{\gamma}_{k+1};\quad \overset{*}{a} = \sum_{n=1}^{\infty} \overset{*}{\beta}_n \overset{*}{Z}^n; \end{aligned}\right\} \tag{31}$$

$\overset{*}{\beta}_n$ is expressed in terms of the coefficients $\overset{*}{\alpha}_n$ by Eq. (19). The average neutron velocity $\bar{v}(\tau)$ is an unknown function which must be found.

If $L_c = \alpha v$, $\varepsilon_1 = 0$, and Eq. (30) goes over into (26). The last two terms in Eq. (30) characterize the loss of particles from the system as a result of capture, and the first term gives the contribution to the distribution function of neutrons which have escaped absorption.

The maximum of the distribution function for the neutrons which have escaped absorption will correspond to an average velocity $\bar{v}(\tau)$ for which the equation

$$\overset{*}{Z}[\bar{v}(\tau),\ \tau] = 0 \tag{32}$$

is satisfied. From Eq. (32) there follows a formula relating the slowing down time of neutrons which have escaped capture and the required velocity $\bar{v}(\tau)$:

$$\tau-\tau_0 = 2\int_{\bar{v}(\tau)}^{v_0} \frac{L_s}{v^2}\, dv - \frac{8}{3}\left[\int_{\bar{v}(\tau)}^{v_0} \frac{L_s^2}{v^2 L_c}\, dv - \frac{\bar{v}}{L_c(\bar{v})}\int_{\bar{v}(\tau)}^{v_0} \frac{L_s^2}{v^3}\, dv\right] + \int_{\bar{v}(\tau)}^{v_0} \sum_{n=3}^{\infty} n c_n \frac{L_s^n \varepsilon_1^{n-1}}{v^{n+1}}\, dv. \tag{33}$$

For this value of the velocity $\bar{v}$ we obtain the following expression for $P[\bar{v}(\tau), \tau]$:

$$P \equiv -\overset{*}{J} = -2\int_{\bar{v}}^{v_0} \frac{L_s}{L_c v}\, dv - \int_{\bar{v}}^{v_0} \sum_{n=2}^{\infty} c_n \frac{L_s^n}{v^{n+1}} \varepsilon_1^{n-1}\left[\frac{v}{L_c} + (n-1)\frac{\bar{v}}{L_c(\bar{v})}\right] dv. \tag{34}$$

If $L_S/L_C \ll 1$, it can be shown that Eqs. (33) and (34) agree with the analogous relations in [1] if we neglect terms of second order and higher in L_S/L_C. We note that the theory developed in [1] is valid only for $L_S/L_C \ll 1$. Our method does not impose such a restriction.

Equation (30) can be simplified near the maximum of the distribution function. Expanding it in a series in the small parameter $\varepsilon = [\bar{v}(\tau) - v]/v$, we find

$$P(v, \tau) = -\overset{*}{J}(\tau) - \frac{1}{2}\overset{*}{K}(\tau)\,\varepsilon^2, \tag{35}$$

where $\overset{*}{J}$ is given by (34) and $\overset{*}{K}$ by

$$\overset{*}{K} = \overset{*}{K}^{(0)}\left\{1 - \frac{3}{4}[I_{(3)}^{(2)}(\bar{v})]^{-1}\int_{\bar{v}}^{v_0} \sum_{n=3}^{\infty} \binom{n}{2} c_n \frac{L_s^n}{v^{n+1}} \varepsilon_1^{n-2}\, dv\right\}^{-1} - \frac{2L_s(\bar{v})}{L_c(\bar{v})}\left(1 - \frac{\bar{v}}{L_c(\bar{v})}\frac{dL_c(\bar{v})}{d\bar{v}}\right). \tag{36}$$

Here $\overset{*}{K}^{(0)}$, the expression in the absence of capture, is determined by Eq. (24).

If capture obeys the $1/v$ law, then, as one should expect, $\overset{*}{K} = \overset{*}{K}^{(0)}$. If $L_S/L_C \ll 1$,

$$\overset{*}{K} = \overset{*}{K}^{(0)}\left\{1 + \frac{5}{2}[I_{(3)}^{(2)}(\bar{v})]^{-1}\left(\int_{\bar{v}}^{v_0} \frac{L_s^3}{v^3 L_c}\, dv - \frac{\bar{v}}{L_c(\bar{v})}\int_{\bar{v}}^{v_0} \frac{L_s^3}{v^4}\, dv\right)\right\} - \frac{2L_s(\bar{v})}{L_c(\bar{v})}\left[1 - \frac{\bar{v}}{L_c(\bar{v})}\frac{dL_c(\bar{v})}{d\bar{v}}\right]. \tag{37}$$

It can be shown that the rather cumbersome expression for K derived in [1] reduces to the simple relation (37) which is easily analyzed.

For constant scattering cross sections it follows from Eq. (22) that

$$P(v, \tau) = -\frac{3}{2}\frac{(x-1)^2}{x^2(1-\beta^2)}\left\{1 + \frac{5}{6}\frac{x-1}{x}\frac{1-\beta^3}{(1-\beta^2)^2} + \frac{27}{32}\frac{(x-1)^2}{x^2(1-\beta^2)^3}\left[\frac{250}{135}\frac{(1-\beta^3)^2}{1-\beta^2} - \frac{136}{135}(1-\beta^4)\right]\right\}. \tag{38}$$

By using (23)-(25) it follows from the theory developed in [1] that

$$\overset{*}{P}(v, \tau) = -\frac{3}{2}\frac{(x-1)^2}{1-x^2\beta^2}\left[1 - (x-1)\left(\frac{2}{1-x^2\beta^2} - \frac{5}{6}\frac{1-x^3\beta^3}{(1-x^2\beta^2)^2}\right)\right]; \tag{39}$$

$$x \equiv \frac{2L_s}{v(\tau-\tau_0+2L_s/v_0)};\quad \beta \equiv v/v_0. \tag{40}$$

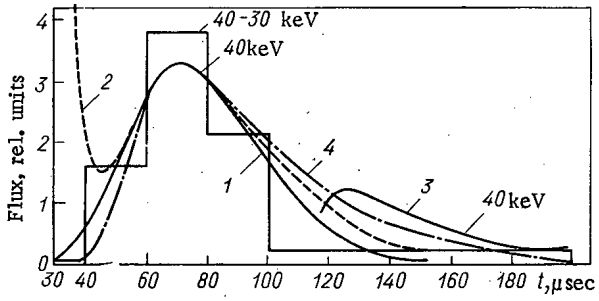

Fig. 1. Comparison of theory with calculations by the Monte Carlo method and results of theory of M. V. Kazarnovskii.

If $\beta \ll 1$ and $\tau \gg \tau_0$,

$$P(v, \tau) = -\frac{3}{2}\left(\frac{z-1}{z}\right)^2\left[1+\frac{5}{6}\frac{z-1}{z}+\frac{57}{80}\left(\frac{z-1}{z}\right)^2+\ldots\right]; \tag{41}$$

$$\overset{*}{P}(v, \tau) = -\frac{3}{2}(z-1)^2+\frac{7}{4}(z-1)^3+\ldots; \quad z \equiv 2L_s/v\tau. \tag{42}$$

Near the point $z \sim 1$ Eqs. (41) and (42) agree up to $(z-1)^3$ terms. According to [1] the simplest approximation for practical calculations is the Gaussian curve

$$n(z) = \sqrt{\frac{3}{2\pi\eta}}\exp\left[-\frac{3}{2\eta}(z-1)^2\right], \tag{43}$$

which is obtained from Eq. (42) by retaining only the first term of the expansion in powers of $(z-1)$.

Figure 1 shows the functions

$$\Psi_1 = A(r, v, t_{max})\, e^{P/\eta} \text{ (curve 1)};$$
$$\overset{*}{\Psi}_1 = A(r, v, t_{max})\, e^{\overset{*}{P}/\eta} \text{ (curve 2)};$$
$$\overset{*}{n}_1 = A_1(r, v, t_{max}) \exp\left[-\frac{3}{2\eta}(z-1)^2\right] \text{ (curve 3)}$$

and a histogram calculated by the Monte Carlo method [10] for a velocity v corresponding to an energy of 40 keV as a function of the time t in μsec; $t_0 = \tau_0/\eta \approx 27.5\,\mu\text{sec} = 120\ \text{m}/v_0$, which corresponds to the transit time for a neutron in air (L = 22 m) from a pulsed point source with $E_0 = 100$ keV to the observation point r = 120 m without collisions.

An analysis of Fig. 1 shows that the proposed method yields results in good agreement with those calculated by the Monte Carlo method. The theory developed in [1] gives a good description of the trailing edge of the curve and of the leading edge near the maximum of the distribution function. However, the behavior of the curve for $t \leq 45\,\mu$sec is at variance with the physical meaning of the problem. We note that if only the first term of the expansion is retained in Eq. (39) (the value in square brackets is set equal to unity), the corresponding curve 4 of Fig. 1 agrees better with the Monte Carlo calculation for the time interval considered than the more accurate curve 2 (39).

Conclusions. We have presented a new approach to the solution of the unsteady kinetic equation for neutron transport in an infinite homogeneous heavy medium with a source uniformly distributed in space and arbitrary energy dependences of the scattering and capture cross sections. The solution derived is valid for the whole range of variables v and t, and therefore can be used as a Green's function. It agrees with the results calculated by the Monte Carlo method within the limits of statistical error of the calculations. The final expression for the function $\Psi(u, t)$ is in the form of a sum of a convergent series whose terms are convenient for calculations. The solution permits a significant simplification of the relation for $\Psi(u, t)$ derived in [1], and correctly determines the limits of its applicability: the solution in [1] is valid only near the maximum; the use of the second term $(\sim\xi^3)$ in the expansion in powers of ξ in the M. V. Kazarnovskii theory gives satisfactory results for large values of the time, but leads to qualitatively incorrect results in the calculation of the leading edge for times $t \leq 0.6\, t_{max}$; by taking account of only the first term $(\sim\xi^2)$ in the expansion in powers of ξ, the function $\Psi(u, t)$ is correctly described only over a very narrow region near the maximum $(0.8\, t_{max} \leq t \leq 1.2\, t_{max})$.

LITERATURE CITED

1. M. V. Kazarnovskii, Tr. Fiz. Inst. Akad. Nauk, 11, 176 (1959).
2. E. V. Metelkin and G. Ya. Trukhanov, At. Energ., 35, 192 (1973).
3. Trine-Yie Dawn and Chio-Min Yang, Nucl. Sci. Eng., 61, 142 (1976).
4. D. A. Kozhevnikov, At. Energ., 40, 338 (1976).
5. L. É. Él'sgol'ts, Differential Equations and the Calculus of Variations [in Russian], Nauka, Moscow (1970).
6. E. T. Whittaker and G. N. Watson, A Course of Modern Analysis, Univ. Press, Cambridge (1915).
7. M. A. Lavrent'ev and B. V. Shabat, Methods of the Theory of Functions of a Complex Variable [in Russian], Nauka, Moscow (1973).
8. P. F. Fil'chakov, Numerical and Graphical Methods of Applied Mathematics [in Russian], Naukova Dumka, Kiev (1970).
9. S. Glasstone and M. Edlud, The Elements of Nuclear Reactor Theory, Van Nostrand, New York (1952).
10. B. M. Stepanov and G. Ya. Trukhanov, in: Problems of the Transport of Penetrating Radiations in the Earth's Atmosphere [in Russian], Nauka, Moscow (1977), p. 39.

MEASUREMENT OF THE $^{238}U(n, 2n)^{237}U$ CROSS SECTION IN THE NEUTRON ENERGY RANGE 6.5-10.5 MeV*

N. V. Kornilov, B. V. Zhuravlev,
O. A. Sal'nikov, P. Raich,
Sh. Nad', Sh. Darotsi,
K. Sailer, and I. Chikai

UDC 539.172.4

The study of the $^{238}U(n, 2n)$ excitation function from threshold to 10 MeV is important primarily from the point of view of practical requirements [1]. At the present time two papers are known which report results of systematic studies of the excitation function in this range. Knight et al. [2] in 1958 measured the cross section in the energy range 6-10 MeV by a radiochemical method. Fréhaut and Mosinski [3] obtained the cross section of this reaction in the range 8-15 MeV by using a large scintillation tank. In the overlapping energy range the difference of the results was $\leq 8\%$.

We report the measurement of the $^{238}U(n, 2n)$ cross section in the neutron energy range 6.5-10.5 MeV by an activation method using a Ge(Li) detector to record γ rays of the induced ^{237}U activity. Samples of ^{238}U ~18.5 mm in diameter and 1.0-1.7 mm thick having a total mass of 1.9-2.8 g were made by thermal sintering of U_3O_8. The percentage content of uranium was $90.0 \pm 0.6\%$. The ^{238}U content relative to the other uranium isotopes was >99.99%.

Neutrons with energies from 6.5 to 10.5 MeV were obtained from the ÉGP-10M tandem generator in the $D(d, n)^3He$ reaction using a deuterium gas target. The target was 40 mm long. For neutron energies of 6.54 and 6.78 MeV the target was filled with deuterium to a pressure of 66.6 kPa, and in the remaining cases to 106.6 kPa. The entrance window was made of molybdenum foil 14.3 ± 0.3 mg/cm^2 thick. The experimentally determined energy spread of the deuterons penetrating the target window was 32 keV (1σ, $E_d = 6$ MeV). The bottom of the target was covered with platinum 0.2 mm thick to decrease the background of neutrons from structural materials. The construction of the target is similar to that shown in [4]. The average energy of the neutrons incident on the sample, their energy spread as a result of the kinematics of the reaction, and the

*Work supported by the Ministry of Education and the Academy of Sciences of the Hungarian People's Republic.

Physics and Power Institute, Obninsk. Institute of Experimental Physics, L. Kossuth University, Debrecen, Hungary. Translated from Atomnaya Énergiya, Vol. 49, No. 5, pp. 283-286, November, 1980.

 0038-531X/80/4905-0722$07.50

TABLE 1. Measured Values of the $^{238}U(n, 2n)$ Cross Section

$E_n \pm \Delta E_n^*$, MeV	Flux, 10^6 neutrons/cm^2 · sec				Average flux, 10^6 neutrons/cm^2 · sec	$\sigma(n, 2n)$, 10^{-31} m^2
	n, α	n, p	n, f	K		
$6{,}54^{+0{,}09}_{-0{,}07}$	2,01	—	2,28	2	2,19±0,13	72±5
$6{,}78^{+0{,}08}_{-0{,}06}$	1,66	1,65	1,87	2	1,76±0,08	251±13
$7{,}00^{+0{,}10}_{-0{,}07}$	—	3,32	3,57	2	3,49±0,12	402±18
$7{,}50^{+0{,}10}_{-0{,}07}$	3,48	3,32	3,64	1	3,48±0,09	830±30 } 831±30
7,50	4,02	3,69	4,06	1	3,92±0,12	832±32 }
$7{,}99^{+0{,}10}_{-0{,}08}$	3,73	3,57	3,74	1	3,68±0,06	1077±31
$8{,}50^{+0{,}10}_{-0{,}08}$	3,81	3,92	4,09	1	3,94±0,08	1244±41
$8{,}99^{+0{,}10}_{-0{,}08}$	4,14	4,24	4,22	1	4,20±0,04	1345±35 } 1344±35
8,99	4,36	4,62	4,62	1	4,53±0,09	1343±42 }
$9{,}49^{+0{,}08}_{-0{,}08}$	2,74	—	2,69	0,5	2,72±0,03	1371±36
10,00±0,08	4,07	4,03	4,19	0,5	4,08±0,04	1413±37
10,50±0,08	4,17	4,39	4,76	0,5	4,38±0,15	1466±63

*$\pm\Delta E_n$ – 68% confidence interval.

losses in the gas and window were calculated by using data from [5, 6], and are listed in the first column of Table 1. The energy distribution of the neutrons incident on the samples is shown in Fig. 1.

The neutron flux was determined by using the reactions $^{238}U(n, f)$, $^{27}Al(n, \alpha)^{24}Na$, and $^{56}Fe(n, p)^{56}Mn$. The uranium samples were placed between two aluminum and iron foils and mounted on a fission ionization chamber 40.0 ± 0.5 mm from the end of the target at an angle of 0° with the deuteron beam (cf. Fig. 1). The flow-type fission chamber contained a layer of ^{238}U 0.28 mg/cm^2 thick and 19 mm in diameter. The amount of uranium in the chamber was determined to within 2%. In determining the flux by using the chamber, corrections were made for the loss of fragment pulses as a result of discrimination, self-absorption, and the change in the angular distribution of fragments in transforming to the laboratory coordinate system.

Discrimination was adjusted so that the α particles from uranium and the products of neutron reactions on structural materials of the chamber were not recorded. The total correction for all these effects did not exceed 2.5 ± 1.0%. In addition, the contribution of background neutrons from the D(d, np) and (d, n) reactions on the structural materials of the target was taken into account. The background of (d, n) neutrons was measured in an experiment with an empty target before and after bombardment; it varied from 1.0 ± 0.5 to 11 ± 1% for E_n = 6.54–10.50 MeV. The contribution of parasitic neutrons from the D(d, np) reaction calculated from data in [7] was 1.0 ± 0.5%–18 ± 4% for E_n = 8.50–10.50 MeV. Thus, without taking account of the error in the fission cross section, the accuracy of the flux determination with the fission chamber was 1–4%.

The ^{24}Na and ^{56}Mn activities were determined with an error of 1–3% by using a $\beta-\gamma$ coincidence detector and a Ge(Li) spectrometer; this error was controlling in calculating the neutron flux. The neutrons leaving the target were monitored with a detector employing a stilbene crystal and an FÉU-30 with recording thresholds of 3 and 6 MeV, and a current integrator. The contribution of background (d, n) neutrons was taken into account by performing a further irradiation at E_d = 8.1 MeV, which corresponds to a neutron energy of 10.5 MeV in the irradiation with a filled target. The contributions of these neutrons to the ^{24}Na, ^{56}Mn, and ^{237}U activities were 3.9, 2.0, and 1%, respectively. In calculating the background for other values of the energy, the readings of the neutron detector with a 6-MeV threshold were taken into account. The variation of the neutron flux through the thickness of the sample was determined by comparing the activities of the foils on both sides of the sample; it amounted to 3%/mm. Since the half-life of ^{237}U is considerably different from the half-lives of ^{24}Na and ^{56}Mn, fluctuations in the neutron flux during the bombardment period were taken into account in calculating the activity. The maximum correction for ^{56}Mn was 12%.

Gamma rays from ^{237}U, ^{24}Na, ^{56}Mn, and standard sources were recorded by a DGDK-70V Ge(Li) detector with a sensitive volume of 42 cm^3. The spectra were measured with an ATsP-4096 equipped with a stabilization system [8]. The spectrometer was constructed from equipment of the Physical Measurement Center

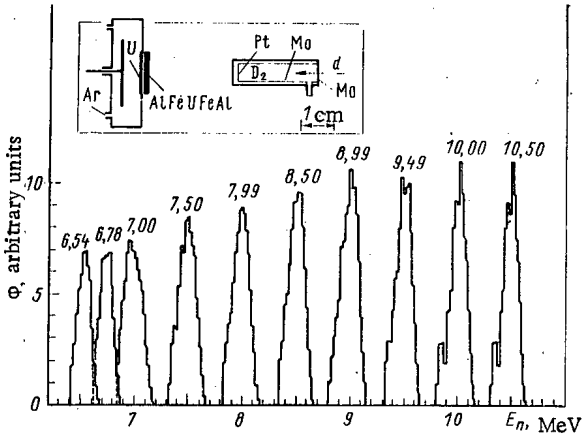

Fig. 1. Geometry of the experiment and calculated energy distribution of neutrons from the D(d, n)^{3}He reaction incident on samples. The neutron flux is given in arbitrary units; the gas pressure and the angular distribution of the neutrons are taken into account.

of the FEI. Correction for the dead time and pulse pile-up was measured with a precision amplitude generator; it did not exceed 10% for 10^3 counts/sec. Corrections for the coincidence of cascade γ rays were calculated by using the measured efficiency of total absorption in the detector and recommended decay schemes; they did not exceed 10%. The absolute efficiency and its dependence on the sample–detector distance was measured in the 60-1500 keV range by using standard sources. The 19-mm-diameter sources were ^{226}Ra (error of absolute activity < 2%), ^{149}Nd, and ^{182}Ta [9]; the 6-mm-diameter sources were ^{241}Am, ^{57}Co, ^{139}Ce, ^{137}Cs, ^{54}Mn, and ^{65}Zn (error of absolute activity ~1.5%). The values of the detector efficiency obtained with the 6-mm-diameter sources were renormalized to the 19-mm-diameter sources. The working value of the sample–detector distance was 15 mm. The error in the determination of the efficiency for γ energies between 200 and 1500 keV was 2%. The γ spectra and the decay curves were processed with a MULTI-20 minicomputer.

The activity of ^{237}U with a half-life of 6.75 days [10] was determined from the yield of 208.00-keV γ rays, which amounts to 21.80% [11]. The resolving power of the spectrometer (total width at half-height equal to 2.6 keV) did not permit separation of the ^{235}U (E_γ = 205.33 keV) and the ^{239}Np (E_γ = 209.73 keV) γ lines. The contribution of ^{235}U γ rays was determined by measuring the background spectra of samples before irradiation, and the contribution of the ^{239}Np line was determined from the measured intensity of the accompanying γ radiation with E_γ = 277.60 keV. They did not exceed 6 and 10%, respectively. The contribution of γ rays from fission fragments after 15 h was negligibly small. The bombardment time for an average deuteron current of 2 μA was varied from 7 to 30 h depending on the anticipated value of the ^{238}U(n, 2n) cross section. The ^{237}U activity was measured for times from 20 to 300 h. The statistical errors in the determination of the initial activity for neutron energies of 6.54 and 6.78 MeV were 3 and 2%, and in other cases < 1%. The experimentally determined correction for self-absorption for a γ energy of 208 keV varied from 0.61 to 0.72 depending on the sample thickness.

Table 1 lists the values of the neutron flux determined from three reference reactions. The ^{238}U(n, f) cross sections were taken from [12], and the ^{27}Al(n, α) and ^{56}Fe(n, p) cross sections from [13]. In spite of the fact that the (n, α) and (n, p) cross sections are more accurate than the (n, f) cross section, we did not take this into account in determining the average neutron flux. At the same time, taking into account the difference in the methods of measuring the flux with the chamber and foils and their sensitivity to background neutrons, the cross sections were calculated by averaging the fluxes in the following way:

$$\overline{\Phi} = \frac{\Phi(n, \alpha) + \Phi(n, p) + K\Phi(n, f)}{2 + K},$$

where K is the relative weight of the flux determined with the fission chamber. The values of K are given in Table 1 together with the values of the average neutron fluxes, the values obtained for the ^{238}U(n, 2n) cross section, and their estimated errors without taking account of the errors in the recommended cross sections of the reference reactions. The error of the (n, 2n) cross section includes the following: the flux (mean-

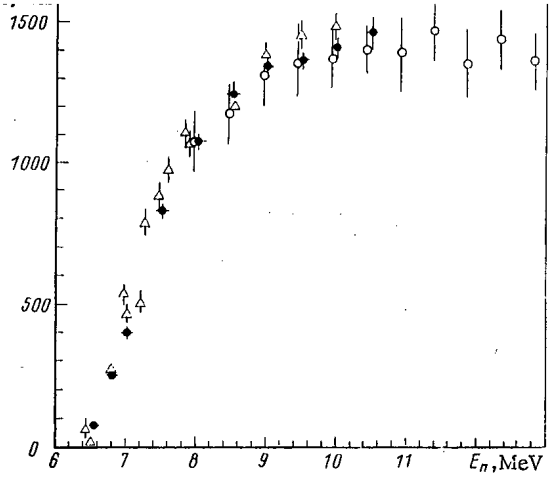

Fig. 2. Experimental values of the ^{238}U (n, 2n) cross section: ●) our results; △, ○) data from [2] and [3], respectively.

square error of weighted mean), number of ^{238}U nuclei (0.6%), efficiency of Ge(Li) detector (2%), corrections for self-absorption (1.5%), yield of 208-keV γ rays (1%).

Measurements at neutron energies of 7.50 and 8.99 MeV were repeated to test the reproducibility of the results. It is clear from Table 1 that the experimental results agree within the estimated limits of accuracy. Our results are compared with published data in Fig. 2. The good agreement with the results in [3] should be noted, while the data of [2] give systematically higher cross sections.

The authors thank V. A. Tolstikov for making it possible for us to use the Ge(Li) detector, G. P. Makhovaya and S. A. Kremenetskaya for performing the chemical analyses of the samples, A. I. Gonchar for help in repairing the electronic equipment, the staffs of the Physical Measurement Center of the FÉI and the ÉGP-10 M accelerator for help with the work, and L. Vash (Institute of Experimental Physics of the L. Kossuth University) for making the preamplifier for the fission chamber.

The authors are grateful to the Ministry of Education and the Academy of Sciences of the Hungarian People's Republic for their attention to the work and for financial support.

LITERATURE CITED

1. WRENDA 76/77: INDC/SEC/-55/URFS, R. Lessler (ed.), IAEA, Vienna (1976).
2. J. Knight, R. Smith, and B. Warren, Phys. Rev., 112, 259 (1958).
3. J. Frehaut and G. Mosinski, CEA-R-4627 CEN-Saclay, Gif-sur-Yvette, France (1974), in: Proc. Conf. Nucl. Cross Sections and Technology, Vol. 2, Washington, March 3-7 (1975), p. 855.
4. N. S. Biryukov et al., Prib. Tekh. Eksp., No. 3, 66 (1971).
5. H. Liskien and A. Paulsen, Nucl. Data Tables, A11, 569 (1973).
6. C. Williamson, J. Boujot, and J. Picard, CEA-R-3402 CEN-Saclay, Gif-sur-Yvette, France (1966).
7. D. Smith and J. Meadows, ANL/10M-9, Aug. (1974).
8. A. I. Gonchar, in: All-Union Conf. on the Automation of Scientific Research in Nuclear Physics [in Russian], Inst. of Nucl. Research, Academy of Sciences of the Ukrainian SSR, Kiev (1976), p. 167; A. I. Gonchar, S. I. Chubarov, and B. V. Nesterov, Prib. Tekh. Eksp., No. 4, 69 (1974).
9. S. Nagy et al., Magy Fiz. Foly., 22, 323 (1974).
10. Nuclear Data Sheets, Vol. 6 (1971), p. 539.
11. R. Gunnink, "Gamma-library file output," Lawrence Livermore Laboratory Special Commun., Univ. Cal., Livermore, Oct. 1 (1975).
12. M. Sowerby, B. Patrick, and D. Mather, Ann. Nucl. Sci. Eng., 1, 409 (1974).
13. V. Kanda and R. Nakasima, in: Proc. Conf. Neutron Cross Sections and Technology, Vol. 1, Washington, March 4-7 (1968), p. 193.

INVESTIGATION OF THE COMBINED ADSORPTION OF KRYPTON, XENON, AND WATER VAPOR OF THE OFF-GAS OF ATOMIC POWER STATIONS

I. E. Nakhutin, D. V. Ochkin, and S. A. Tret'yak

UDC 621.039.73:66.074.7

A radiochromatographic system of purifying the off-gas from the short-lived krypton, xenon, and iodine nuclides is presently used in Russian atomic power stations and in foreign atomic power stations equipped with the aid of the USSR. The basic elements of the system are filter-adsorbers filled with activated carbon and a drying unit [1-3]. Dynamic adsorption and radioactive decay in the adsorber cause stationary conditions at which the concentration of the radioactive gas decreases along the height of the sorbent layer. The adsorber is designed for operation as "perpetual column" without regeneration of the activated carbon.

The composition of the off-gas strongly influences the efficiency of adsorber operation. For example, the adsorption of radioactive rare gases on the activated carbon is affected by the presence of carbon dioxide [4], water vapor, ammonia, freon [5], and various volatile organic materials the relatively high concentration of which in the gas phase may "poison" the adsorbent and reduce the efficiency of gas purification. For this reason the greatest admissible concentration of the admixtures must be determined.

The drying unit usually comprises two alternatingly working adsorption columns, i.e., one is in operation while the other one is regenerated by hot atmospheric air or is on standby. Since the adsorbents designated for drying the gas have many shortcomings [6], one must in each case consider all the factors influencing the process and select the optimum adsorbent. In particular, it is indispensable to consider the adsorbent capacity of rare gases, which determines the size of the protective radiation shielding of the drying unit and the release of radioactive gas during regeneration of the adsorbent.

We have investigated the combined adsorption of water vapor, krypton, and xenon from air on activated SKT-6A carbon under equilibrium conditions at various temperatures and from the nitrogen flow on NaA, NaX, CaA, CaX, and NaM zeolites, Polish "Molecular Sieves 4A" zeolite, KSM silica gel, A-1 alumogel, and activated SKT-3 carbon under dynamic conditions at room temperature.

Method and Results of the Measurements under Equilibrium Conditions. The distribution of the rare gases between the gas phase and the adsorbent was determined in a closed circulation circuit by the technique of labeled atoms (intensity of the gamma radiation as a measure of the concentration of ^{85}Kr and ^{133}Xe radionuclides). The partial pressure of the xenon did not exceed $8 \cdot 10^{-3}$ Pa, that of krypton did not exceed 6.7 Pa. The water vapor pressure was maintained at a particular level with a humidifier placed into a cryostat and included in the closed circuit. The combined adsorption of water vapor and air was measured by the mass increase on a spring balance with a quartz spiral.

Figure 1 represents the kinetic adsorption curves of water vapor adsorbed on activated SKT-6A carbon at temperatures between −30 and +20°C and at a relative humidity (p/p_s) between 0.30 and 0.73. The time after the beginning of the experiment is plotted to the abscissa; the amount of adsorbed moisture (expressed in grams per gram adsorbent) is plotted to the ordinate.

At a low pressure of the water vapor, the adsorption equilibrium established itself relatively rapidly. In the range of the so-called "polymolecular adsorption and capillary condensation," the rate at which the equilibrium was established decreased – the process lasted several days.

The equilibrium values of the water vapor adsorption on activated carbon were used to plot the isotherms shown in Fig. 2. The relative humidity p/p_s of air is plotted to the abscissa, the amount of adsorbed

Translated from Atomnaya Énergiya, Vol. 49, No. 5, pp. 286-289, November, 1980. Original article submitted November 23, 1979.

0038-531X/80/4905-0726$07.50

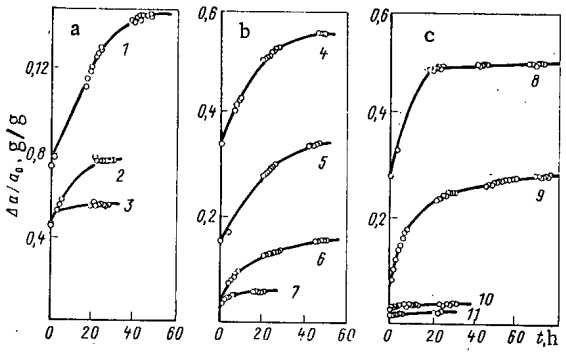

Fig. 1. Kinetic curves of the adsorption of water vapor on activated SKT-6A carbon at a) −30 °C; b) 0°C; c) +20°C and p/p_S = 0.73 (1); 0.56 (2); 0.39 (3); 0.71 (4); 0.60 (5); 0.49 (6); 0.40 (7); 0.68 (8); 0.60 (9); 0.45 (10); 0.30 (11).

moisture, to the ordinate. The curve does not start from the coordinate origin: the relative weight at moisture zero corresponds to the adsorption of dry air. The isotherms at 0 and 20°C are S-shaped, which is characteristic of the adsorption of water vapor on activated carbon. The same figure shows the equilibrium coefficients of adsorption of rare gases, Γ/ρ (cm^3/g), the coefficients referred to the unit mass of activated carbon.

Method and Results of the Measurements under Dynamic Conditions. Technical nitrogen with a relative humidity $p/p_S = 0.83 \pm 0.02$ was at room temperature admitted to the column with the adsorbent; the moisture of the gas leaving the column was continuously monitored.

During the experiment, the adsorbent became gradually moist and the H_2O front was shifted along the height of the column. At specific moments, which corresponded to various positions of the front, indicator quantities of ^{85}Kr or ^{133}Xe were pulsewise admitted to the gas flow at the entry to the column. The radioactivity of the gas at the outlet of the column was measured with a flow-type ionization chamber whose ionization current was recorded with a recording instrument. The partial pressure of the krypton and xenon did not exceed $5.3 \cdot 10^{-2}$ and $8.2 \cdot 10^{-4}$ Pa in the experiments.

Figure 3 shows a series of eluent curves of krypton, which were obtained in the NaX zeolite-filled column while it became moist; the curves correspond to various positions of the chromatographic H_2O front. Curve 1 corresponds to dry adsorbent, curve 4 to completely moist adsorbent. Curves 2 and 3 characterize intermediate states.

The eluent curves were used to calculate the average time of the passage of the chromatographic front of krypton and xenon, $\bar{\tau}$, in accordance with the formula

$$\bar{\tau} = \int_0^\infty \tau I(\tau)\, d\tau \Big/ \int_0^\infty I(\tau)\, d\tau,$$

where I denotes the current of the ionization chamber and τ, the time, reckoned from the moment at which the radioactive gas was admitted.

The results of some of the calculations are shown in Fig. 4, where the amount of gas that passed through the column since the beginning of the experiment is indicated on the abscissa, and the average time of passage of the radioactive "marker" is indicated on the ordinate. The passage time of the chromatographic front of radioactive rare gases decreases from a maximum, which corresponds to the dry adsorbent and depends upon the equilibrium coefficient of adsorption, to a minimum, which corresponds to the completely moist adsorbent.

The figure includes curves representing the relative moisture p/p_S: at the beginning of each experiment, the relative moisture of the gas leaving the column was insignificant; after that, when the H_2O front approached the column exit, the relative moisture increased and gradually reached a constant value equal to the moisture of the gas admitted to the column.

Discussion of the Results. The experimental data indicate that moisture significantly influences the ad-

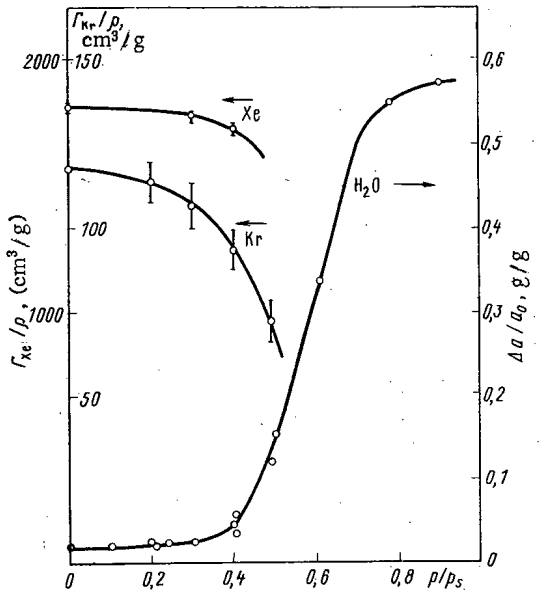

Fig. 2. Combined adsorption of krypton and xenon, along with water vapor, on activated SKT-6A carbon at 0°C; o denotes the experimental points.

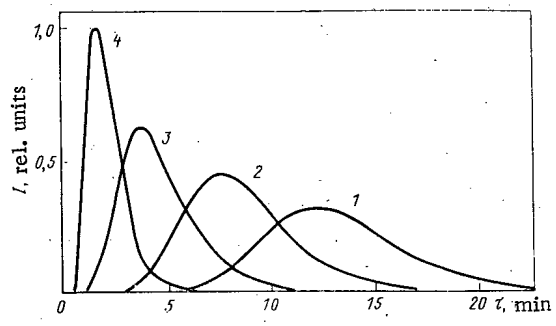

Fig. 3. Eluent curves of xenon which were obtained with a column filled with NaX zeolite; various degrees of adsorbent moisture.

sorption of rare gases on activated SKT-3 and SKT-6A carbon, NaX, CaA, CaX, and NaM zeolites, KSM silica gel, and A-1 alumogel.

The "poor" adsorption kinetics of the water vapor adsorbed on activated carbon in the region of the so-called capillary condensation (see Fig. 1) made it possible to calculate the effective coefficient of thermal diffusion with the method of [7]. For example, the D_{eff} value estimated from the kinetic curve and corresponding to 20°C and the relative humidity $p/p_S = 0.6$ was $(5.6\text{-}9.5) \cdot 10^{-4}$ cm²/sec. This relatively low rate of the diffusion of water vapor in the granules of activated carbon influences the dynamics of the process. Thus, when the moist gas is admitted, an "overswing" of moisture is immediately observed at the exit of the column containing activated SKT-3 carbon; the chromatographic H_2O front is strongly "smeared."

The equilibrium coefficients of krypton and xenon adsorption on activated carbon change only slightly under the influence of adsorbed water in the interval of relative humidity corresponding to the initial portion of the isotherm (see Fig. 2). The coefficients decrease sharply in the region of polymolecular adsorption and capillary condensation. This fact determines the degree of the required drying of the gas sent to the radiochromatographic system of an atomic power station.

The isotherm of water vapor adsorption on zeolite depends only slightly on the temperature and is clearly convex [8]. Therefore, the H_2O front in a column containing zeolite has the form of a step, which means that the moisture capacity of zeolite can be almost fully used in practice.

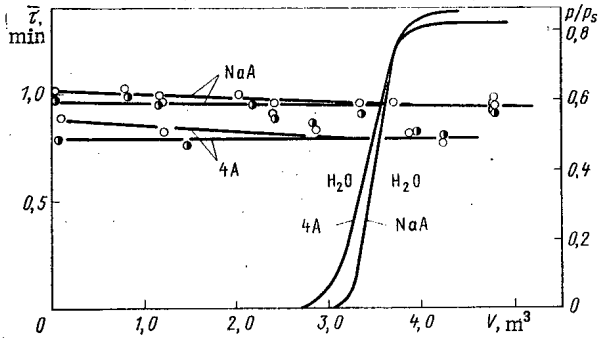

Fig. 4. The average passage time of the chromatographic front of Xe (○) and Kr (◑) in an NaA zeolite column and in a "Molecular Sieves 4A" zeolite column and the relative humidity of the nitrogen leaving the column as functions of the amount of gas sent through the column.

The strongest adsorption of krypton and xenon was observed on CaA zeolite; the rare gases are slightly less adsorbed on NaX and CaX zeolites. The adsorption coefficient of xenon is for these three zeolites greater than the adsorption coefficient of krypton. The inverse pattern was observed on acid-resistant NaM zeolite on the basis of H-mordenite. The adsorption coefficient of krypton was greater than the adsorption coefficient of xenon, which obviously results from the relation between the effective dimensions of the pores and the molecules. Unfortunately, this fact cannot be used for separating krypton from zenon in the gas purification system of a nuclear fuel regeneration unit. The relatively poor adsorption kinetics of krypton on NaM zeolite smears the chromatographic front and the eluent peaks of krypton and xenon in the column are not separated.

Zeolites of the types NaM and "Molecular Sieves 4A," practically speaking, do not adsorb krypton and xenon (see Fig. 4). These zeolites are used to dry gas in radiochromatographic gas purification systems of atomic power stations [3]. Drying apparatus filled with this sorbent requires very little biological shielding. Furthermore, during the regeneration of the zeolite by hot air, a relatively small amount of radioactive elements is released; this release is associated with the free volume of the apparatus.

The isotherm of water vapor adsorption on fine-pore silica gel and alumogel depends rather strongly upon the temperature [9]. The liberation of heat during the adsorption of water vapor on the adsorbents of this type causes a "protraction" of the chromatographic H_2O front: a premature overswing of the moisture is observed. It was impossible under dynamic conditions to make full use of the static moisture capacity of these adsorbents.

The width of the eluent peaks observed in the dynamic experiments (see Fig. 3) cannot be explained by longitudinal diffusion of the radioactive marker in the gas phase within the column. Estimates of peak blurring caused by this mechanism yield values smaller than the experimental values by at least one order of magnitude. Nevertheless, the eluent curves are well described by the theoretical function, provided that a finite diffusion rate of the rare gases in the adsorbent granules or an external mass transfer in a thin gas layer surrounding the granules is assumed in the calculations. Then details such as the asymmetry of the eluent peak can be explained. However, the available experimental data do not make it possible to estimate the separate contributions of internal diffusion and external mass transfer.

The linear dependence of the passage time of the chromatographic front of rare gases on the moisture concentration of the adsorbent is interesting and of practical importance. For example, by introducing an indicating amount of a radioactive rare gas into the gas stream and by measuring the time of passage through the piled-up adsorbent layer, it is possible to estimate the degree of adsorbent poisoning by moisture, organic material, etc. This method is conveniently used to determine the degree of poisoning of activated carbon in the adsorber of a radiochromatographic gas purification system of an atomic power station and to estimate its efficiency. Obviously, the method is suitable also for determining the degree of poisening of the adsorbent by hydrocarbons of high molecular weight in the gas- and petroleum-refining industry.

Conclusions. A significant influence of moisture in the adsorption of rare gases on activated carbon was established. In a radiochromatographic system, in which activated carbon is employed, the relative humidity of the gas must not exceed values at which polymolecular adsorption sets in.

In estimating the transition processes in the adsorber during changes in the conditions of operation, one must take into account the considerable adsorption of the carrier gas on the activated carbon.

In gas-purification systems of atomic power stations, the Russian NaA zeolite and the Polish "Molecular Sieves 4A" zeolite, which are characterized by considerable moisture capacity and good dynamic properties, can be recommended for the drying of gas. The moisture capacity of these zeolites depends only slightly on the temperature, and the adsorbents hardly sorb any krypton and xenon, which is very important for the biological shielding aspects of equipment.

The linear dependence of the time in which rare gases pass through the layer can be used in practice to determine the degree of adsorbent poisoning.

The authors thank A. N. Dekalova for help in the present work.

LITERATURE CITED

1. I. E. Nakhutin and D. V. Ochkin, Inzh.-Fiz. Zh., 9, No. 1, 112 (1965).
2. I. E. Nakhutin, D. V. Ochkin, and Yu. V. Linde, Zh. Fiz. Khim., 43, No. 7, 1811 (1969).
3. I. E. Nakhutin et al., At. Energ., 44, No. 3, 251 (1978).
4. A. M. Trofimov and A. N. Pankov, Radiokhimiya, 7, No. 3, 293 (1965).
5. R. Adams et al., Ind. Eng. Chem., 51, No. 12, 1467 (1959).
6. C. Colley, Brit. Chem. Eng., 17, No. 3, 229 (1972).
7. D. P. Timofeev, Kinetics of Adsorption [in Russian], Akad. Nauk SSSR, Moscow (1962), p. 95.
8. V. A. Sokolov, N. S. Torocheshnikov, and N. M. Kel'tsev, Molecular Sieves and Their Use [in Russian], Khimiya, Moscow (1964), p. 38.
9. O. M. Dzhigit, A. V. Kiselev, and G. G. Muttik, Kolloidn. Zh., 23, No. 5, 553 (1961).

THIN FOILS OF METAL NUCLIDES FOR NUCLEAR RESEARCH

L. G. Lishenko, V. N. Medyanik, T. S. Nazarova, A. A. Rozen, and G. V. Shula

UDC 539.216.2

The development of methods of obtaining thin foils of metal nuclides employed as targets in nuclear research [1] was initiated in 1956 in Kharkov Physicotechnical Institute. At the present time four methods are employed; the methods differ in the way in which the material is admitted and in the temperature conditions of the deposition: electrolysis of aqueous solutions of metal salts, evaporation of the metal in vacuum, vacuum-thermal reduction of the metal from compounds, and decomposition of volatile metal halides on a heated substrate. All the methods, except for the evaporation method, imply chemical reactions. Therefore, vacuum-thermal processes can be used to obtain foils at a low temperature from compounds which do not decompose under normal pressure. It should be noted that for obtaining foils from metal nuclides by evaporation, a molecular flow of metal vapor is required. In order to improve the uniformity of foil deposition, the equipment is usually provided with a device for shifting the substrate relative to the evaporator.

Each method has its particular advantages and shortcomings. Summarizing, it should be noted that evaporation is used mainly for obtaining thin foils, whereas the chemical techniques, which are characterized by high yields, are used to produce foils of greater thickness.

Electrolytic Deposition. Only a few of the many known electrolytes are used to deposit foils of metal nuclides [2]. The reason is that in the case of a small amount of a nuclide, the electrolytes employed have a low concentration of the metal to be deposited and are continuously depleted. The electrolytic technique is characterized by low temperature of deposition, by relatively low losses (up to 3%) of the nuclide, and by high

Translated from Atomnaya Énergiya, Vol. 49, No. 5, pp. 290-293, November, 1980. Original article submitted January 30, 1979; revision submitted March 18, 1980.

 0038-531X/80/4905-0730$07.50

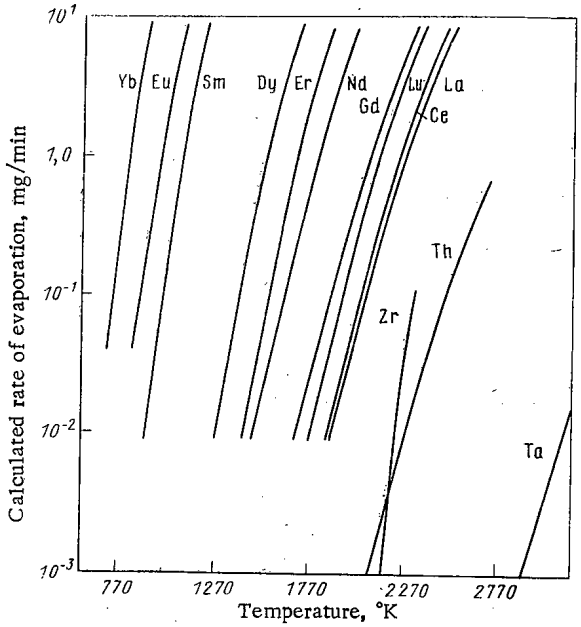

Fig. 1. Temperature dependence of the rate of evaporation of metals.

yield (90%) of the metal. In the majority of cases, sulfates of the metal nuclides (Fe, Ni, Co, Cu, Zn, Cd, Rh, In, and Ag) are used as the components of the electrolyte; in some cases, chlorides or complex chlorides (Bi, Sn, Ir, Ru, Pd, and Pt) or synthetized salts [2-5] of organic complex acids (Pb and Os) are employed. Cu, Ta, steel alloys, and Al are used as substrates. In order to facilitate the mechanical separation of the foils, the substrates are polished before their use. Copper substrates are dissolved in acids or solvents of various compositions, depending upon the nature of the foil deposited [5].

The internal stress is increased in Cr, Fe, Ru, and Rh foils obtained by electrolytic deposition. Therefore such foils are destroyed when they are removed from the substrate or when they are stored. Changes in the conditions of deposition (current density, temperature of the electrolyte, and its composition) have little influence upon the internal stress. The internal stress is substantially reduced when the electrolysis is performed with an asymmetric alternating current or by subsequent annealing of the foil in vacuum [2, 3].

Electrolytically deposited foils are characterized by rather uniform thickness (within the limits ±5%), which depends upon the composition of the electrolyte, the electrolysis conditions, and the geometry of the electrodes [5]. Since it is impossible to deposit foils of many metals by electrolysis, it is interesting to consider the use of organic solvents in which either a salt of the metal or organometallic compounds can be dissolved. Significant progress has not been achieved in this field and only sparce information on Ge [6] and Al [7] foils produced with this method has been published.

Evaporation of Metal Nuclides in Vacuum. Though metallization by evaporation in vacuum is widely employed, the foils obtained from metal nuclides in this manner have been treated in only a few papers. The possibilities of the technique can be assessed with the known values [8] of the vapor pressure and the evaporation rate of the metals. It follows from the data that the deposition rate of a foil is rather high at a metal vapor pressure of more than 1 Pa. The majority of metals have such a vapor pressure at temperatures of up to 2000°K, and heating to a higher temperature is required for a much smaller number of metals. The internal stress developing within the foil limits the deposition rate.

The evaporators are usually made from refractory materials, mainly W and Ta, and also Mo, Nb, Pt, Ni, and ceramics. In order to obtain foils of metals which are hard to evaporate, electron beam heating of a molten droplet is usually employed so that the evaporator and the heating unit are not contaminated by the material. The uniformity of the foil thickness depends mainly upon the geometry of the system, the type of the evaporator, and the solid angle of the vapor flow. High uniformity of ± (3-5)% is obtained by eccentrically positioned evaporators at a rotating substrate.

Substrates which do not dissolve or which dissolve in acids, organic solvents, and water are used for depositing foils. The foils are mechanically removed from unsoluble substrates (of tantalum or steel alloys). The linear foil thickness depends upon the parameters of the process such as the vapor pressure of the metal

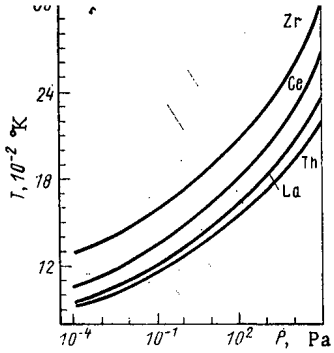

Fig. 2. Pressure dependence of the temperature of deposition of metal nuclide foils.

evaporated, the rate of evaporation, and the deposition time. The quality of the foil is substantially influenced by the vacuum which restricts the amount of gaseous contaminants introduced. Usually metal is evaporated under a residual pressure of 10^{-7}-10^{-4} Pa.

The technique of producing foils from the nuclides of certain metals has been described in several papers. Foils of Se [9, 10], Mn and Ge [9], Mg [11], Tl [12], Er and Sc [13], and Ti, Zr, and Hf [14] are deposited by evaporation from a tantalum (molybdenum) microevaporator at 600-1700 °K. Lavsan 1-2 μm thick, steel alloys, or tantalum is used as the substrates. When thallium is deposited, one also employs a substrate of zinc foil which is afterwards dissolved in hydrochloric acid; Ti, Zr, and Hf are deposited on Cu and Mo which are separated by dissolution in diluted (1:1) nitric acid. Thin target foils made from metals which are hard to evaporate (Mo, Ta, Nb, W, Re, Os, Zr, and Hf) are deposited on a carbon substrate by evaporation performed with the aid of electron beam heating [15].

Reduction of Compounds in Vacuum. Thermal reduction in vacuum allows the use of oxides of metal nuclides for obtaining metal foils. The method is limited by the following details:

1. High vapor pressure and high evaporation rate of the reduced metal and relatively low volatility of the metal-reducing agent.

2. Extremely low temperature of the reduction reaction.

3. High degree of purity of the metal-reducing agent.

4. High vacuum of the reaction chamber ($P_{res} \sim 10^{-4}$ Pa).

It follows from Fig. 1 that Ce, La, Zr, and Th [16] are the most convenient reducing agents of rare-earth metals; Ta is conveniently employed as the material of the evaporator and reaction vessel. In some cases, tantalum acted as the reducing agent at the same time. According to the thermodynamic data (Fig. 2), the temperature of reduction of rare-earth metals from oxides in a thermal process in vacuum can be decreased with increasing vacuum in the reaction chamber; thorium is the reducing agent of highest efficiency in this respect [17].

It was established in investigations of the kinetics [17-20] of thermal reduction of rare-earth metal oxides in vacuum that the rate of deposition and the yield of the metal depend strongly upon the pressure with which the reducing agent was compacted, the composition of the layer, and the temperature of the reducing agent. Practically no metal leaves a layer which was not compacted. The optimum compaction pressure is 250-300 MPa. A thin (δ = 1.0 μm) foil of Dy, Er, Nd, Gd, Lu, Sm, Eu, and Yb nuclides was obtained [16, 21, 22] by rolling vacuum condensates when the oxides of these metals were reduced with La and Th. However, high plasticity of the condensates and precision rolling equipment are required for this purpose.

When one wishes to obtain plastic foils, particularly those of rare-earth metals, both high vacuum in the chamber and a preliminary treatment of the initial materials are of great importance. The initial oxide of the nuclide must be calcined in air at 1100°K to remove organic impurities, and, before the reduction, the charge must be degassed in vacuum for a long time in the reaction vessel proper and at a temperature slightly below the temperature of reduction [23]. In the preliminary treatment, the total concentration of admixed oxygen, nitrogen, hydrogen, and carbon in the foil is reduced to about 10^{-2}%, which increases the plasticity of the foil and, in addition, also allows the use of the purified metal, which previously was degassed in vacuum, as reducing agent.

TABLE 1. Optimum Conditions for Producing Foils of Metal Nuclides by Thermal Reduction of Oxides in Vacuum

Group (metal)	Reducing agent	Optimum compos. of charge (oxide: metal), moles	Optimum temp. °K, of reducing agent	Ref.
Alkali and earth-alkali metals	La	1 : 1,7	900—1100	[29, 30]
Mg	Ti	1 : 1,25	1300	[27]
Mg	Ta	—	2100	[21]
Zn	Ti	—	1200	[28]
Ca	Ta	—	1950	[24]
Rare-earth metals				
Yb, Tm, Sm, Dy	La	1 : 4,5	300—1700	[16, 20, 23]
Yb	Zr	1 : 3	1200	[20, 21]
Ho, Er, Dy, Sc	Th	1 : 3	1800	[13, 16, 17, 19, 31]
Ti	Ta	—	2200	[21]
Cr	Ta	—	—	[25]
Fe	Al	—	1900	[26]

By reduction of the corresponding oxides with tantalum in high vacuum, the nuclides of Mg and Ti [21], Ca [24], and Cr [25] were obtained in the form of films on substrates or in the form of foils. Though the use of tantalum implies a higher reaction temperature, it appears promising to use tantalum because it eliminates additional contamination of the foil by the metal of the reducing agent. Since no data are available, it is not possible to reliably calculate the thermodynamically possible interval of the reduction temperatures and to assess tantalum as a reducing agent. It is known from experiments that Ti and Mg [21], as well as Ca [24], are reduced by Ta at relatively low temperatures (see Table 1). The method was used to produce foils of nuclides of Fe (reduction of Fe_2O_3 by aluminum) [26], Eu (reduction of Eu_2O_3 by lanthanum) [21], Mg [27], and Zn [28] (reduction of MgO and ZnO by titanium). It should be noted that the uniformity of a foil obtained by thermal reduction of compounds in vacuum is affected by the same factors as in the case of vacuum evaporation.

Decomposition of Volatile Metal Halides. The decomposition of volatile compounds of metals, mainly of iodides and chlorides, on a heated substrate in vacuum is an efficient method of producing thin foils of metal nuclides. The method is based on well-known work on producing titanium and zirconium of high purity by the decomposition of tetraiodides of those metals in a closed evacuated volume [32]. In the KhFTI there were developed a method and equipment [33-36] for obtaining foils of metal nuclides having a high melting point compared to the decomposition temperature of the halide, low volatility, and a tendency to form highly volatile halides.

In investigating the thermodynamics of the decomposition of halides [37], it was established that foils are most easily produced from Ti, Zr, and Hf tetraiodides, Nb, Ta, Mo, and Re pentachlorides, W hexachloride, and V and Cr diodides. The decomposition temperature of those compounds decreases with decreasing pressure as shown in Fig. 2, and the yield of the metal increases at the same time. With increasing atomic number of the element and decreasing valency of it, the deposition temperature of the foil increases. Since the deposition temperature of a foil must be much lower than the melting point of the metal, one can say that a foil of metals of increased valency can be obtained by decomposotion of halides at increased pressure, i.e., accordingly, at an increased rate, than foils of tetravalent metals.

Investigations of the kinetics of metal-foil deposition from halides [38-42] have revealed that the characteristic bell-shaped curve of the temperature dependence of the deposition rate results from the simultaneous occurrence of three competing processes on the heated substrate: decomposition of the halide under formation of the metal, reaction of the deposited metal with the halide vapor under formation of not-very-volatile halides, and evaporation of the deposited metal. The halides of the metal nuclides used to produce foils are synthetized directly from the elements in a degassed, evacuated glass apparatus and distilled into tubes [33, 34]. If necessary, the metal nuclide is initially obtained from oxides by thermal reduction with calcium.

TABLE 2. Optimum Conditions for Producing Foils of Metal Nuclides by Decomposition of Nonvolatile Halides

Metal	Halide	Temperature, °K		Material of substrate	Ref.
		Evaporator	Substrate		
Ti	TiI_4	440	1400	Mo	[33]
Zr	ZrI_4	540	1500	»	[33]
Hf	HfI_4	540	1500	»	[41]
Nb	$NbCl_5$	400	1400	»	[35]
Ta	$TaCl_5$	400	1400	»	[35]
Mo	$MoCl_5$	500	1200	Cu	[43]
W	WCl_6	400	1600	Mo	[36]
Cr	Cr_2I_4	1070	1300	Mo	[33]
V	V_2I_4	700	1300	Be	[35]
Dy	DyI_3	1200	1400	»	[44, 45]
Ho	HoI_3	1100	1500	»	[44, 45]
Tm	TmI_3	1100	1300	»	[44, 45]
Lu	LuI_3	1100	1300	»	[44, 45]

The halides are decomposed in a vacuum chamber ($P_{res} \approx 10^{-3}$ Pa) on a hot molybdenum substrate. The halide vapors arrive from the evaporator at the substrate via a vapor duct. The decomposition products, as well as the unreacted halide, are retained in a trap cooled with liquid nitrogen [33, 34] and regenerated thereafter. At $P_{res} > 1$ Pa the foil absorbs a considerable amount of gas and becomes brittle. The foil is separated by dissolving the substrate in diluted (1:1) nitric acid.

Optimum conditions for producing foils of metal nuclides by decomposition of volatile halides are listed in Table 2. The yield of the nuclide in the foil usually does not exceed 50%. The uniformity of a foil over its thickness depends strongly upon the geometry of the halide vapor flux relative to the substrate and varies within ±6%. Since the method implies that metal foils are deposited on a substrate heated to a high temperature, the foils are contaminated by the material of the substrate. For example, the concentration of molybdenum in Ti, Zr, and Hf foils increases at increasing temperature of the substrate and decreases when the rate of deposition is increased. The maximum amount of molybdenum is observed in titanium foils [46].

LITERATURE CITED

1. A. P. Klyucharev and N. Ya. Rutkevich, Zh. Eksp. Tekh. Fiz., 38, 2857 (1960).
2. V. N. Medyanik, V. N. Karev, and A. P. Klyucharev, Ukr. Fiz. Zh., 9, No. 7, 798 (1964).
3. V. N. Karev et al., Zh. Prikl. Khim., 39, No. 11, 2525 (1966).
4. V. N. Medyanik, V. N. Karev, and A. P. Klyucharev, Ukr. Fiz. Zh., No. 5, 560 (1966).
5. V. N. Karev and V. N. Medyanik, in: Physics of Metals [in Russian], No. 26, Naukova Dumka, Kiev (1969), p. 97.
6. C. Fink and V. Dakras, J. Electrochem. Soc., 95, No. 2, 80 (1949).
7. E. Peled and E. Gileadi, J. Electrochem. Soc., 123, No. 1, 15 (1976).
8. R. Honig, Radio Corp. Am., 23, No. 4, 567 (1962).
9. T. S. Nazarova and A. A. Rozen, Prib. Tekh. Eksp., No. 3, 226 (1974).
10. J. Galant, in: Proc. Annual Conf. on Nuclear Target Development, Atomic Energy Ltd., Chalk River (1975), p. 171.
11. J. van Andenhove et al., in: Proc. Annual Conf. on Nuclear Target Development, Atomic Energy Ltd., Chalk River (1975), p. 127.
12. T. S. Nazarova and A. A. Rozen, Prib. Tekh. Eksp., No. 1, 217 (1972).
13. T. S. Nazarova and A. A. Rozen, Prib. Tekh. Eksp., No. 6, 246 (1975).
14. R. Glover, F. Rogers, and T. Tuplin, Nucl. Instrum. Methods, 102, 443 (1972).
15. P. Maier, Nucl. Instrum. Methods, 102, 485 (1972).
16. L. Westgaard and G. Byornholm, Nucl. Instrum. Methods, 42, 7780 (1966).
17. T. S. Nazarova and A. A. Rozen, in: Problems of Atomic Science and Technology, Ser. General Physics and Nuclear Physics [in Russian], No. 3 (3) (1978), p. 65.
18. G. G. Gvelesiani and D. I. Bagdavadze, Soobch. Akad. Nauk Gruz. SSR, 42, No. 1, 151 (1966).
19. G. Schiffmacher and F. Trombe, Ct. Rd. Acad. Sci., C 268, No. 2, 159 (1969).
20. V. N. Karev et al., in: Metal Physics, No. 26 [in Russian], Naukova Dumka, Kiev (1969), p. 92.
21. S. Maxman, Nucl. Instrum. Methods, 50, No. 1, 53 (1967).

22. E. Kobisk and W. Grisham, Mater. Res. Bull., 4, No. 9, 651 (1969).
23. L. G. Lishenko et al., Prib. Tekh. Eksp., No. 1, 19 (1968).
24. G. Stinson, in: Proc. Annual Conf. on Nuclear Target Development, Atomic Energy Ltd., Chalk River (1975), p. 100.
25. C. Bouchard, in: Proc. Annual Conf. on Nuclear Target Development, Atomic Energy Ltd., Chalk River (1975), p. 74.
26. W. Riel, in: Proc. Annual Conf. on Nuclear Target Development, Atomic Energy Ltd., Chalk River (1975), p. 167.
27. I. Sugai, Preprint Inst. Nucl. Study, Tokyo Univ., No. 150 (1975).
28. I. Sugai, Preprint Inst. Nucl. Study, Tokyo Univ., No. 149 (1975).
29. A. D. Bondar', V. N. Karev, and A. P. Klyucharev, Prib. Tekh. Eksp., No. 4, 136 (1961).
30. A. D. Bondar', V. N. Karev, and A. P. Klyucharev, Prib. Tekh. Eksp., No. 2, 177 (1961).
31. T. S. Nazarova and A. A. Rozen, in: Problems of Atomic Science and Technology, Ser. General Physics and Nuclear Physics [in Russian], No. 2(8) (1979), p. 31.
32. A. E. van Arkel, in: Methods of Obtaining Pure Metals [Russian translation], IL, Moscow (1957), p. 80.
33. A. D. Bondar' et al., Izv. Akad. Nauk SSSR, Ser. Fiz., 24, No. 7, 929 (1960).
34. L. G. Lishenko et al., Prib. Tekh. Eksp., No. 4, 37 (1968).
35. V. N. Karev et al., Izv. Akad. Nauk SSSR, Ser. Fiz., 32, 328 (1968).
36. L. I. Kovalenko and A. A. Rozen, Prib. Tekh. Eksp., No. 3, 260 (1970).
37. L. G. Lishenko and A. A. Rozen, in: Problems of Atomic Science and Technology, Ser. General Physics and Nuclear Physics [in Russian], No. 3(3) (1978), p. 57.
38. A. P. Klyucharev et al., Izv. Akad. Nauk SSSR, Ser. Met., No. 6, 81 (1968).
39. L. G. Lishenko et al., Izv. Akad. Nauk SSSR, Ser. Met., No. 3, 91 (1971).
40. L. I. Kovalenko et al., Zh. Fiz. Khim., 47, No. 6, 1606 (1973); VINITI Dep. No. 5513-73.
41. L. G. Lishenko and A. A. Rozen, in: Problems of Atomic Science and Technology, Ser. General Physics and Nuclear Physics [in Russian], No. 3(3) (1978), p. 60.
42. B. S. Lysov, A. N. Tumanov, and V. N. Anikin, Izv. Vyssh. Uchebn. Zaved., Tsvetn. Metall., No. 4, 75 (1975).
43. A. P. Klyucharev et al., Prib. Tekh. Eksp., No. 4, 197 (1966).
44. L. G. Lishenko, T. S. Nazarova, and A. A. Rozen, Prib. Tekh. Eksp., No. 4, 243 (1972).
45. L. G. Lishenko et al., Zh. Neorg. Khim., 18, No. 4, 921 (1973).
46. L. G. Lishenko and A. A. Rozen, in: Problems of Atomic Science and Technology, Ser. General Physics and Nuclear Physics [in Russian], No. 2(8) (1979), p. 33.

CURRENT LIMITATION IN AN ACCELERATOR WITH VARIABLE-PHASE FOCUSING

A. S. Belei, V. S. Kabanov,
S. S. Kaplin, N. A. Khizhnyak,
and N. G. Shulika

UDC 621.384.64

In recent years, successes have been achieved in the creation of small-sized accelerating structures of heavy-particle linear accelerators, in which the stability of the motion is provided by means of variable-phase focusing (VPF) [1, 2]. The VPF method is simple in application and, by using it, favorable conditions are created for increasing the rate of acceleration. The acceleration process is started at a quite low injection energy (0.07-0.08 MeV for protons), which is of decisive importance in the development of linear small-sized heavy-particle accelerators.

However, there is an opinion [3] that the VPF method is unsuitable for providing stable acceleration of intense beams of ions. For example, in [3] for a 1.8-MeV proton accelerator with asymmetric phase-variable focussing (APVF), the limiting value of the accelerated current obtained does not exceed 32 mA and, by the numerical computation of the effect of the space-charge forces within the scope of the "large particle" model, the value is 15 mA. Such cautious estimates have originated as the result of the nonoptimum choice of the operating characteristics of the accelerating–focusing channel. Using a new approach to the choice of accelerator parameters with VPF [4], a heavy-particle linear accelerator can be developed with a higher value of the limiting current, which also is the purpose of the present paper.

When investigating different versions of design of the accelerating–focusing channel, it was established [4] that with a different distribution of the synchronous phase over the focusing period (containing several hf accelerating periods), there is an optimum value of the number of hf periods n occurring in one focusing period, which depends on the initial relative velocity β at the channel inlet and the specific rate of acceleration. In order to maintain the working current in the center of the stability diagram, it is necessary with increase of β to increase n also. By means of the method introduced, the accelerating–focusing channel in a small-sized 3-MeV deuteron accelerator with VPF [5], consisting of three focusing periods, was calculated. The first period contains a 3.5 hf period (structure in a π-wave), the second – 4, and the third – 4.5. The synchronous phase distribution over the hf periods of the accelerator obtained in this way is given in Table 1.

The accelerator is described in more detail in [5]. The principal parameters of the MLUD-3 accelerator are given below (data relating to capture by the accelerator in the longitudinal and transverse planes, obtained without taking account of space-charge forces):

Range of energy of accelerated particles, MeV	0.15-3
Operating wavelength, m	3
Strength of accelerating field in the gap, MV/m	7.8-8.0
Total length of accelerator, m	1.2
Diameter of resonator, m	0.5
No. of accelerator periods	24
Diameter of drift tubes, m:	
first	0.01
last	0.041
Extent of phase capture region at the synchronous energy level, deg	60
Transverse normalized acceptance for particles with energy spread of ±1%, cm·mrad	0.2π

In this present paper, an investigation was carried out of the Coulomb current limit in the MLUD-3 accelerator. The results were obtained by the numerical modeling method, using the "coarse particle" model. The motion of the particles in the accelerator was investigated beforehand by the method of mathematical modeling of the particles, without taking account of space-charge forces [6]. The regions of capture (accep-

Translated from Atomnaya Énergiya, Vol. 49, No. 5, pp. 294-295, November, 1980. Original article submitted February 27, 1980.

 0038-531X/80/4905-0736$07.50

TABLE 1. Synchronous Phase Distribution with Respect to Accelerator Gaps

No. of gaps	Phase, deg	No. of gaps	Phase, deg	No. of gaps	Phase, deg
1	—35	9	0	17	—25
2	—10,5	10	55	18	40
3	43,5	11	55	19	55
4	65	12	50	20	60
5	31,5	13	25	21	50
6	—12	14	—15	22	15
7	—42,2	15	—47,5	23	—30
8	—42,2	16	—47,5	24	—73,1

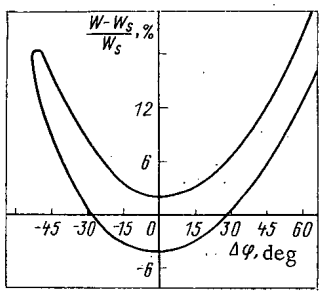

Fig. 1. Separatrix of the MLUD-3 accelerator, without taking account of the space-charge forces of the particles.

tance) in the longitudinal and transverse planes were determined. Figure 1 shows the separatrix of the accelerator in the coordinates $(W - W_S)/W_S$, $\Delta\varphi$. Here, W is the energy of an arbitrary particle; W_S is the synchronous energy; $\Delta\varphi$ is the deviation of the phase of the arbitrary particle from synchronous. At the energy level of motion of the synchronous particle for W_S = 150 keV, the extent of the longitudinal capture region amounted to 60° (accelerator capture coefficient 0.17)

The numerical modeling, taking account of the repulsive action of the space charge, was carried out by using a program developed in [3]. For the numerical calculations, the spread of particles with respect to initial energy was assumed to be equal to ±1%, the radius of the beam at the accelerator inlet was 0.25 cm, initial slope of the trajectory was 30 mrad, and the accelerating field in the gaps was approximated by a "square wave." The transverse acceptance of the accelerator, obtained without taking account of Coulomb forces, is given in Fig. 2. In the course of the investigations, the current at the accelerator inlet I_{acc} was determined for different values of the injection current I_{inj}. The normalized emittance of the beam $\pi\beta ab$, in accordance with Fig. 2, was assumed to be equal to $\pi \cdot 0.09$ mrad·cm (Fig. 3). It can be seen that the accelerator current increases linearly at first with increase of the injection current, then the increase slows down, reaching ~0.325 A with an injection current of 4 A. With further increase of the injection current, a drop in the accelerator output current is observed. On the linear section, the accelerator capture coefficient right up to an injection current of ~1 A is very close to the value obtained with zero intensity. This result is explained by the fact that the main limitations of the beam current in the accelerator are due to longitudinal movement, as the transverse emittance of the beam was chosen less than the emittance of the accelerator [7].

The dependence of the accelerator current on the emittance of the beam at the inlet is shown in Fig. 4. The injection current is chosen equal to 4 A, which corresponds, according to Fig. 3, to the maximum accelerated current. On the axis of abscissa, the maximum slope of the particle trajectory is $R' = dR/dz$, which for a given beam radius R is proportional to the emittance. The curves in Figs. 3 and 4 are drawn by taking account of the mean statistical spread, proportional to $1/\sqrt{N}$, where N is the number of "coarse" particles.

The maximum value of the current at the accelerator outlet corresponds to conditions of total coincidence of the beam emittance with the channel acceptance (see Fig. 2), which are achieved for R' = 50 mrad. With increase of the beam emittance, the accelerator current falls, as limitation with respect to the transverse motion begins, because the beam emittance exceeds the channel acceptance. Somewhat unexpected is the drop in the accelerator current with reduction of the beam emittance. It is possible that this is associated with the conditions of its overfocusing or the development of instability with increase of the phase density of the particles in the beam.

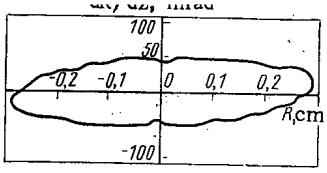

Fig. 2. Radial acceptance of accelerator for an energy spread of the particles at the inlet within the limits of ±1%.

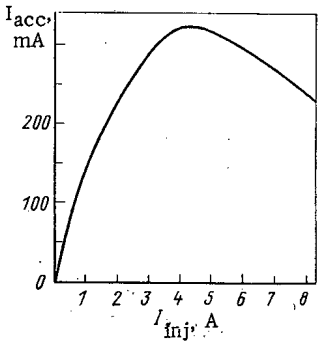

Fig. 3. Dependence of accelerated ion current on the injection current.

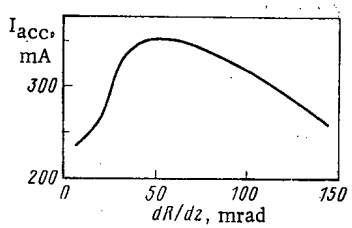

Fig. 4. Dependence of accelerated ion current on the maximum initial slope of the particle trajectory.

The results given show that the VPF method is quite promising for the development of small-sized linear heavy-particle accelerators with a beam intensity of the order of several hundred milliamperes.

LITERATURE CITED

1. Ya. Fainberg, in: Proc. Symp. on High Energy Accelerators and Pion Physics, Vol. 1, Geneva CERN, (1956), p. 91.
2. M. Good, Phys. Rev., 92, 538 (1953).
3. Linear Ion Accelerators, Vol. 1, Problems and Theory [in Russian], Atomizdat, Moscow (1979), p. 264
4. V. G. Papkovich, N. A. Khizhnyak, and N. G. Shulika, in: Problems of Nuclear Science and Technology, Ser. Techniques of Physics Experiment [in Russian], No. 2(2) (1978), p. 51.
5. L. N. Baranov et al., in: Problems of Nuclear Science and Technology, Ser. Linear Accelerators [in Russian] (1977), p. 12.
6. V. Yu. Gonchar et al., Ukr. Fiz. Zh., 24, No. 11, 1705 (1979).
7. I. M. Kapchinskii, Dynamics of Particles in Linear Resonance Accelerators [in Russian], Atomizdat, Moscow (1966).

STEADY PROTON BEAM INJECTOR WITH A CURRENT OF 1 A AND ENERGIES OF 100 keV WITH AN ION SOURCE OF THE "ION PUMP" TYPE

G. A. Koval'skii, D. V. Karetnikov, M. I. Men'shikov, N. V. Pleshivtsev, and B. K. Shembel'

UDC 621.384.644

In this paper, a constant proton beam injector* is described, for injection into a high-powered continuous-action accelerator [1] with an input acceptance of 10 cm · mrad. At the start of the project, only one injector [2] was known with an intensity close to 0.75 A, but it was insufficient for the problem posed and had a beam energy of 100 keV.

The operation of a steady injector with a high beam intensity is characterized by considerable thermal loads in the formation region and by a high electric field. The electrical strength of the accelerating interelectrode gaps in this region can be maintained only under good vacuum conditions which, in their turn, are provided by small flows of a neutral gas from an ion source. In the injector described in [2], and also in injectors [3, 4] capable of creating beams with an intensity of up to 0.6 A, the pressure of the gas in the discharge chamber of the source amounts to 1-10 Pa.

In the source developed by us, the discharge chamber is connected with the region of formation by a large-area opening. The gas pressure in the discharge chamber is reduced to approximately 10^{-1} Pa. The pressure drop between the discharge chamber and the precathode discharge region (in which it amounts to 1 Pa) is created because of the use of the ion pumping effect. This mechanism for removal of the gas was used for the first time in the vacuum ion pump [5]. In this paper, a ratio of the values of the pressure between the precathode region and the discharge chamber of ~500 is obtained.

The diagram of the "ion pump" source is shown in Fig. 1. The low-vacuum region 1, where the heated cathode 2 with an extended emission surface is located, is joined by a narrow channel 3 with the main discharge chamber 4, in which a higher vacuum is created. The plasma of the gas discharge 5, collimated by a longitudinal magnetic field, extends to the anticathode 6. The body of the chamber 7 serves as the anode. The plasma flow from the source into the vacuum takes place through the opening in the anticathode 8.

A stable discharge is established with a longitudinal magnetic field of 0.02-0.04 T. The maximum plasma output also corresponds to these values of magnetic induction. With increase of the field above 0.06 T, the intensity of the oscillations in the plasma increases strongly and, correspondingly, the radial flow of ions due to Bohm diffusion. With increase of the arc current, in all cases there corresponds an increase of the proton components which, in long chambers with a voltage in the discharge of U = 200 V, can reach 80-90%.

*Work carried out in 1967.

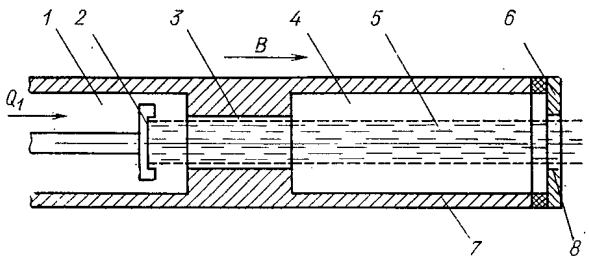

Fig. 1. Schematic diagram of an ion source (the direction of flow of the gas in the ion source is shown by the arrow).

Translated from Atomnaya Énergiya, Vol. 49, No. 5, pp. 296-299, November, 1980. Original article submitted November 30, 1979.

0038-531X/80/4905-0739$07.50

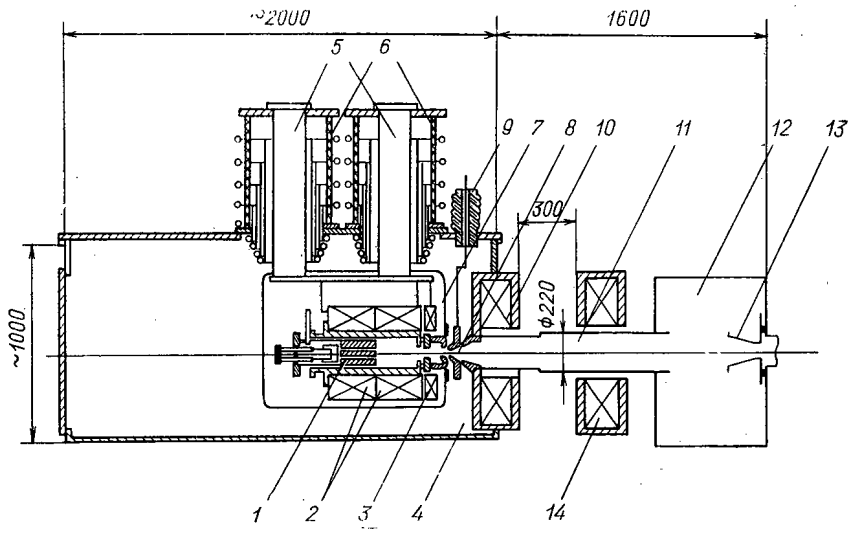

Fig. 2. Diagram of the proton injector.

The structural design of the ion source, to a considerable degree, is dictated by the beam shaping conditions. One of the most important elements of the shaping system is the plasma boundary of the ion emission. The position of the boundary (in the absence of a magnetic field, perpendicular to the direction of the ion take-off) is determined by the condition of equivalence of the pressure of the plasma electron gas and the pressure of the external electrostatic field

$$\varepsilon_0 E/2 = n_e k T_e, \tag{1}$$

where ε_0 is the dielectric constant of the vacuum; E is the strength of the external electrostatic field; n_e is the concentration of the electron gas at the boundary of the plasma, and T_e is the temperature of the electron gas.

The saturation ion current density at the plasma probe was found from the relation [6]

$$j = 0.4 e n_0 \sqrt{2kT_e/m_i}, \tag{2}$$

where $n_0 = 1.65 n_e$; e is the charge of the electron; m_i is the mass of the ion. Using this relation, expression (1) was reduced to the form

$$E = 4.96 \cdot 10^3 j^{1/2} (M\theta)^{1/4}, \text{ V/m}. \tag{3}$$

Here j is the ion current density; M is the mass of the ion, amu, and θ is the electron temperature, eV.

In characteristic operating conditions of the ion source ($j = 0.1$ A/cm^2, $\theta = 5$ eV), the strength of the field at the plasma boundary amounts to several kV/cm. By fixing the plasma density distribution over the cross section of the ion take-off region, by choosing the geometry of the take-off system and taking account of the relations given above, a configuration of the plasma boundary which is favorable for shaping the beam can be created. The flow of primary electrons markedly increases the pressure on the plasma side. As a result, the boundary of the plasma is deformed according to the density distribution of the dishcarge current. In this source, in order to eliminate the effect of the primary electrons on the plasma boundary, a cylindrical electrode is introduced, which is located behind the anticathode and has the identical potential. The primary electrons are reflected electrically in the discharge column in the vicinity of the anticathode opening, without penetrating the cavity of the cylindrical electrode, and the plasma flows freely from the source. In the majority of ion sources, the plasma reaches the beam shaping region through the central opening of the output electrode of the gas discharge chamber. Therefore, the maximum density of the plasma appears on the axis. The increased plasma density in the central region and the weakened (due to the presence of the opening in the accelerating electrode) external field lead to the appearance of a bulge at the boundary take-off surface, which significantly worsens the beam shaping condition. In the source being considered, a discharge column of tubular configuration is used. With the motion of the plasma in the cavity of the cylindrical electrode, the preaxial region as a result of radial diffusion also is filled with plasma, but its density is lower. Therefore, during the ion take-off, a concave surface of the plasma is formed and a beam which is close to laminar is formed.

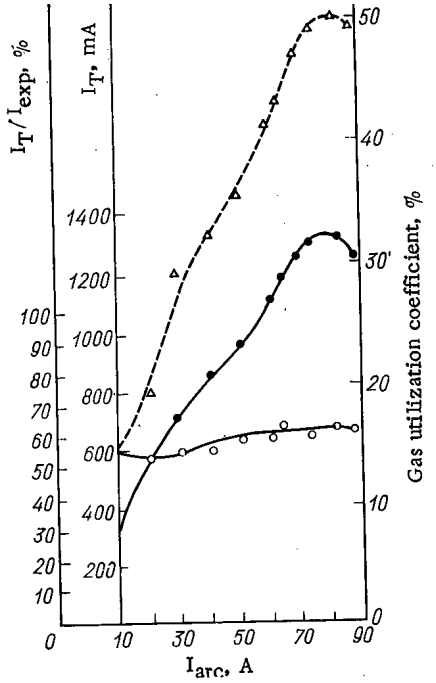

Fig. 3. Dependence of proton beam current on the arc discharge current for an accelerating energy of 100 keV: collimating opening with diameter 70 mm located at a distance of 1.6 m from the source; Δ) utilization factor of the gas flow for creating the proton beam; ●) proton beam current; ○) current utilization factor of the high-voltage rectifier for creating the proton beam.

Construction and Characteristics of the Proton Injector. The injector is shown diagrammatically in Fig. 2. The gas-discharge unit 1, with the magnetic coils 2 and 3, is insulated from the body of the injector to the total value of the accelerating voltage. It is installed in the vacuum container 4. The source is suspended on tubular rods 5 at the upper collars of two straight-through high-voltage insulators 6. In order to increase the electrical strength of the source, it is installed in the jacket 7 of polished copper plates. In the container, the inside walls of which are plated with polished copper plates, the electrodes of the beam shaping system 8 are installed. The second electrode, with a negative potential relative to the injector casing, is mounted on a separate rod which has an insulated lead-out 9. The third electrode is fixed to the wall of the container. A powerful focusing coil 10 creating a field of up to 0.7 T is installed on the outside of the front wall of the container. The ion duct 11 joins the container space with the collimator space 12, in which a collimating copper cone 13 is positioned at a distance of 1600 mm from the ion source (in front of the inlet to the preaccelerator [1]); the diameter of the straight-through opening in the collimating cone depends on the conditions of the experiment. The second focusing coil 14 is separated from the first by a distance of 300 mm. All the subassemblies of the injector which are irradiated by the ions are cooled intensively with water, and the high-voltage part of the injector by distilled water. The vacuum of $4 \cdot 10^{-3}$ Pa is provided by five oil-vapor pumps, provided with nitrogen traps. The total pumping rate amounts to 15,000 liters/sec. The majority of the running current measurements of the ion beam are carried out by an electrical method. The measurement error due to secondary electrons originating as the result of bombardment of the target by ions was eliminated by superposing a transverse magnetic field on the inlet section of the Faraday cylinder. All the principal measurements were necessarily duplicated by a calorimetric method. Measurements were carried out also by noncontact methods [7] developed in the course of the investigations.

At the outlet from the injector, the shaped beam contains ~70% of the protons. After passing through the focusing coils and the collimator, the proton content in the beam was increased up to 95%. The beam intensity with an energy of 100 keV attained 1.3 A. For this, 50% of the gas flow reaching the source was converted into the proton beam. The beam current amounted to ~60% of the current load of the high-voltage rectifier. The dependence of the beam current on the arc discharge current in the source is shown in Fig. 3. Figure 4 shows the dependence of the beam current on the energy in the range from 40 to 110 keV. With extension of the channel up to 3.3 m, a beam current of 1.0 A with an energy of 85 keV is recorded after passing through the colli-

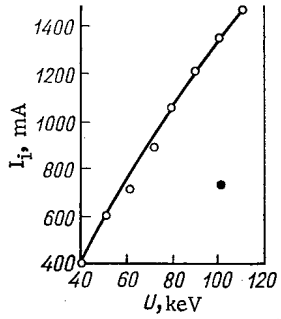

Fig. 4. Values of the proton beam current with a different accelerator energy: collimating opening with diameter 70 mm located at a distance of 1.6 m from the source; ●) data of [2]; ○) experiment.

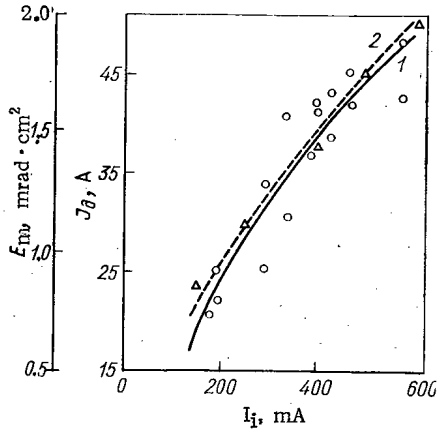

Fig. 5. Dependence of beam emittance on the ion current intensity (—, Δ) and the value of the discharge current corresponding to a given beam intensity (– – –, ○) with a voltage at discharge of 70 V.

mating opening with a diameter of 85 mm (in this case, the second solenoid was separated from the first by 1.5 m). The beam emittance, because of the inadequate thermal stability of the measurement equipment, was determined for an energy of 70 keV (Fig. 5). The measurements were carried out at a distance of 1.6 m from the source and with a diameter of the collimator opening of 70 mm. The beam intensity was controlled by the change of the discharge current with a constant discharge voltage. A distinct correlation between changes of emittance and the discharge current can be clearly seen in Fig. 5. It should be noted that the direct current entering the current collector was always modulated by hf oscillations with amplitude at the 20% level of the average intensity. The level of the modulations in the beam is above the level of the modulations by the hf oscillations of the discharge current. The maximum intensity of the oscillations corresponds to the range from a few tens to several hundreds of kHz.

On completion of development of the ion source, before connecting to the accelerator the accelerator was tested in defined conditions (beam current 1.0 A, beam energy 100 keV) during three months over 8-10 h per day, and it displayed stable operation with a high stability of the parameters.

Combined Operation of the Injector with the Accelerator. A diagram of the accelerator is shown in [1]. The total length of the beam channel up to the current collector of the accelerator amounted to 6.7 m. Owing to the separating action of the five series-installed focusing coils, the content of protons in the beam at the inlet to the current collector of the accelerator amounted to more than 99%. Below, the parameters of the injector are given for a beam of protons with an intensity of 0.6 A reaching the accelerator current collector (without switching on the hf acceleration).

Heating power of cathode, kW	5.5
Discharge current in source, A	55
Discharge voltage, V	75
Magnetic field in the ion source channel, T	0.02
Gas flow arriving at the source, $m^3 \cdot Pa/sec$	$4.0 \cdot 10^{-2}$
Beam energy, keV	95
Voltage on first electrode relative to earth, kV	-24
Load of high-voltage rectifier of injector, A	1.3
Diameter of opening in collimator cone, mm	50
Vacuum in injector, Pa	$2.7 \cdot 10^{-3}$

When the hf resonators of the accelerator were switched on, a proton current of 0.25 A with an energy of 500 keV was recorded in the current collector.

In conclusion, the authors express their thanks to participants in this project, in particular M. A. Nikitin, K. N. Nikitin, A. S. Skvortsev, E. N. Knyazev, O. A. Gusev, Yu. G. Gendal', and O. G. Matveenko, and also to the director of operations on the startup and investigation of the accelerator, A. P. Fedotov.

LITERATURE CITED

1. B. K. Shembel' et al., At. Energ., 31, 1, 45 (1971).
2. W. Lamb and E. Lofgreen, Rev. Sci. Instrum., 27, 11, 907 (1956).
3. R. A. Demirkhanov et al., Prib. Tekh. Eksp., 2, 19 (1964).
4. N. V. Pleshivtsev et al., Prib. Tekh. Eksp., 6, 23 (1967); At. Energ., 22, 2, 128 (1967).
5. E. Lawrence, Science, 122, 3180, 1127 (1955).
6. M. D. Gabovich, Physics and Technology of Ion Plasma Sources [in Russian], Atomizdat, Moscow (1972).
7. G. A. Koval'skii et al., Prib. Tekh. Eksp., 5, 47 (1968).

PROBLEMS OF THE RADIATION HAZARD OF ^{14}C

I. Ya. Vasilenko, P. F. Bugryshev, A. G. Istomina, and V. I. Novosel'tseva

UDC 621.039.58:539.16.01

Nuclear explosions, the total power of which has reached 530 megatons, have been accompanied by the formation of a substantial amount of radiocarbon – ^{14}C – characterized by a long half-life (5760 yr) and a low β radiation energy (0.156 MeV). The maximum concentration of this nuclide in the atmosphere was registered in 1965, when its level exceeded the natural background by approximately 100%. The total amount of accumulated radiocarbon was 5.8 MCi in 1972 [1, 2]. As a result of the limitation of atmospheric nuclear explosions, the concentration of "bomb" ^{14}C in the atmosphere is gradually falling. However, it still exceeds the natural level by approximately 30%. By the year 2000, it is expected to have fallen to 3% (Fig. 1).

At the present time, the main sources of the ever increasing penetration of ^{14}C into the environment are the atomic energy enterprises. According to generalized data, the ejection of gaseous ^{14}C from energy reactors comes to hundredths of a Ci/MW(el) · yr [3]. In this case ~95% of the ^{14}C is in the form of $^{14}CO_2$, 2.5% in the form of ^{14}CO, and 2.5% in the form of hydrocarbonates [4]. By the year 2000, this situation may lead to an approximately 200% increase in the concentration of radiocarbon in the atmosphere (Fig. 2). We should note that the increase [5, 6] in the content of stable carbon in the atmosphere as a result of the combustion of mineral fuel is leading to a certain drop in the ^{14}C concentration as a result of its dilution.

Processes of exchange of ^{14}C between the atmosphere, biosphere, and hydrosphere proceed rather intensively and are characterized by time constants of the order of several years. The period of half purification of the atmosphere is assumed equal to 1.5-5 yr [1, 2]. Ultimately the bulk of the radiocarbon passes into the world's ocean, which plays the role of a unique "buffer" and where, reacting with metals, ^{14}C forms carbonates and bicarbonates. The time constant of the exchange of the surface layers of the ocean is ~5-25 yr,

Translated from Atomnaya Énergiya, Vol. 49, No. 5, pp. 299-303, November, 1980. Original article submitted September 28, 1979.

0038-531X/80/4905-0743$07.50

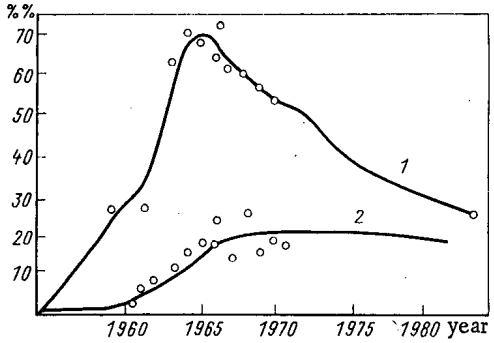

Fig. 1. Content of "bomb" ^{14}C in the atmosphere (1) and surface layer of the ocean (2) [1, 2]. The excess amount of ^{14}C in comparison with natural content is plotted along the y axis in Figs. 1 and 2.

and of the deep layers 100-1000 yr. It is believed that a complete exchange of the ^{14}C in the atmosphere, like that of stable carbon, occurs in 300-500 yr.

During the process of photosynthesis ^{14}C is accumulated in plants, and then in the organism of animals and humans. Moreover, terrestrial plants fix only 1/10 of the radiocarbon; the remaining 9/10 is absorbed by marine plants, chiefly by phytoplankton. The coefficient of transfer in the chain atmosphere–terrestrial plants is equal to unity [7]. Equilibrium is established very rapidly, within 2-3 months. Radiocarbon can pass into plants in small amounts from the soil through the root system as well. The content of ^{14}C in the animal organism is correlated with the past years' content of it in plants [8]. In 1963-1964 the concentration of the radionuclide in plants approximately doubled in comparison with the natural level [9]. Close to pollution sources, the concentration of ^{14}C in the atmosphere is higher than the average, which naturally leads to an increased accumulation of radiocarbon in plant and animal organisms in these zones. Thus, plants at a distance of 1-2 km from the stack of an atomic power plant contain 50-90% more ^{14}C than those at a distance of 20-30 km [6]. Consequently, local foci of contamination by radiocarbon may be created.

Radiocarbon penetrates into the human organism with food products of vegetable and animal origin and with water in the forms of various organic and inorganic compounds, as well as with air in the form of $^{14}CO_2$. The accumulation of radiocarbon in plants in the process of photosynthesis is the basic link in the biological chain through which ^{14}C is taken into the human organism with foods.

The penetration of artificial radiocarbon into the atmosphere leads to an increase in its content in the human organism. Thus, the amount of ^{14}C in the bodies of people who died in 1964-1965 exceeded the natural level by approximately 50% [9]. Practically the same amount of ^{14}C was in the bodies of people who died in 1973 [10]. The additional dose of irradiation on account of bomb radiocarbon is negligible, and in recent years has been ~1 mrd/yr for the whole body. In the years to come it will gradually fall, since the levels of contamination of food products by bomb ^{14}C are decreasing. The period of half purification of products of animal origin is equal to 6 yr [11]. The integral dose in the year 2000 will be 7, 22, and 19 mrd for the gonads, endosteal cells, and on the average for the organism, respectively [1, 2]. During the entire lifetime of ^{14}C, its integral dose significantly exceeds the dose from other radionuclides of fission products. It will be created for 10^3 yr. We note that the fraction of irradiation of the whole body on account of natural radiocarbon is equal to ~1.2 mrd/yr and comes to ~1% of the dose of the background irradiation. The doses of irradiation on account of the ejection of ^{14}C by nuclear energy enterprises are gradually increasing (Fig. 3).

In an evaluation of the biological aspects of global pollution of natural media by radiocarbon, we should keep in mind that carbon is one of the basic biogenic elements and is contained in all living tissues (fats, proteins, carbohydrates, nucleic acids, enzymes, vitamins, and other biologically important compounds); thus it may act as an internal irradiator of biomolecules. During the metabolic process, the radionuclide is displaced from one class of compounds to another.

The biological action of the radionuclide is associated not only with radiation effects, i.e., its processes of ionization and excitation of atoms and molecules by β-particles in the decay of ^{14}C and by the formation of highly biochemically active radicals, but also with the chemical action as a result of transformations of the disintegrated carbon atoms into nitrogen atoms [$^{14}C(n, p) \rightarrow {}^{14}N$]. The transmutation factor (changes in the chemical nature of the atoms and molecules) takes on special significance if radiocarbon is incorporated into

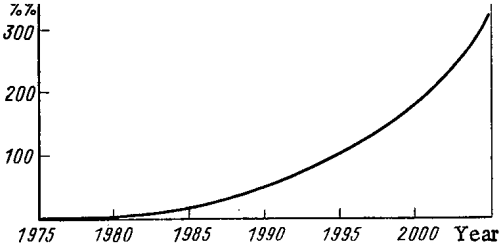

Fig. 2. Concentrate of ^{14}C in the atmosphere due to ejection by nuclear energy enterprises expected in the year 2000 [5, 9].

the molecule, damage to which determines the biological effect. Local changes in the chemical composition of DNA (conversion of ^{14}C to ^{14}N) lead to gene and chromosome mutations which are not repaired. The probability of damage due to β particles formed in the decay of ^{14}C is immeasurably lower [12]. We note that the repairing enzymes in most cases repair single breaks in DNA induced by radiation effects. Double breaks are repaired with greater difficulty. Mutations in the germ cells, if they do not lead to their death, may be manifested in the progeny in the form of deviations from normal development, and also in the form of hereditary diseases. Mutations in somatic cells can cause various disorders over long periods, including malignant neoplasms.

Pauling was the first to call attention to the possibility of an increased mutagenic action of incorporated ^{14}C [13]. Many researchers attribute great significance to the transmutation action of radiocarbon. considering that the biological effectiveness per unit of sorbed dose is increased [14-17]. However, we should make special note of the fact that the International Commission on Radiological Protection, analyzing the results of these and other investigations, recommended the acceptance of an RBE of ^{14}C equal to one. The same conclusion was reached by the Scientific Committee on the Effect of Atomic Radiation of the United Nations Organization (UNSCEAR), the National Academy of Sciences of the United States [18], and the National Commission on Radiological Protection of the USSR [19].

In evaluating the biological effects of radiocarbon, the investigation of the kinetics of exchange of the nuclide is of great significance. The necessity for conducting such investigations is due to the fact that the peculiarities of the exchange of various compounds of radiocarbon are not always taken into account in its standardization [19, 21]. Only in Publication 10 of the International Commission on Radiological Protection was attention paid to the peculiarities of the metabolism of certain compounds of ^{14}C (bicarbonate, glycine, acetate). These compounds, however, are not the main sources of the contribution of radiocarbon to the human diet.

In our investigations [22, 23], a comparative study was made of the kinetics of the metabolism of the basic inorganic and organic radiocarbon compounds, contained in carbohydrates, proteins, and fats, as well as alcohols. The inorganic compounds $Na_2^{14}CO_3$, $K_2^{14}CO_3$, $Ca^{14}CO_3$ are characterized by a high absorbability (90-100%), a relatively uniform distribution of ^{14}C in the organs and tissues, and a rapid elimination from the organism, chiefly through the lungs in the form of $^{14}CO_2$. During the first hour, rats eliminate 77, 79, and 35% of the introduced amount of radiocarbon in the form of the above-mentioned compounds, respectively, through the lungs. By the end of 24 h, only 1-3% of the introduced ^{14}C remains in the organism. Organic compounds ([^{14}C]glucose, [^{14}C]succinic acid, [^{14}C]glycine, [^{14}C]palmitic acid, [^{14}C]ethanol, [^{14}C]methanol) are also characterized by high absorbability (95-100%) and a relatively uniform distribution of ^{14}C in the organs and tissues. Radiocarbon is eliminated from the organism chiefly through the lungs; however, it is eliminated more slowly in comparison with inorganic compounds, since the ^{14}C of these compounds is utilized as an energy and plastic material. After 24 h, the rat organism contained approximately 15, 50, 60, 10, 12, and 34% of the activity after the administration of [^{14}C]glucose, [^{14}C]glycine, [^{14}C]palmitic acid, [^{14}C]succinic acid, [^{14}C]ethanol, and [^{14}C]methanol, respectively. In the initial period, a large concentration of ^{14}C was registered in the organs and tissues with a high level of metabolism (liver, kidneys, gastrointestinal tract), and subsequently in the adipose tissue and bone.

In the case of long-term intake of radiocarbon, an equilibrium state was established in rats after a month from the beginning of the introduction of $Na_2^{14}CO_3$, three months after the beginning of administration of [^{14}C]glucose, and four months after the beginning of administration of [^{14}C]glycine and [^{14}C]palmitic acid. By this period, 7, 200, 1200, and 1300 daily introduced amounts of radiocarbon had been accumulated in the

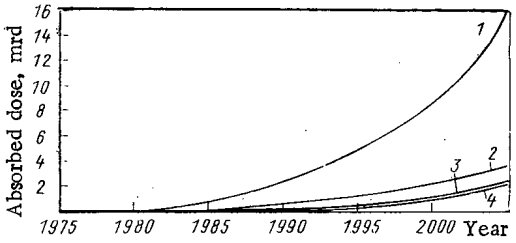

Fig. 3. Presumed doses of irradiation due to ejection of ^{14}C by nuclear energy enterprises: 1) adipose tissue; 2) whole body; 3) bone marrow; 4) gonads.

organism, respectively. The peculiarities of the metabolism of various radiocarbon compounds affected the rate and value of the irradiation doses formed. When organic compounds were administered, the doses of irradiation of the organs and tissues were 10 times as great as when inorganic compounds of ^{14}C were taken in.

When the experimental data obtained are extrapolated, it may be assumed that in man, when ^{14}C is received in the standard diet, an equilibrium state is established 1.5 yr after the beginning of the intake of radiocarbon, with a multiplicity of accumulation ~30 (the ratio of the radiocarbon content in the organism to the amount consumed daily). These values are in good agreement with the recommendations of the USNCEAR, according to which the time of an equilibrium state is 1.4-1.8 yr [1, 2], while the multiplicity of accumulation of ^{14}C agrees with the multiplicity of accumulation of stable carbon and radiocarbon of natural origin (30-40 and 30-33, respectively). The nature of the irradiation depends on the form of the compound in which radiocarbon is taken into the organism. When ^{14}C is consumed in the diet, the maximum doses are formed in the adipose tissue and bone marrow (yellow) and are approximately four times as great as the average dose of irradiation of the body.

The doses of irradiation due to anthropogenic radiocarbon make a negligible contribution to the dose of background radiation. The effect of low doses is of a stochastic nature and may be manifested chiefly in various kinds of genetic disorders (deviation from normal development and hereditary diseases) and malignant neoplasms. The hazard of the risk for society increases with increasing number of persons irradiated in the population. The International Commission on Radiological Protection and the UNSCEAR, in evaluating the risk, recommend that one proceed from the concept of a thresholdless action of radiation and a linear dose vs effect relationship. It is emphasized in this case that any irradiation that is unnecessary should not occur. Such an approach is the best guarantee of reliability of radiation protection of man.

The results of estimates of the possible genetic and somatic consequences of environmental pollution with ^{14}C are presented in Table 1. The following initial assumptions were used in this:

global pollution of the environment and the established equilibrium in the chain air–food products–human organism (coefficient of discrimination assumed equal to unity);

cessation of nuclear explosions in the atmosphere;

thresholdless linear dose vs effect relationship (the increase in the biological effect on account of the transmutation effect is neglected).

As was noted above, the biological hazard of the accumulation of ^{14}C in natural media is associated primarily with its transmutation action. The transmutation of ^{14}C incorporated into DNA is especially important to consider for such effects as gene and chromosome mutations, reproductive death of cells, which are associated with direct damage to DNA. The quantitative evaluation of these effects encounters great methodological difficulties. In an experimental determination of the relative genetic effectiveness (RGE) of ^{14}C according to the indices of gene mutations (experiments on phage, yeasts, Drosophila), chromosome aberrations (experiments on onion rootlets, bean sprouts), and reproductive death (experiments on bacteria, human cells in tissue culture), contradictory data were obtained; the RGE was 1-20 [14-17, 24-30]. The standards used were x rays and γ radiation with low values of the linear energy loss. Such discrepancies are due to the great variety of experimental material and the various experimental conditions. There are no sufficiently substantiated materials on the value of the RGE of ^{14}C at the present time. In our investigations the value of the biological effectiveness of ^{14}C was estimated by the coefficient 10 [23]. If we use this value of the RGE, the yield of malignant neoplasms and congenital defects cited in Table 1 must be increased by an order of magnitude.

TABLE 1. Possible Somatic and Genetic Consequences of Irradiation of a Population of 10^6 Persons on Account of Anthropogenic ^{14}C (number of cases in the whole life from a dose in 1 yr)

Nature of disorders	1980	1985	1990	1995	2000	2005
Malignant tumors	0,01	0,04	0,1	0,2	0,4	0,8
Serious congenital defects *	0,004	0,01	0,03	0,06	0,1	0,15

*Per 10^6 newborn.

It should be noted that even in this case it is impossible to detect the influence of anthropogenic ^{14}C: the mortality from malignant neoplasms of various localizations reaches 1500-1600 cases per year per 10^6 persons [32]; the natural frequency of genetic damages is considered equal to 60,000 cases per 10^6 children, including 16,000 severe cases [33].

In the estimates cited the possibility of accumulation of a genetic burden in the population as a result of the mutagenic action of ^{14}C in an infinite series of cell generations and the consequent increase in unfavorable effects in future generations was not taken into account. In this case the value of the RGE of ^{14}C may be substantially increased. In the opinion of Academician N. P. Dubinin [34, 35], 25% of the natural mutations are associated with the radiation background, and great significance is attributed to radiocarbon in this case. The possibility remains that radiocarbon has been of vital importance as a factor of variability in the process of evolution of life on earth. It can be assumed that the bulk of the mutations are eliminated in the process of evolution.

The investigations of the resistance of the plant and animal world to an increased concentration of ^{14}C in the biosphere remain insufficient. The possibility remains that the ecosystems may have less stable links than man. Therefore, the increase in ^{14}C concentration presents not only a hygienic, but also an ecological problem on a global scale. To answer these questions, it will be necessary to conduct further complex systematic investigations on various species of plants and animals, including higher animals.

LITERATURE CITED

1. Radioactive Pollution as a Result of Nuclear Explosions, Report of the UNSCEAR, A/AC 82/R, 298, June 17, 1975.
2. Sources and Action of Ionizing Radiation, Report of the UNSCEAR at the U.N. General Assembly, New York, Vol. 1 (1978), p. 226.
3. Production of Nuclear Energy, Report of the UNSCEAR, A/AC 82/R, 329, June 15, 1976.
4. C. Kunz, W. Mahoney, and J. Miller, Trans. Am. Nucl. Soc., 21, 91 (1975).
5. A. D. Turkin, Dosimetry of Radioactive Gases [in Russian], Atomizdat, Moscow (1973).
6. V. P. Rublevskii, S. P. Golenetskii, and G. S. Kirdin, in: A. D. Turkin (ed.), Radioactive Carbon in the Biosphere [in Russian], Atomizdat, Moscow (1979).
7. W. Broccer and A. Walton, Science, 130, No. 3371, 309 (1959).
8. A. P. Vinogradov, A. L. Devirts, and É. I. Dobkina, Dokl. Akad. Nauk SSSR, No. 3, 688 (1961).
9. R. Nydal and K. Lovseth, Nature, 206, No. 4988, 1029 (1965).
10. M. Steinhouse and M. Baxter, Nature, No. 5614, 828 (1977).
11. Data and Reports, 14, No. 11, 679 (1973).
12. L. M. Gracheva and V. G. Korolev, Genetic Effects of the Decay of Radionuclides in Cells [in Russian], Atomizdat, Moscow (1977).
13. L. Pauling, Science, 128, 1183 (1958).
14. A. M. Kuzin, Effectiveness of the Biological Action of ^{14}C When It is Incorporated into Living Structures [in Russian], Akad. Nauk SSSR, Moscow (1960).
15. A. M. Kuzin et al., Radiobiologiya, No. 6, 805 (1964).
16. A. M. Kuzin et al., in: Radiation Genetics [in Russian], Akad. Nauk SSSR, Moscow (1962), p. 267.
17. S. N. Aleksandrov, D. K. Popov, and N. K. Strel'nikova, Gig. Sanit., No. 3, 63 (1971).

18. Radiation Protection Recommendations of the International Commission on Radiological Protection, ICRP, Publication 10, Pergamon Press, Oxford (1968).
19. Standards of Radiation Safety NRB-76 [in Russian], Atomizdat, Moscow (1978).
20. Recommendations of the International Commission on Radiological Protection [Russian translation], IL, Moscow (1958).
21. Radiation Protection. Recommendations of the International Commission on Radiological Protection. Second Publication [in Russian], Gosatomizdat, Moscow (1964).
22. I. Ya. Vasilenko et al., in: Radioecology of Animals. Materials of the First All-Union Conference [in Russian], Nauka, Moscow (1977), p. 203.
23. I. Ya. Vasilenko et al., in: Summaries of the All-Union Conference: Long-Term Effects and Estimation of the Risk of the Influence of Radiation [in Russian], Moscow (1978), p. 61.
24. J. Beal and N. Scully, Bot. Gas., 112, 232 (1950).
25. E. Suomolainen, O. Jurpeinen, and R. Niini, Nature, 178, No. 4529, 337 (1956).
26. H. McQuade, M. Friedkin, and A. Atchison, Exptl. Cell Res., 11, No. 2, 249 (1956).
27. C. Purdon, Mutation Res., 2, No. 2, 156 (1965).
28. V. S. Skobkin and L. A. Mineeva, Genetika, 1, No. 3, 97 (1965).
29. G. Pluchennik, Genetika, 2, No. 5, 117 (1966).
30. R. Oliver, in: Biological Effects of Transmutation and Decay of Incorporated Radioisotopes, IAEA, Vienna (1968), p. 165.
31. S. Apelgot, ibid., p. 147.
32. Morbidity of the USSR Population with Malignant Neoplasms and Cancer Mortality [in Russian], Meditsina, Moscow (1970).
33. The Effects on Populations of Exposure to Low Levels of Ionizing Radiation. National Academy of Sciences, National Research Council, Washington (1972).
34. N. P. Dubinin, Evolution of Populations and Radiation [in Russian], Atomizdat, Moscow (1966).
35. N. P. Dubinin, General Genetics [in Russian], Nauka, Moscow (1976).

OPERATIONAL METHOD FOR STUDYING ^3H IN THE OCEAN AND ATMOSPHERE UNDER MARINE CONDITIONS

V. N. Soifer, E. A. Boroukhin,
V. A. Goryachev, Yu. S. Pozdeev,
and A. F. Sergeev

UDC 539.1.551.4

An important place in the realization of long-term complex programs in the study of the circulation and agitation of water masses in the world's ocean is occupied by the application of radioactive tracers, such as ^3H, ^{14}C, ^{226}Ra, and ^{137}Cs [1]. Tritium, along with deuterium and ^{18}O, is the most promising indicator of movement of water masses and is used to study the processes of circulation and water exchange of a mesoscale character (mass exchange across a thermocline, the interaction of the atmosphere with underlying water surfaces, the ascent and descent of water masses). Their use is also promising in the study of vortex formation in the ocean.

Apart from measurements of ^3H and ^{14}C conducted recently (e.g., by the Scripps Oceanographic Institute), there was a gap for several years [2] between the selection of significant volume samples at separate stations and labor-intensive technological analysis of them after set-up in coastal laboratories. This excluded the possibility of an effective use of tritium and radiocarbon methods during work on areas in the ocean. Besides this, additional difficulties arose in the protection of deep-water samples with ultralow concentrations of ^3H from contamination by ^3H atmospheric moisture during analysis on dry land, where the concentrations of ^3H are 1-2 orders of magnitude higher than in the atmosphere above the ocean surface.

Translated from Atomnaya Énergiya, Vol. 49, No. 5, pp. 303-307, November, 1980. Original article submitted December 24, 1979.

 0038-531X/80/4905-0748$07.50

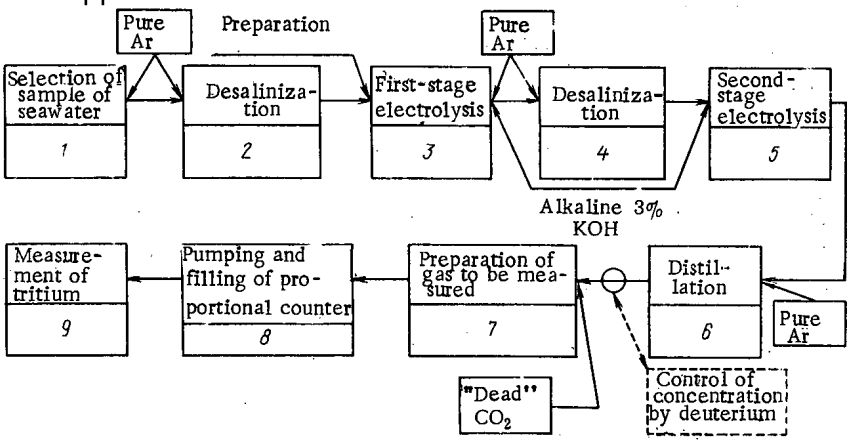

Fig. 1. Design of tritium measurements in ocean water (sensitivity $0.2 \cdot 10^{-18}$ $^3H/H$: 1) plastic bathometers, V = 6 liters; 2) vacuum still, P = 3.6 kW, output 1 liter/h; 3) C_0 = 3% KOH, C_f = 30%; 4) distillation battery with 5 tanks, V_0 = 500 ml, Δt = 2h; 5) C_0 = 3% KOH, C_f = 40%; 6) 9 tanks, V_0 = 30 ml, Δt = 1 h; 7) synthesis units and pure methane, V_f = 16 liters, Δt = 8 h, output 96-99%; 8) pumping units and counter filling, vacuum 10^{-2} torr (1 torr = 133.322 Pa), pressure 400 kPa, Δt = 2 h; 9) detection block with 5 channels, ^3H "window" 1-19 keV, σ = 1-2%, Δt = 10 h.

Sharp changes in the hydrometeorological conditions in the boundary zone of the atmosphere lead to significant variations in the coefficient of the turbulent volume of moisture. Therefore, for the correct solution to moisture–exchange problems on the area of water studied, it is necessary to have immediate measurements of tritium on the vessel during field work. The variability observed in the concentration of tritium in the vertical sections of the area of the ocean studied has, quite correctly, an unprecedented character. Obtaining preliminary data about the tritium field of a definite region during the work of the expedition allows one to plan studies during the course of the entire voyage. It is evident that in the given case, not only is there a saving in time and valuable material, but the possibility appears of conducting unique experiments in the study of the circulation and movement of water masses in the ocean as well as in moisture-exchange on the ocean–atmosphere boundary.

The presence of a tritium laboratory consisting of a measuring complex on the research vessel (RV) allows one to reduce to several days the time from the moment of sampling to the moment when the results are obtained and also lessens the danger of contaminating deep samples with atmospheric moisture during storage and analysis.

In 1971 on the RV "Academician Kurchatov," the first experiment was conducted on ^3H radiometry in marine conditions, in the Pacific Ocean Oceanography Institute (POI) DVNTs AN SSSR Marine Tritium Laboratory devoted to work under expeditionary conditions with a complex program of studying the ocean and atmosphere using tritium and, eventually, radiocarbon methods.

Unfortunately, an ultralow level of ^3H radioactivity in the ocean and, especially, the techniques of its measurement do not allow one to conduct uninterrupted recording. At present, the concentration of ^3H in deep and surface waters is 0.1-1.0 parts per 10^{18}, and in the atmosphere it is 10-100 parts per 10^{18}. Taking this into consideration, the basic problems in creating a marine measuring complex are the following:

1) analysis of the means and methods of selection of samples of atmospheric moisture for gradient measurements of the flow of ^3H (test volume 30-100 ml);

2) mastery of techniques of sample selection of deep water, studied for ^3H, without contact with the atmosphere and with simultaneous determination of the hydrological background: temperature, salinity, chemical composition of water at depth (approximate sample volume 3-5 liters);

3) reanalysis of the tuning and set-up of a marine measuring complex for a precise analysis of water for ^3H with a sensitivity to 0.2 per 10^{18}.

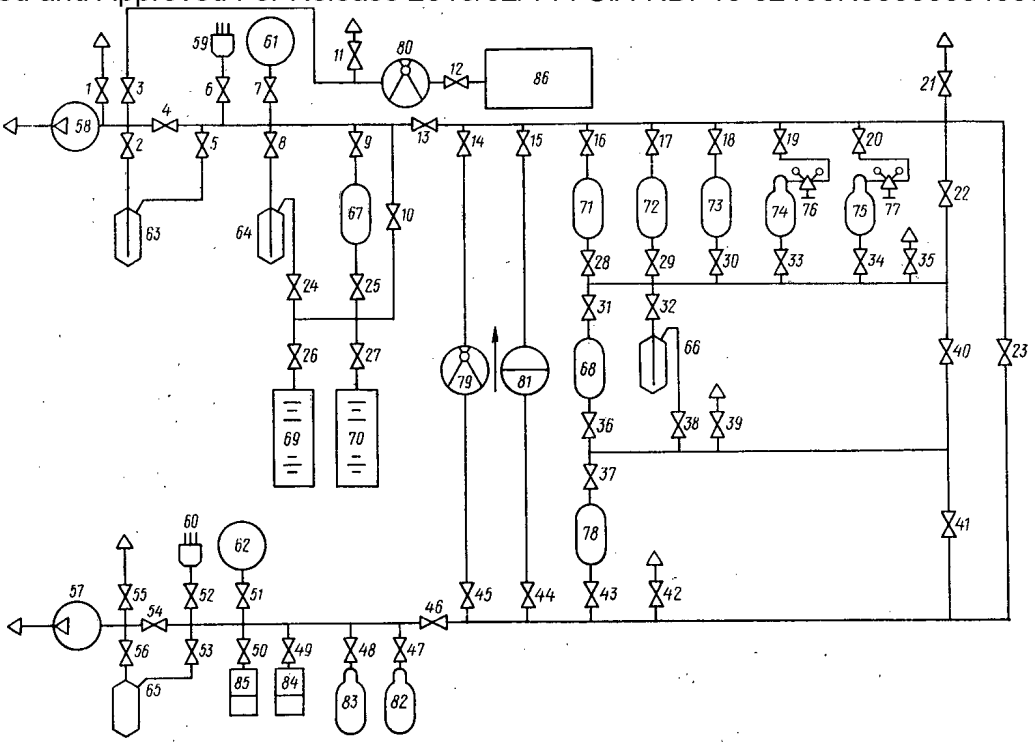

Fig. 2. Design of the pumping system: 1-56) valves; 57-58) vacuum hoses; 59-62) vacuum meters; 63-68) traps; 69-70) reactors for methane synthesis; 71-73, 78, 81-83) loops to purify methane; 74-75) tanks with CO_2 and H_2; 84-85) proportional counters; 76-77) reducers; 79, 80) buffer capacities.

A marine measuring system was created on the TOI to study ^3H, ^{14}C, and other radionuclides: we included a marine tritium laboratory, automated thermohaline probe-γ-spectrometer, a system for rapid analysis of data, and automated meteorological stations for the gradient measurements with an apparatus for sampling the atmospheric moisture.

Analysis in the marine tritium laboratory was accomplished by a concentrating electrolysis apparatus, apparatus for distillation of samples (distillation batteries), vacuum apparatus with a sealed system and a detection block with a protective shield (Figure 1).

The electrolysis arrangement consists of electrolyzers of the first and second stages (in 6 parts),* arranged in a support and cooled by running water with a consumption of not more than 3.5 m^3/h. The dimensions of the apparatus are 1340 × 1800 × 700 mm, mass ≈380 kg. The current for first-stage electrolysis is 100 A, and for the second stage 25 A. At the first stage the initial volume of the sample water is V_0 = 3200 ml, the final volume is V_f = 500 ml; for the second stage V_0 = 500 ml, V_f = 20-50 ml. To supply the electrolyzer we use individual regulating rectifiers of the bridge design with silicon diodes VK-200 with water cooling.

The distillation battery of the second stage consists of five tanks with condensers (volume 1.2 liters), arranged in one thermal block and cooled by running water with flow of not more than 1.2 m^3/h. The power of the heater was 2 kW. The dimensions of the battery are 196 × 360 × 400 mm, the mass is 70 kg.

The distillation battery of the second stage consists of nine tanks with a volume of 100 ml with refrigerators cooled by running water with flow of not more than 1 m^3/h, and a heating block. The dimensions of the batteries are 720 × 200 × 360 mm, the mass is ≈20 kg.

The vacuum arrangement for the synthesis of the counting gas and filling of the proportional counters, built as a single testing unit, consists of the following loops: metallic vacuum system (negative pressure 4.3 Pa) with a loop of pure gas and circulating pumps,† two reactors for the synthesis of gas with an automatic

*In several cases it was necessary to reduce the final volume of electrolysis to 1-2 ml. This was accomplished by using electrolyzers of the third stage which are glass test tubes with electrodes of iron and nickel plates placed in them.

† Pumps are designed and prepared in the Department of Molecular Physics of the IAE im. I. V. Kurchatova.

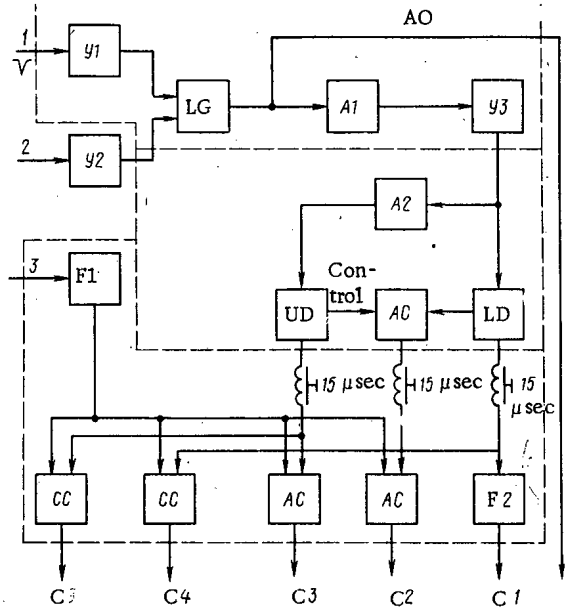

Fig. 3. Schematic of the "Baikal" electronic system: Y1) basis amplifier, amplitude of input signals 1-100 mV, bandwidth 1 kHz-1 MHz, amplification coefficient 30 dB, variation of amplification coefficient 1.5%; Y2) amplifier for muon detector, amplification coefficient 10^3, bandwidth 1 kHz-1 MHz; Y3) auxiliary amplifier, amplification coefficient 30 dB; A1) attenuator, coefficient 0-30 dB; A2) attenuator, coefficient 0-20 dB; UD, LD) upper- and lower-level discriminators, sensitivity 500 mV, accuracy of threshold and window width 2%, stability of threshold over the temperature range from +10 to −35°C 5% for a time not less than 15 h; AC) anticoincidence circuit; CC) coincidence circuit; LG) linear gate, linearity coefficient 2% in the range 0-3 V, stability of transmission coefficient not less than 1%; AO) analyzer output; F1, F2) pulse shapers.

system of regulating the temperature of the reactors, a membrane pump* for the overpumping of gas inside the system, two fore-vacuum pumps VN-461M and four 5-liter containers for storing the hydrogen, carbonic, and synthesized gases. The dimensions of the system are 1500 × 750 × 140 mm, the mass is 360 kg. The consumed power is 3.5 kW.

Methane is used as the counting gas under a pressure to 400 kPa. The concentrated test water is spread out on the zinc, isolated by hydrogen. Then a synthesis of methane is produced by the scheme

$$CO_2 + 4H_2 \rightleftarrows CH_4 + 2H_2O$$

in the presence of a ruthenium catalyst, further

$$2H_2O + 2Zn = 2H_2 + ZnO \text{ etc.}$$

This method of methane synthesis in one stage, demanding not less than a day for its realization, was proposed by Lal [3]. In order to refine the method a corresponding apparatus (Fig. 2) was constructed and prepared, including reactors with two regulating heaters in the upper and lower parts [4]. Plates with zinc powder and a catalyst are placed inside the reactor. By industrial standards, the zinc powder contains up to 15% oxide which prolongs oxidation during storage and rarely reduces its chemical activity. This latter was enhanced by the addition of bromide steel. The control tests showed that the vapor of bromide steel destroys the oxide film, forming zinc bromide permeable to water, which with time is removed from the reaction zone by sublimation. For this part, the powder is 10 wt.% of bromide steel, which provides practically a 100% yield of the synthesis for 5 h during the decomposition of 15-40 ml of tritium-enriched water.

The methane was cleaned with the help of chemical absorbers: from traces of moisture with anhydrous phosphorous, from hydrogen by copper oxide shavings. Having been formed in the secondary reactions, the

*Pumps are designed and prepared in the Department of Molecular Physics of the IAÉ im. I. V. Kurchatova.

TABLE 1. Results of Determining α for the Second Stage of Electrolysis

V_0, ml	V, ml	N_0, counts/min	N, counts/min	$\frac{V_0}{V}$	$\frac{N}{N_0}$	α
500	33,70	10	120,0	14,8	12,0	12,8
500	19,28	10	188,2	26,0	18,8	10,0
500	30,63	10	129,0	16,3	12,9	11,9
500	26,75	10	144,0	18,7	14,4	11,3

oxide of carbon was initially oxidized on copper oxide shavings to dioxide, and carbonic acid gas was absorbed by askarit or by waterless caustic potassium.

The circulation of the gas throughout the absorber is guaranteed by a squeezed greaseless hose with a large square piston, small working stroke and a frequency of 120 strokes/min. The gas in the system is pumped by a vacuum-compressor with a nonstress membrane and pneumatic driving gear. The seal in the counter with 400 kPa of gas is provided for by a residual pressure in the loop of less than 10 kPa.

The detector block with the protective shield was designed to measure ^3H with the help of liquid scintillators which do not require long preparation of the sample. However, the efficiency of such measurements does not exceed 30%, and the background is impossible to reduce below 10 counts/min, and the volume of the sample is limited to several millimeters.

A greater detection efficiency (to 100%) and a large test volume (to 40 ml) at this background level are the primary purpose of the counter of the inner filling. By an analysis of the form of the impulse, the background of the counter may be reduced to several pulses/min. Thus, proportional counters possess a sensitivity an order of magnitude higher than that of liquid scintillators. This determined its selection for a marine measuring complex.

A proportional counter of a volume of 4 liters is used by the marine tritium laboratory. This may be filled to a pressure of 400 kPa. A gold-plated tungsten thread with a diameter of 28 μm served as an anode, the cathode was the external noncontacting body of the counter. The feed of the counter was a pair of two high-voltage rectifiers of type B5-24. Methane was used as the counting gas. The internal isolation of the cathode fluoroplastic ribbon and adjusting ring of plastic prevents leakage during voltage on the cathode up to 3 kW, which allows one to conduct measurements at a counter pressure up to 400 kPa. The counter supplies a charge-sensitive preamplifier collected on two pole transistors IP 303G. The feed of the preamplifier is $\pm$ 12 V, the amplification coefficient is not less than 50. There is a beryllium window for calibration by an external source on the face of the counter. The counter is surrounded by a mercury screen and ringed multiwire proportional chamber filled with a mixture of argon and methane (pressure 50 kPa) that includes, in our design, anticoincidence. The counter, mercury shield, and chamber are found inside the iron external screen with a wall thickness of 20 cm; for this we used radiation-pure materials. The mass of the shielding equipment is 3.5 tons.

Electrical anticoincidence signals from the counter and chamber act on the electric detecting setup "Baikal",* which realized amplitude and temporal selection of pulses and their recording (Fig. 3). Pulses arrive at input 1 from the proportional counter, at input 3 from the anticoincidence shields, and at input 2 as an inhibit signal. The differential discriminators form pulses at the upper and lower levels and also in the "window." A linear gate admits pulses at the input of the discriminators in the absence of a signal at input 2. The design of "Baikal" has 5 counters, the capacity of each being 10^6 counts. The first counter records the pulses exceeding the lower-level discriminator (general counts), the second records all pulses falling in the "window" in anticoincidence with the signals at input 3 (tritium canal). The third counter records all pulses triggering the upper-level discriminator in anticoincidence with input 3 (background from extraneous radioactivity). In the fourth and fifth counters, pulses accumulate which fire the lower-level discriminator in coincidence with input 3 (cosmic background).

Laboratory experiments with marine tritium were conducted in 1976-78 in the Mediterranean Sea and the Scotia Ocean (Southern Ocean). During the time of the experiments with the measuring complex, we ob-

*Electric equipment and detector block are manufactured in SO AS USSR in our technological shop, established on the basis of preliminary experiments of a model of the set-up on ten trips of the RV "Academician Kurchatov." The authors express thanks to all participants of this work.

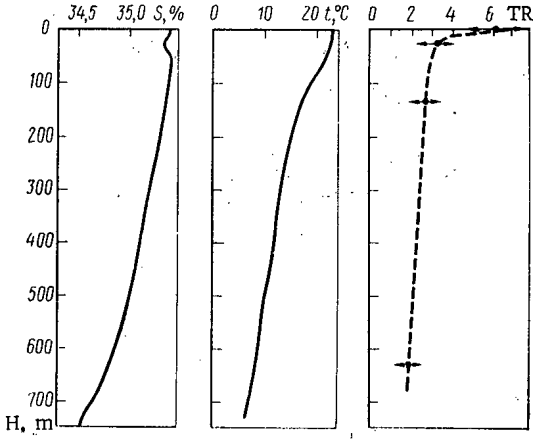

Fig. 4. Salinity distribution, temperature, and tritium ratio (TR) at station No. 3109 in the Southern Ocean.

tained the basic characteristics of the design, the recording characteristics of the detector, the background of the counter, and the coefficients of concentration for tritium samples during all stages of electrolysis.

On the starboard side of the vessel inside the protective shield, the background of the counter during filling to a pressure of 200 kPa was 6.6 counts/min. Assuming an efficiency of 100%, this corresponds to a minimum recorded activity of 150 GBq.

The values of the fractionation coefficient α at the first and second stages were determined by a well-known method of calibrated solutions by the formula

$$N/N_0 = (V_0/V)^{(\alpha-1)/\alpha},$$

where N_0, N and V_0, V are the tritium concentrations and test sample volumes before and after electrolysis.

Experimental results are presented in the table. The mean coefficient of fractionation for the second stage at current of 25 A and a water-cooled temperature of 14°C is equal to 11.5 ± 1.0. Analogously, the value obtained for the first stage of electrolysis at current of 90 A and a cooling water temperature of 14°C is 4.9 ± 0.8. As an example, see Fig. 4, where we present the temperature distribution, salinity, and ^3H concentration for station No. 3109 in the Southern Ocean (20°E, 38°S).

For a radiocarbon analysis of ocean water, a useful method is preparation of a counting gas. However, one should not use "dead" carbon monoxide and hydrogen from water, but instead use carbon monoxide taken from the seawater with a volume of 60-200 liters and hydrogen free of tritium.

Preceeding the selection of a water sample to measure ^3H and ^{14}C using a special bathometer, a vertical band of ocean is analyzed by a developed probe-γ-spectrometer to separate the structure of the water strata and operational depth of sampling at the station. Most promising is the use of a developed system for analysis of the samples with the goal of measuring ^3H and ^{14}C which allows one to measure successfully and economically to fulfill complex long-term programs of studying the world's oceans.

Collaborators at the Laboratory of Nuclear Oceanography TOI DVNTs AN SSSR took an active role in this work: N. A. Vorontsova, V. V. Kobylyanskii, S. B. Zverev, R. M. Amal'skaya, and V. N. Kanchuk.

For the successful operation of the tritium laboratory, the authors are thankful for the great help from the following group of collaborators at all stages of the work, from preparation to the marine experiments at the site: the I. V. Kurchatov Institute for Atomic Energy (I. K. Kikoin, S. S. Yakimov, K. I. Balashov, et al.), the Institute for Nuclear Physics and Experimental Factory SO AN SSSR (A. V. Sidorov, V. M. Aul'chenko, S. E. Baru, et al.), Arctic and Antarctic Scientific-Study Institute (N. P. Smirnov, E. I. Sarukhanyan, et al.), and also the crew of the RV "Professor Bogorov" and "Professor Zubov." The authors are deeply indebted to them all.

LITERATURE CITED

1. H. Craig, Earth Planet. Sci. Lett., 16, 47 (1972).
2. R. Michel and H. Suess, J. Geophys. Res., 80, 4139 (1975).
3. D. Lal and R. Athavale, Proc. Indian Acad. Sci., A63, No. 3 (1966).
4. V. N. Soifer et al., in: Problems in the Study and Use of Water Resources [in Russian], Nauka, Moscow (1972), p. 131.

SOME PHYSICAL CHARACTERISTICS OF FAST REACTORS WITH HETEROGENEOUS CORE GROUPING

E. P. Kunegin, L. N. Yurova,
O. M. Kovalevich, S. D. Yurchenko,
and A. N. Shmelev

UDC 621.039.5

The development and assimilation of fast reactors are linked with finding the best optimum grouping of the core both for the reactor-breeder cycle and for the reactor-converter cycle. The assumption is expressed in [1] that a high-powered fast power-generating reactor with a high breeding factor (BF) can be arranged from several cores (modules) of relatively small dimensions with highly enriched fuel, and located in the breeding zone of metallic uranium. However, in order to achieve this course, in addition to the advantages (high BF) there are also difficulties, e.g., in providing the increased power loading of the fuel, with compensation of the change of reactivity during operation. In [2], the requirements are analyzed for the fuel of such a reactor in order to achieve a sufficiently low specific investment of nuclear fuel in the reactor and in the whole fuel cycle. It is shown that by comparison with reactors with a diluted core of the BN type, the heterogeneous modular reactor in providing the necessary conditions of power release has advantages in both cycles of interest. Within the bounds of the heterogeneously grouped core, there is the possibility of varying its degree of heterogeneity. The question arises as to whether or not the change of the degree of heterogeneity whilst maintaining the neutron spectrum leads to improvement of the physical characteristics.

Breeding Factor. A study of the breeding factor of an individual module with highly enriched fuel and also of an infinite lattice of fuel modules of different dimensions, "linked" to the neutron flux, has shown that in a number of cases a higher breeding factor can be achieved than the BF of the individual module. Table 1 shows the results of a calculation of the cylinderical cells of a lattice of fuel moduli with enriched oxide fuel and sodium coolant (ratio of the volume fraction of the core components $\varepsilon_{fuel}/\varepsilon_{Na}/\varepsilon_{steel} = 0.25/0.5/0.25$ for uranium fuel, and $\varepsilon_{fuel}/\varepsilon_{Na}/\varepsilon_{steel} = 0.45/0.33/0.22$ for mixed uranium–plutonium fuel, isotopic composition of the plutonium $^{239}Pu/^{240}Pu/^{241}Pu/^{242}Pu = 0.62/0.28/0.06/0.04$), distributed in the breeding zone, and containing as the raw material metallic uranium, sodium and steel [2]. The calculations were performed in P_1-transport approximation, using an 18-group catalog of microconstants obtained from the 26-group BNAB-70 library [3], averaged over the integrated neutron fluxes in one-dimensional cylindrical geometry by the M-26 program [4].

It was found that for the compositions of the fuel module being considered and the breeding zone, the transition from the individual module to the even more finely divided lattice of modules "linked" to the neutron flux in almost all cases allows the BF to be increased. With a change of density of the breeding zone and its composition, the relationships may be changed, as a change of ratios of ^{238}U and ν_{eff} of the principal fissile isotope occurs, which mainly also determines the BF. Thus, it follows from the examples considered that the BF can be increased by comparison with a single module and, obviously, only investigations using specific compositions of the fuel modules and of the breeding zone will show the advantages of one or other core grouping from the point of view of achieving a high BF.

Change of Breeding Properties during Burn-Up. The results given in Table 1 of the calculation of the change of reactivity for 10% burn-up of heavy nuclei showed that the reactivity of an isolated fuel module decreases with time. Despite the fact that in the breeding zone more fuel is formed than is burned up in the fuel module, its contribution to the reactivity is insufficient. With the finely divided lattice of fuel modules, the contribution to the reactivity of the fuel which is formed is increased, and with certain characteristic lattice dimensions, to a significant degree it compensates the effect of fuel burn-up in the fuel module. With transition to an almost homogenized medium, the contribution to the reactivity from the fuel which is formed even exceeds the reduction of reactivity in the fuel modules. Thus, in the cases being considered, transition to

Translated from Atomnaya Énergiya, Vol. 49, No. 5, pp. 309-310, November, 1980. Original article submitted June 4, 1980.

0038-531X/80/4905-0755$07.50

TABLE 1. Calculated Characteristics of Fuel Critical Cells with a Metallic Breeding Zone

Parameter	Enrichment							
	Uranium fuel				Uranium–plutonium fuel			
	30 % ^{235}U		90 % ^{235}U		35 % Pu		75 % Pu	
Radius of core, cm	2,5	52	2,5	22	2,5	22,05	2,5	11,9
Thickness of shield, cm	0,42	56	0,17	56	1,23	56	2,74	56
Breeding ratio	1,19	1,08	1,49	1,35	2,31	2,26	2,5	2,57
Change in reactivity, %	+9,7	−9,8	+6,1	−3,1	+18,1	−7,8	+11,2	−5,3

smaller modules linked to the neutron flux, for certain characteristic dimensions of the lattice, allow a small change of reactivity during operation to be provided, which is inherent in fast reactors with a diluted core.

Conclusions. The advantage in the BF of some or other heterogeneous grouping of the core depends on the relation between the dimensions and the composition of the core and the breeding zone.

The heterogeneous grouping of the core of high-powered fast reactors combines the advantages in the BF of reactors with a high-power neutron spectrum and the advantages in change of reactivity during operation and smoothing of the energy release field of high-powered reactors with a diluted core. It may be mentioned that the advantages of heterogeneous grouping are more completely achieved with an increased power loading of the fuel and with deeper burn-ups; this obviously requires the development of fuel elements capable of operating in conditions of increased thermal loads but with a smaller fluence [2].

LITERATURE CITED

1. S. M. Feinberg and O. M. Kovalevich, in: State and Prospects of Work on the Construction of Nuclear Power Stations with Fast Neutron Reactors, COMECON Symposium [in Russian], Vol. 1, Fiz.-Energ. Inst., Obninsk (1968), p. 165.
2. O. M. Kovalevich and E. P. Kunegin, in: Nuclear Reactor Physics [in Russian], No. 5, Atomizdat, Moscow (1977), p. 70.
3. A. P. Abagyan et al., Group Constants for the Calculation of Nuclear Reactors [in Russian], Atomizdat, Moscow (1964).
4. N. S. Nikolaishvili et al., in: COMECON Symposium, op. cit., Vol. 2, p. 75.

MATRIX SCREW DIE METHOD FOR THE CALCULATION OF A COMPLEX LATTICE IN P_3-APPROXIMATION

V. E. Raevskaya and B. Z. Torlin

UDC 621.039.51.12:539.125.52

As shown in [1], the calculation of the neutron distribution inside the multiring slugs of a complex lattice in P_3-approximation can be carried out by means of the matrix folding method. A detailed description of a one-group program for the calculation of square or hexagonal multicells based on this is given in [2].

The results of calculations of complex annular slugs in a heterogeneous lattice by the procedure of [1] and by other procedures [3, 4] have proved to be in good agreement [2, 5]. All comparisons, however, have been carried out for slugs of average blackness. It was obvious that for slugs with black layers, the matrix folding method – which is attractive in its simplicity – is found to be inapplicable. Numerical verification has shown that a significant error arises when the slug has layers with $\Delta/l_a > 3$, where Δ is the thickness of the layer; l_a is the neutron moderation length in it. Analysis of the error of the method of matrix folding has allowed an upper estimate of the relative error to be obtained in a layer with diffusion length L, which was found to be proportional to $\exp(2\Delta/L)$.

We shall consider a method of calculation which is free from this drawback. In its structure it is similar to the matrix screw die method [6] but does not lead to the accumulation of an error. Usually, this method is used for the approximate solution of equations in finite-difference form. In this present paper, it will be used as a stable method for synthesizing the exact solution of the problem in an annular slug, consisting of uniform layers.

In [1, 2], a six-component representation of the vector of the neutron flux density in P_3-approximation is used. We shall find the solution in the form of two three-component vectors φ and j. The components of φ will be, respectively, the first, fourth, and third, and of j – the second, sixth, and fifth components of the previous six-component vector. In this case, for the i-th zone of the n-th slug, the equations

$$\begin{cases} \varphi_{n,i}(r) = \hat{K}^{(1)}_{n,i}(r)\,A_{n,i} + \hat{I}^{(1)}_{n,i}(r)\,B_{n,i} + C^{(1)}_{n,i}(r); \\ j_{n,i}(r) = \hat{K}^{(2)}_{n,i}(r)\,A_{n,i} + \hat{I}^{(2)}_{n,i}(r)\,B_{n,i} + C^{(2)}_{n,i}(r) \end{cases} \tag{1}$$

are valid. The matrices $\hat{I}^{(1)}_{n,i}(r)$ and $\hat{I}^{(2)}_{n,i}(r)$ with size 3×3 are composed of the elements of the first three, and the matrices $\hat{K}^{(1)}_{n,i}(r)$ and $\hat{K}^{(2)}_{n,i}(r)$ of the same size are composed of the other three columns of the matrix $\hat{M}(r)$ of the sixth order given in [1, 2]. In order to formulate the matrix with superscript (1) we shall use the elements of the first, fourth, and third, and for the matrix with superscript (2) – elements of the second, sixth, and fifth lines of the matrix $\hat{M}(r)$.

In Eq. (1), $A_{n,i}$ and $B_{n,i}$ are constant three-component vectors for the i-th zone of the n-th slug, and for the central zones of slugs, $A_{n,1} = 0$. Retaining the nomenclature of [1, 2], we obtain for the source vectors

$$C^{(1)}_{n,i}(r) = l_{n,i}\,\mathrm{col}\,(c_1, c_4, c_3);$$
$$C^{(2)}_{n,i}(r) = l_{n,i}\,\mathrm{col}\,(c_2, c_6, c_5).$$

The matrices formed in this way will have the following important properties:

all elements of the matrices $\hat{I}^{(1)}_{n,i}(r)$ and $\hat{I}^{(2)}_{n,i}(r)$ are proportional to the modified Bessel functions I(r) and will increase with increase of the radius r;

all elements of the matrices $\hat{K}^{(1)}_{n,i}(r)$ and $\hat{K}^{(2)}_{n,i}(r)$ are proportional to the modified Hankel functions K(r) and will decrease with increase of r;

Translated from Atomnaya Énergiya, Vol. 49, No. 5, pp. 310-311, November, 1980. Original article submitted October 22, 1979.

0038-531X/80/4905-0757$07.50

in the zones with weak absorption, only the matrix $\hat{I}^{(2)}_{n,i}(r)$ can be singular.

We shall number the zones of the slugs and the boundaries between them, starting from the center (r_i is the outside radius of the i-th annular zone of the slug). Taking expression (1) into consideration, the following relations of the matrix screw die method can be obtained:

$$\varphi_{n,\,i+1}(r_i) = \hat{E}_{n,\,i+1}\varphi_{n,\,i+1}(r_{i+1}) + \sigma_{n,\,i+1}; \tag{2}$$

$$j_{n,\,i+1}(r_{i+1}) = \hat{\gamma}_{n,\,i+1}\varphi_{n,\,i+1}(r_{i+1}) + D_{n,\,i+1}, \tag{3}$$

where

$$\hat{E}_{n,\,i+1} = \hat{L}^{(1)}_{n,\,i+1}(r_i)\,[\hat{L}^{(1)}_{n,\,i+1}(r_{i+1})]^{-1}; \tag{4}$$

$$\hat{\gamma}_{n,\,i+1} = \hat{L}^{(2)}_{n,\,i+1}(r_{i+1})\,[\hat{L}^{(1)}_{n,\,i+1}(r_{i+1})]^{-1}; \tag{5}$$

$$\begin{aligned}\sigma_{n,\,i+1} = {} & [\hat{K}^{(1)}_{n,\,i+1}(r_i) - \\ & - \hat{E}_{n,\,i+1}\hat{K}^{(1)}_{n,\,i+1}(r_{i+1})]\,[\hat{f}^{(1)}_{n,\,i+1}]^{-1}\alpha_{n,\,i+1} - \\ & - \hat{E}_{n,\,i+1}C^{(1)}_{n,\,i+1}(r_{i+1}) + C^{(1)}_{n,\,i+1}(r_i);\end{aligned} \tag{6}$$

$$\begin{aligned}D_{n,\,i+1} = {} & [\hat{K}^{(2)}_{n,\,i+1}(r_{i+1}) - \\ & - \hat{\gamma}_{n,\,i+1}\hat{K}^{(1)}_{n,\,i+1}(r_{i+1})]\,[\hat{f}^{(1)}_{n,\,i+1}]^{-1}\alpha_{n,\,i+1} - \\ & - \hat{\gamma}_{n,\,i+1}C^{(1)}_{n,\,i+1}(r_{i+1}) + C^{(2)}_{n,\,i+1}(r_{i+1});\end{aligned} \tag{7}$$

$$\hat{L}^{(l)}_{n,\,k}(r) = \hat{f}^{(l)}_{n,\,k}(r) + \hat{K}^{(l)}_{n,\,k}(r)\,[\hat{f}^{(1)}_{n,\,k}]^{-1}\hat{f}^{(2)}_{n,\,k};$$

$$\hat{f}^{(1)}_{n,\,i+1} = \hat{K}^{(2)}_{n,\,i+1}(r_i) - \hat{\gamma}_{n,\,i}\hat{K}^{(1)}_{n,\,i+1}(r_i);$$

$$\hat{f}^{(2)}_{n,\,i+1} = \hat{\gamma}_{n,\,i}\hat{I}^{(1)}_{n,\,i+1}(r_i) - \hat{I}^{(2)}_{n,\,i+1}(r_i);$$

$$\alpha_{n,\,i+1} = \hat{\gamma}_{n,\,i}C^{(1)}_{n,\,i+1}(r_i) - C^{(2)}_{n,\,i+1}(r_i) + D_{n,\,i}.$$

In the center of the slug $\hat{\gamma}_{n,0} = 0$ and $D_{n,0} = 0$,* and all other matrices $\hat{E}_{n,i+1}$ and $\hat{\gamma}_{n,i+1}$, just like the vectors $\sigma_{n,i+1}$ and $D_{n,i+1}$, are calculated successively by means of the recurrent relations (4)-(7), starting from the outside boundary of the first zone and up to outer boundary of each slug r_{out}.

At the outside boundary of all N nonequivalent slugs of the multicell, according to [1, 2], we have

$$\begin{cases}\varphi_n(r_{III}) = \sum\limits_{k=1}^{N}\hat{F}^{(1)}_{n,\,k}A_k + C^{(1)}_n; \quad n = 1, 2, \ldots, N; \\ j_n(r_{III}) = \sum\limits_{k=1}^{N}\hat{F}^{(2)}_{n,\,k}A_k + C^{(2)}_n; \quad n = 1, 2, \cdots, N,\end{cases} \tag{8}$$

where $\hat{F}^{(1)}_{n,k}$ and $\hat{F}^{(2)}_{n,k}$ are matrices with size 3×3 and with elements for which the computation algorithms are described in [2].

From expression (8), by eliminating $A_1, \ldots, A_N$, it is easy to obtain

$$J \equiv \hat{\Gamma}\Phi + D, \tag{9}$$

where

$$\hat{\Gamma} = \hat{F}_2\hat{F}_1^{-1}; \quad D = C_2 - \hat{\Gamma}C_1;$$

$$\Phi = \mathrm{col}\,(\varphi_1, \varphi_2, \cdots, \varphi_N); \quad J = \mathrm{col}\,(j_1, j_2, \cdots, j_N);$$

$$\hat{F}_1 = \{\hat{F}^{(1)}_{n,\,k}\}, \quad F_2 = \{\hat{F}^{(2)}_{n,\,k}\};$$

We form likewise the vector $D_{Sl} = \mathrm{col}\,(D_1, D_2, \ldots, D_n)$ and the diagonal-cellular matrix $\hat{\gamma}_{Sl} = \{\gamma_n\}$, where D_n and $\hat{\gamma}_n$ are the vector and matrix, calculated respectively by means of Eqs. (5) and (7) for the outer boundary of the n-th slug.

Using expressions (3) and (9), we obtain

$$\Phi = (\hat{\Gamma} - \hat{\gamma}_{Sl})^{-1}(D_{Sl} - D). \tag{10}$$

After calculating the neutron flux density Φ at the outer boundary of the slugs, relations (2) and (3) can be used for determining the neutron flux density also at the inner boundaries of the zones. Since in the overwhelm-

*We note that $[\hat{K}^{(2)}_{n,\,1}(0)]^{-1} = 0$ and $\hat{I}^{(2)}_{n,\,1}(0) = 0$.

ing majority of cases interest lies only in the first component of the vector φ (zero harmonic), an appreciable economy of computer memory can be achieved by not storing the matrix $\hat{\gamma}_{n,i}$ and the vector $D_{n,i}$ completely. In order to calculate the first component of the vector j (first harmonic, used for determining the average neutron fluxes in the zones [1, 2]) it is sufficient to store only the first lines of the matrices $\hat{\gamma}_{n,i}$ and the first components of the vectors $D_{n,i}$.

The matrix screw die of the vectors $A_{n,i}$ and $B_{n,i}$ can be limited by a procedure identical to that explained. Although in order to obtain the same information about the neutron flux density distribution over the slugs, it is necessary to store appreciably larger bulks of matrices, in some cases (e.g., in order to determine the average neutron fluxes in zones without absorption) this limitation of the computational processes can be justified.

After generating the first version of the program for calculating the complex lattice in P_3-approximation by the matrix screw die method, it was found possible to carry out the calculations of multicells with slugs containing layers with a high ratio of Δ/l_a. In order to verify the procedure and to estimate the errors due to the assumed approximations, in particular, the results of the calculation of a uniform lattice with multilayered slugs in P_3-approximation and the calculation of the effective cell with the same slug by the integral equation method [7] were compared. It was found that even in a slug washed from both sides with water with an absorbing layer with $\Delta/l_a \approx 5$, the maximum divergence in the neutron distributions did not exceed 15% and it occurred in the zone with weak absorption. The error in the determination of the thermal neutron utilization factor amounted to a total of 0.12%.

The program was written in FORTRAN language for the BÉSM-6 computer. The calculation time for a single version was ~20 sec for double lattices of uniform slugs, and ~40 sec for double lattices of 30-zone slugs. The maximum time of ~4 min is required for the calculation of the multicell with size 8 × 8, containing 20 nonequivalent 30-zone slugs of twenty kinds.

LITERATURE CITED

1. A. D. Galanin and B. Z. Torlin, At. Energ., 36, 2, 125 (1974).
2. V. E. Raevskaya and B. Z. Torlin, Preprint Institute of Theoretical and Experimental Physics No. 60 (1977).
3. V. V. Smelov, At. Energ., 33, 5, 915 (1972).
4. Ya. V. Shevelev (ed.), Methods of Calculating Thermal Neutron Fields in Reactor Lattices [in Russian], Atomizdat, Moscow (1974).
5. A. D. Galanin, V. V. Smelov, and B. Z. Torlin, At. Energ., 37, 1, 76 (1974).
6. G. I. Marchuk and V. I. Lebedev, Numerical Methods in Neutron Transport Theory [in Russian], Atomizdat, Moscow (1971).
7. A. Ya. Burmistrov and B. P. Kochurov, Preprint Institute of Theoretical and Experimental Physics No. 49 (1976).

INVESTIGATION OF THE RATE OF GROWTH OF A FATIGUE CRACK IN STRUCTURAL STEELS

L. A. Vainer and V. F. Vinokurov

UDC 620.171

When investigating modern methods of assessing the efficiency of structures under conditions of cyclic loading, it is necessary to know the mechanisms of development of fatigue cracks. The first investigations of the kinetics of fatigue crack development in irradiated low-strength steels of foreign manufacture showed that as a result of neutron irradiation – causing significant changes of the strength and plasticity characteristics – the rate of growth of cracks is essentially unchanged [1]. At the same time, for irradiated cylindrical samples of high-strength steel with an annular notch of the types 12KhN3MFA and 10KhSND, a marked increase of the rate of growth of the crack was established [2]. The results do not agree and they are difficult to compare, in consequence of the complexity of the procedure for investigating the kinetics of growth of a fatigue crack in irradiated materials. It is of definite interest, therefore, to establish a correlation between the results of tests of samples with cyclic and static loading.

As the material for the investigations, steels 12KhN3MFA and 15Kh3MFA were chosen, and steel 15Kh3MFA was investigated in two states differing in tempering temperature, which ensured a different level of strength. Compact samples were investigated by eccentric tension. The thickness of the steel 15Kh3MFA samples was 16 mm, and of the steel 12KhN3MFA – 10 mm. These samples were irradiated in the core of the VVR-M research reactor (see Table 1). The samples were tested on a special remote-control hydraulic machine by means of pulsating tension at room temperature with a frequency of 3-5 cycles/min [3]. During the tests, a diagram was plotted of the load vs expansion of the crack, which allowed the length of the crack to be determined by an experimentally established calibration graph of sample pliability vs length of crack.

The results of the tests, processed in accordance with Paris's expression [4]

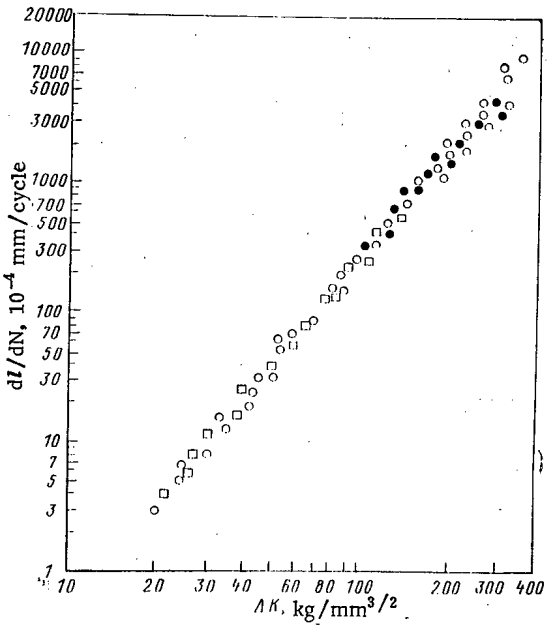

Fig. 1. Relation between the rate of growth of the crack and ΔK for steel 15Kh3MFA: ○, □) tempered at 690 and 620°C; ●) tempered at 690°C, irradiation up to a fluence of $1 \cdot 10^{19}$ neutrons/cm^2 at 120 ± 10°C.

Translated from Atomnaya Énergiya, Vol. 49, No. 5, pp. 311-313, November, 1980. Original article submitted November 5, 1979.

0038-531X/80/4905-0760$07.50

TABLE 1. Mechanical Properties of the Steels Investigated

Material	Fluence, neutrons/cm²	$\sigma_{0.2}$, MPa	$\sigma_в$, MPa	δ_5, %	$\Psi_к$, %	σ_H^{max}, MPa·m
12KhN3MFA	—	940	990	17	75	110
tempered at 670°C	$1 \cdot 10^{20}$	1240	1260	4	27	40
15Kh3MFA	—	560	700	20	73	180
tempered at 690°C	$1 \cdot 10^{19}$	730	820	17	65	170
15Kh3MFA tempered at 620°C	—	965	1050	17	65	100

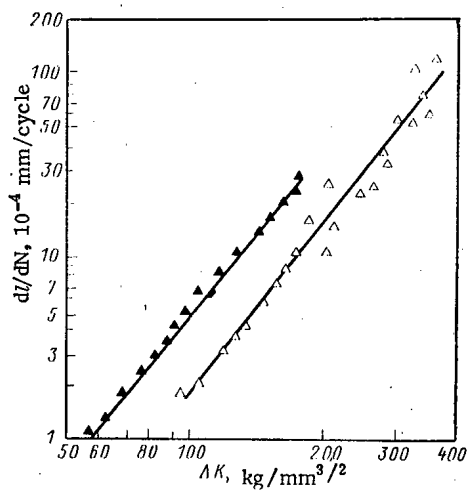

Fig. 2. Relation between rate of growth of the crack and ΔK for steel 12KhN3MFA, when irradiated up to a fluence of $1 \cdot 10^{20}$ neutrons/cm² at 200°C (▲) and without irradiation (△).

$$dl/dN = C(\Delta K)^m \qquad (1)$$

(here ΔK is the spread of the stress intensity factor during the cycle; l is the length of the fatigue crack; and C and m are coefficients) are given in Figs. 1 and 2. It can be seen from the data given that a change of both the tempering temperature and the neutron irradiation up to a fluence of $1 \cdot 10^{19}$ neutrons/cm² at 120 ± 10°C leaves the rate of growth of the fatigue crack in steel 15Kh3MFA almost unchanged. At the same time, neutron irradiation up to a fluence of $1 \cdot 10^{20}$ neutrons/cm² at approximately 200°C increased the rate of growth of the fatigue crack in steel 12KhN3MFA. It follows from the data given in Fig. 2 that irradiation has led to a parallel shift of the dl/dN vs ΔK curve to the side of higher values of dl/dN, which corresponds to an increase of C without a significant change of the index m.

Some irradiated and unirradiated samples were tested by static tension at room temperature and a speed of movement of the clamp of 0.1-0.2 mm/min. Values of I_c were determined – the energy necessary to increase the crack at the instant of the start of its increase [5]. In accordance with Paris's procedure [6]

$$I_c = \alpha A/F, \qquad (2)$$

where A is the energy absorbed by the system sample–testing machine at the instant of start of growth of the crack; α is a coefficient; and F is the net cross section of the sample. The value of A is determined by planimetric measurement of the hatched region of the diagram of the load vs movement of the moving clamp, bounded along the axis of abscissa by the value Δ_c, corresponding to the start of growth of the crack (Figs. 3, 4).

It follows from analysis of the data given that the value of I_c for steel 15Kh3MFA was unchanged with

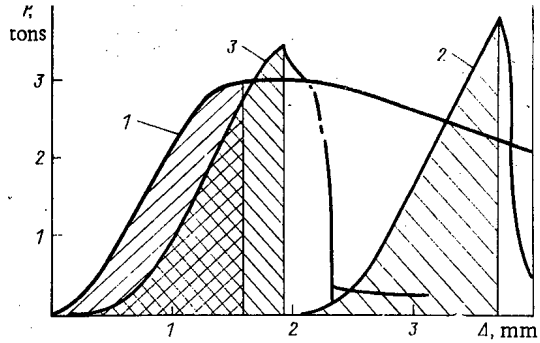

Fig. 3. Diagram of the load vs movement of the moving clamp for samples of steel 15Kh3MFA at 20°C: 1, 2) without irradiation, tempered at 690 and 620°C, respectively; 3) tempered at 690°C, irradiated up to a fluence of $1 \cdot 10^{19}$ neutrons/cm^2 at 120 ± 10°C.

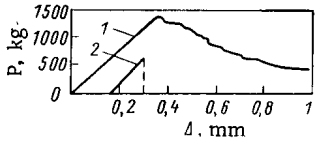

Fig. 4. Diagram of load vs movement of moving clamp for samples of steel 12KhN3MFA at 20°C without irradiation (1) and with irradiation (2) up to a fluence of $1 \cdot 10^{20}$ neutrons/cm^2 (~200°C); P is the load.

both change of tempering temperature and neutron irradiation up to a fluence of $1 \cdot 10^{19}$ neutrons/cm^2 at 120 ± 10°C. At the same time, neutron irradiation up to a fluence of $1 \cdot 10^{20}$ neutrons/cm^2 at 200°C led to an appreciable reduction of I_c for steel 12KhN3MFA.

In comparing the data of the rate of growth of a fatigue crack with the results of the tests on static tension, a relation was established between the resistance characteristics to the development of the crack during static and cyclic loading. Neutron irradiation of steel 12KhN3MFA, having caused a reduction of I_c by a factor of 5.8 (see Fig. 4), led to an increase of the rate of growth of the fatigue crack by a factor of 2.4 (see Fig. 2). Thus, it may be supposed that the coefficient C in (1) is inversely proportional to $\sqrt{I_c} = K_c$, where K_c is the stress intensity coefficient at the start of unstable spreading of the crack, serving as the viscosity index of failure of the material with the thickness being tested.

A similar relation follows from Forman's expression [7]:

$$dl/dN = C_1 \Delta K^m/[(1 - R) K_c - \Delta K], \quad (3)$$

where R is the coefficient of asymmetry of the cycle.

Thus, the results of the tests by static tension can be used for an approximate estimate of the effect of neutron irradiation on the rate of growth of a fatigue crack in structural steels.

LITERATURE CITED

1. P. Shakhinyan et al., Am. Soc. Engineers–Mechanics, Ser. D, 96, No. 4, 1 (1974).
2. V. F. Vinoburov and A. V. Vasil'chenko, Problems of Nuclear Science and Technology. Ser. Physics of Radiation Damage and Radiation Metal Behavior [in Russian], No. 1 (6) (1978), p. 36.
3. L. A. Vainer et al., At. Énerg., 45, 2, 137 (1978).
4. J. Irvine and P. Paris, in: Failure, Vol. 3 [Russian translation], Mir, Moscow (1976).
5. G. S. Pisarenko, V. P. Naumenko, and G. S. Volkov, in: Determination of the Crack Resistance of Materials, Based on the Energy Contour Integral [in Russian], Naukova Dumka, Kiev (1978), p. 6.
6. J. Rice, Trans. ASME, J. Appl. Mech., 35, 379 (1968).
7. R. Forman, V. Kearney, and R. Engle, Trans. ASME, Ser. D, 89, 3, 339 (1967).

SENSITIVITY ANALYSIS IN STUDY OF LAWS GOVERNING RADIATION DISTRIBUTION ACCORDING TO MONTE CARLO DATA

A. M. Zhezlov, A. I. Ilyushkin, V. A. Klimanov, V. P. Mashkovich, and D. N. Rybin

UDC 539.166.2:519.283

The study of the general physical laws governing radiation transfer according to the data of direct calculations by the Monte Carlo method entails a number of difficulties, the main one being the complexity of analysis of the results obtained with appreciable statistical errors, which are particularly large in one-dimensional problems of deep penetration. These difficulties can be overcome by using the method of analysis of the sensitivity of the calculation results to the initial parameters of the problem [1, 2]; this method is based on the application of a dependence of the relative sensitivity of some linear functional R of the radiation field (e.g., dose, heat release, etc.) to some initial parameters X_i (interaction cross section, functions specifying the source, etc.) which are found in general form from [1, 2]

$$p(X_i)=\frac{\delta R/R}{\delta X_i/Y_i}, \tag{1}$$

where δR is the variation of the result with the variation δX_i. In the case of independent δX_i the deviation of the result R with an error to quantities of second-order smallness is of the form

$$\delta R=R\sum_{i=1}^{n} p(X_i)(\delta X_i/X_i). \tag{2}$$

In the Monte Carlo method the procedure used most for calculating the functions $p(X_i)$ has been that of correlated sampling [3], which at times proves to be rather ineffective because of the considerable computer time expended. Analysis of the distinctive features of the Monte Carlo method makes it possible to suggest a general and quite simple way of calculating the functions $p(X_i)$. The essence of this way can be explained by considering the example of analysis of the sensitivity to a source whose perturbation $\delta S(X_i, \xi)$ is given in piecewise-constant form:

$$\frac{\delta S(X_i,\xi)}{S(X_i,\xi)}=\begin{cases}\Delta(X_i) & \text{for } \xi\in\theta_i;\\ 0 & \text{for } \xi\notin\theta_i,\end{cases}$$

where ξ is a point in the studied region of phase space (e.g., an energy group in a spectrum), and $\Delta(X_i)$ is any function specifying the magnitude of the perturbation.

On the basis of the general theory [1, 2, 4], taking account of the last expression for the function of relative sensitivity to the source, we get

$$p_s(X_i,\theta_i)=\frac{1}{R}\int_{\theta_i}\Phi^*(\xi)S(X_i,\xi)\,d\xi,$$

where the integral is the contribution to the functional in question from particles emitted by the source in the region θ_i; this source is taken into account with the conjugate function $\Phi^*(\xi)$. This integral can be calculated by differentiating the contributions to the respective "pockets" of a detector during calculation of the contribution to the detector, e.g., from the initial energy of the particles (from the coordinate or angle of emission from the source), which makes it possible then to get the energy (spatial or angular) dependence of the relative sensitivity to the source. From the last expression there clearly is a possibility of estimating the value function $\Phi^*(\xi)$ on the basis of the results of direct calculations.

Translated from Atomnaya Énergiya, Vol. 49, No. 5, pp. 313-315, November, 1980. Original article submitted December 11, 1979; revision submitted June 23, 1980.

0038-531X/80/4905-0763$07.50

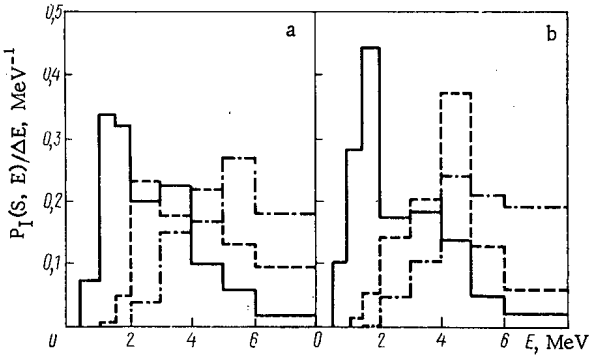

Fig. 1. Energy dependences of relative sensitivities of energy flux density of scattered γ rays to the assignment of a point isotropic source with a fission spectrum in a homogeneous air medium of density 1.225 kg/m^3 (a) and near the air–earth interface for H_S = 10 m (b) at a distance of 0.5 (——), 1.5 (– – –), and 2.5 (–·–·–) km.

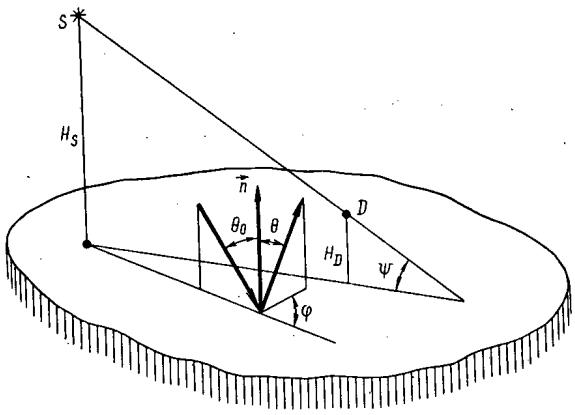

Fig. 2. Geometry of problem and diagram for reckoning angles for reflection of quanta from earth.

To illustrate the possibilities of sensitivity analysis and of the proposed method of calculating $p(X_i)$ let us consider some results of its implementation within the framework of a local estimate with a shift of range by an improved variance-minimizing technique (MDB method [5]) as applied to the practically important problem of transfer of γ rays from a point isotropic source with a fission spectrum [6] in a uniform air medium and near the air–earth interface to distances of up to 3500 kg/m^2. Analysis of various dependences of the relative sensitivity makes it possible to formulate laws of radiation transfer near to and far from the earth. With an increase in the distance an increase is observed in the energy of the quanta which make the main contribution to the principal functionals of the field of scattered radiation (Fig. 1); this can be used for significant sampling of the exit energy of quanta from the source. The main contribution to the complete functionals of the field from those quanta which interact with the earth is made by quanta which collide once with the earth. Their contribution (up to 22% of the energy flux density) is an order of magnitude or more greater than the contributions from quanta with more reflections from the earth. For all of the considered values of the source height H_S ($0.01 \leq H_S \leq 1$ km with a fixed detector height H_D = 1 m) the total contribution of scattered radiation is determined in the main by quanta scattered at low angles relative to the source–detector direction (Figs. 2, 3). With variation of H_S and a fixed distance from source to detector, the quanta determining the contribution of the radiation scattered by the earth have a characteristic angle of incidence, roughly equal to $\pi/2 - \Psi$ and correlating with the polar θ and azimuthal φ angles of reflection. Reflection of the decisive contribution from quanta at low depression angles Ψ (see Fig. 2) occurs in the plane of incidence and at an angle of 90° (see Fig. 3). For $\sin \Psi \leq 0.1$ the sensitivity to the angular parameters of the albedo is markedly anisotropic, while the principal functionals of the flux density of the scattered radiation are 2-3 times smaller

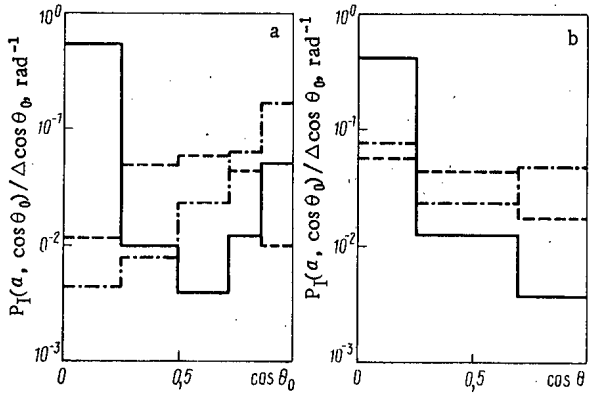

Fig. 3. Relative sensitivity of energy flux density of scattered γ rays to albedo of earth: a) as function of angle θ_0 of incidence of quanta on earth and b) as function of polar angle θ of reflection of quanta by earth, for sin Ψ = 0.1 (——), 0.4 (– – –), and 1.0 (–·–·–).

than for a homogeneous medium. With an equidistant elevation of the source these functionals grow rapidly and for sin $\Psi > 0.4$ coincide within the limits of computational error with the data for a homogeneous medium, starting from a distance ~500 m.

The results are distinguished by clarity and make it possible to clearly isolate the significant parameters in the approximation of the functionals. For example, the intensity of the γ rays scattered at the interface, $I_{int}(R, \Psi)$, can be related to within 15-20% to the intensity $I_\infty(R)$ in an infinite air medium:

$$\frac{I_{int}(R, \Psi)}{I_\infty(R)} = 1 - A(R) \exp(-B \sin \Psi),$$

where the coefficient B ≈ 5 while coefficient A varies little within the limits 0.4-0.65 as R varies from 0.5 to 2.5 km in air with a density of 1.225 kg/cm^3.

LITERATURE CITED

1. H. Goldstein, in: Proc. Fourth Intern. Conf. on Reactor Shielding, OECD, Paris (1973), p. 1332.
2. E. Oblow, General Sensitivity Theory for Radiation Transport, ORNL-TM-4110 (1973).
3. H. Steinberg, Correlated Sampling and Its Implementation in the SAMCEP Code, ORNL-RSIC-33 (1971), p. 161.
4. V. V. Bolyatko et al., in: Problems of Dosimetry and Radiation Protection [in Russian], No. 19, Atomizdat, Moscow (1980), p. 109.
5. V. A. Klimanov et al., Propagation of Ionizing Radiation in Air [in Russian], Atomizdat, Moscow (1979), p. 27.
6. F. Maienschein, Engineering Compendium of Radiation Shielding, Vol. 1, Springer-Verlag (1968), p. 76.

ENERGY SPECTRA OF NEUTRON RADIATION FROM SPENT FUEL OF VVÉR REACTOR

N. S. Shimanskaya

UDC 539.12...126.5:621.039.52.44

The estimation in [1] of the yields of spontaneous-fission and (αn) neutrons for the individual nuclides forming part of the spent fuel of VVÉR (water-moderated water-cooled power reactors) permits the energy spectrum of the neutron radiation from this fuel to be calculated.

It is known that the spectra of neutrons from spontaneous fission as well as neutrons from (αn) reactions usually differ significantly. The spectra of fission neutrons are roughly the same for all fissionable nuclides, have a maximum at 0.8-1 MeV, and have a distribution "tail" extending to 12-15 MeV. The shape of (αn)-neutron spectra depends on the energy of the α-particles and the location of the energy levels of the compound nucleus and the product nucleus and can vary between quite wide limits.

The spectrum of neutrons from the (αn) reaction in oxygen is relatively soft, with a maximum in the region 2.5-3.0 MeV and an upper limit not exceeding 5 MeV. The mean energy of this spectrum ($\bar{E}_n$ = 2.4-2.8 MeV, depending on the α-nuclide) is appreciably higher than for the spectrum of fission neutrons. The theoretical form of the spectrum, calculated in [2] with allowance for the relation of the partial cross sections of the $^{18}O(\alpha n)^{21}Ne$ reaction with transition to the ground and first three excited levels of ^{21}Ne and for the contribution of neutrons from the $^{17}O(\alpha n)^{20}Ne$ reaction, is in agreement with the experimentally measured neutron spectra for oxide compounds of α-emitters.

The energy spectra of the neutron radiation of spent fuel of the VVÉR reactor with an initial ^{235}U enrichment α_5^0 = 3% were calculated at various levels of fuel burn-up and various cooling times after unloading from the reactor. The spectra of neutrons from the spontaneous fission of ^{240}Pu and ^{244}Cm and the spectra of neutrons from (αn) reactions in oxygen at E_α = 5.49 MeV (^{238}Pu), E_α = 5.80 MeV (^{244}Cm), and E_α = 6.10 MeV (^{242}Cm) served as "reference" spectra. The calculations were carried out with experimental data on the isotopic composition of spent fuel from VVÉR-365 and VVÉR-440 reactors [3, 4].

The calculations showed that the energy spectra of neutrons from spent UO_2 fuel change substantially as the burn-up of the fuel increases. Figure 1 gives the normalized spectra of the neutron radiation of fuel with α_5^0 = 3% and a burn-up w = 10-35 kg/ton U. It is seen that as the burn-up fraction increases, the neutron spectrum "softens" and its shape approaches that of the fission-neutron spectrum. This is due to the growth of the relative contribution of ^{244}Cm to the neutron yield of the fuel as it burns up.

The shape of the spectrum of neutron radiation from spent fuel should also change considerably when the fuel is cooled after being removed from the reactor. Table 1 gives the values of $Y_n^{(SF)}$ and $Y_n^{(\alpha n)}$ for fuel with a burn-up w = 30 kg/ton U, characterizing the change in the yields of neutrons from spontaneous fission (SF) and neutrons from (αn) reactions in oxygen as a function of the cooling time. As seen from Table 1, at first, i.e., for the first 5 yr, there is a decrease in the contribution from (αn) neutrons, this being due mainly to the decay of ^{242}Cm. With further cooling, this contribution increases slightly owing to the accumulation of ^{238}Pu and ^{241}Am and decay of ^{244}Cm in the fuel.

TABLE 1. Dependence of $Y_n^{(SF)}$ and $Y_n^{(\alpha n)}$ on Cooling Time of Spent Fuel

t_{cool}, yr	$Y_n^{(SF)}$, %	$Y_n^{(\alpha n)}$, %	t_{cool}, yr	$Y_n^{(SF)}$, %	$Y_n^{(\alpha n)}$, %
0	83,0	17,0	3	96,2	3,8
1	90,3	9,7	5	96,0	4,0
2	94,9	5,1	10	95,6	4,4

Translated from Atomnaya Énergiya, Vol. 49, No. 5, pp. 315-316, November, 1980. Original article submitted December 17, 1979.

0038-531X/80/4905-0766$07.50

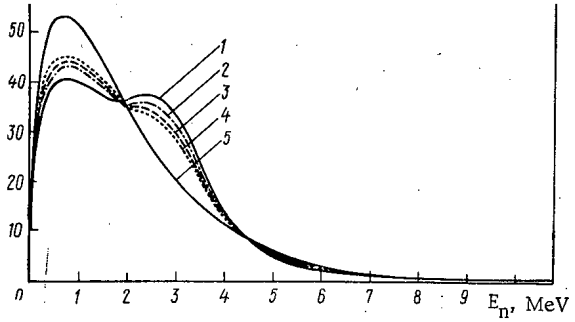

Fig. 1. Energy spectra of neutron radiation of spent VVER fuel (α_5^0 = 3%) at various levels of burn-up w, kg/ton U: 1) 10 ($\bar{E}_n$ = 2.19 MeV); 2) 20 ($\bar{E}_n$ = 2.17 MeV); 3) 30 ($\bar{E}_n$ = 2.14 MeV); 4) 35 ($\bar{E}_n$ = 2.13 MeV); 5) spectrum of ^{244}Cm fission neutrons ($\bar{E}_n$ = 2.03 MeV).

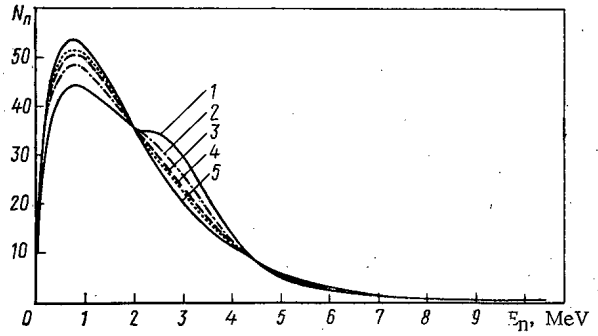

Fig. 2. Variation of energy spectrum of neutron radiation of spent VVER fuel (α_5^0 = 3%, w = 30 kg/ton U) as a function of t_{cool}, yr: 1) 0 ($\bar{E}_n$ = 2.14 MeV); 2) 1 ($\bar{E}_n$ = 2.10 MeV); 3) 2 ($\bar{E}_n$ = 2.07 MeV); 4) 3 ($\bar{E}_n$ = 2.04 MeV); 5) spectrum of ^{244}Cm fission neutrons ($\bar{E}_n$ = 2.03 MeV).

Figure 2 illustrates the variation of the shape of the neutron spectrum of spent UO_2 fuel with w = 30 kg/ton U as a function of the fuel-cooling time after unloading from the reactor. It is seen from Fig. 2 that as t_{cool} increases, the spectrum softens, the mean energy $\bar{E}_n$ of the spectrum decreases, and starting from t_{cool} = 3 yr the spectrum practically coincides with the spectrum of ^{244}Cm spontaneous-fission neutrons.

The energy spectra given in [5] for two different values of the burn-up of UO_2 fuel and t_{cool} = 163 days were calculated by using incorrect values for the specific yields of (αn) neutrons for $^{242}CmO_2$ and $^{242}CmO_2$, as a result of which the energy range 2-4 MeV corresponding to neutrons from the (αn) reaction in oxygen proved to be roughly overestimated by a factor of two. Moreover, the paper does not indicate the kind of fuel, that of a PWR or a BWR, to which the spectra correspond or what the initial enrichment of the fuel was.

The results obtained in the present paper may be of interest in design work on transport containers, the design of spent-fuel storage facilities and radiation protection, as well as in the estimation of the appropriate doses of neutron radiation in various media.

LITERATURE CITED

1. N. S. Shimanskaya, At. Energ., 49, No. 5, 316 (1980).
2. M. Taherzadeh and P. Gingo, Nucl. Technol., 15, No. 3, 396 (1972).
3. V. Ya. Gabeskiriya, V. V. Gryzina, et al., At. Energ., 44, No. 5, 446 (1978).
4. T. P. Makarova et al., in: Zwei Tagung Nukleare Analysenverfahren (Dresden, 1979), Preprints der Vorträge und Posberbeiträge, Dresden (1979), p. 212.
5. H. Bailey et al., Nucl. Technol., 17, No. 3, 217 (1973).

NEUTRON RADIATION YIELD OF SPENT FUEL OF VVÉR REACTOR

N. S. Shimanskaya

UDC 539.12...126.5:621.039.52.44

On the basis of experimental data on the isotopic composition of spent fuel from VVÉR-365 and VVÉR-440 reactors [1, 2] calculations were made of the expected yield of neutron radiation from this fuel at various levels of burn-up and various cooling times after unloading from the reactor.

It is known that when uranium oxide fuel is used the source of neutrons consists of the (αn) reaction in oxygen and the spontaneous fission (SF) of nuclides of heavy elements accumulated in the fuel under irradiation. In the paper we calculate the partial yields of (αn) and SF neutrons for the main components of UO_2 fuel: $^{235,238}U$, ^{236}U, ^{237}Np, $^{238-242}Pu$, $^{241,243}Am$, and $^{242,244}Cm$. The values of the specific yields of SF neutrons and the specific α-activity of the nuclides were taken from [3] where they had been calculated on the basis of the respective estimated half-lives $T_{1/2}(SF)$ and $T_{1/2}(\alpha)$. The yield of (αn) neutrons for the individual nuclides was found from a semiempirical formula [4] relating the yield of neutrons from the (αn) reaction in oxygen and the energy of the α-particles; the formula was converted for a UO_2 target.

Table 1 gives the values of the total neutron radiation yields Y_n ($Y_n = Y_n^{(SF)} + Y_n^{(\alpha n)}$) of the spent fuel for various levels of burn-up w (w = 10-35 kg/ton U) and various cooling times (t_{cool} = 0-10 yr). The change in Y_n with an increase in the burn-up fraction w in the indicated range of burn-up values for freshly withdrawn fuel ($t_{cool} = 0$) corresponds to the relation $Y_n \sim w^{3.2}$. For the cooled fuel the exponent is somewhat higher and varies within the limits 3.2-3.9 for t_{cool} = 0-10 yr.

The contributions to the neutron yield from individual nuclides and the variation of the ratio of these contributions with the variation of the fuel burn-up fraction and cooling time are shown in Fig. 1 for fuel with a burn-up of 20 and 30 kg/ton U. The most significant contribution at $t_{cool} = 0$ is made by ^{242}Cm. When the burn-up increases from 10 kg/ton U to 35 kg/ton U the contribution from this nuclide drops from 87 to 60% with a corresponding increase in the relative contribution of ^{244}Cm neutrons. At burn-up levels exceeding 15 kg/ton U, precisely ^{242}Cm and ^{244}Cm determine the intensity of the neutron radiation from the spent fuel of a VVÉR reactor. At lower burn-ups a noticeable contribution is made by plutonium isotopes, primarily ^{240}Pu

TABLE 1. Dependence of Y_n of Spent VVÉR Fuel ($\alpha_5^0 = 3\%$) on the Fuel Burn-Up and Cooling Time, neutrons/sec · kg U, $\times 10^5$

w, kg/ton U	t_{cool}, yr					
	0	1	2	3	5	10
10	0,156	0,0481	0,0253	0,0204	0,0189	0,0182
20	1,69	0,664	0,434	0,376	0,347	0,301
25	3,36	1,40	0,960	0,844	0,796	0,665
30	5,62	2,49	1,81	1,62	1,47	1,23
35	8,51	4,36	3,38	3,08	2,82	2,34

Translated from Atomnaya Énergiya, Vol. 49, No. 5, pp. 316-317, November, 1980. Original article submitted December 17, 1979.

0038-531X/80/4905-0768$07.50

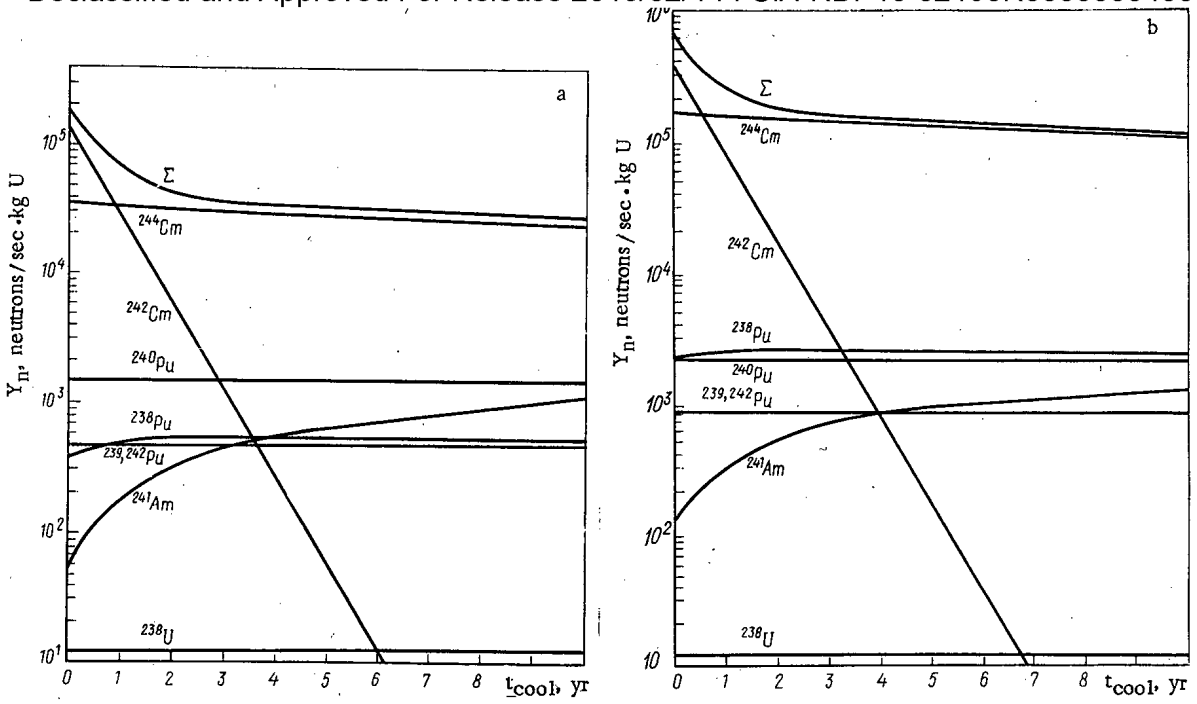

Fig. 1. Plots of the total neutron yield Y_n and partial contributions to it from individual nuclides as function of cooling time for spent VVÉR fuel with initial enrichment $\alpha_5^0 = 3\%$ and burn-up fraction w = 20 (a) and 30 (b) kg/ton U.

(up to 4% at w = 10 kg/ton U) as well as ^{238}Pu and ^{239}Pu. Usually, upon conclusion of a run (w = 30-35 kg/ton U) the total contribution from these isotopes as well as from the isotopes of U, Np, and Am does not exceed 1%.

As the fuel-cooling time grows longer the ratio of the contributions of neutron radiation from the individual nuclides, as follows from Fig. 1, changes substantially. After cooling for three or four years the neutron radiation of the spent UO_2 fuel with a burn-up level w ≈ 20-35 kg/ton U is determined to an extent of more than 90% by the ^{244}Cm spontaneous-fission neutrons.

The accuracy of the Y_n estimates, 15-20%, is limited by the error of burn-up determination in [1, 2] and the correctness of the correlations established there between the burn-up and isotopic composition of the fuel. The results of similar calculations carried out for the water-moderated water-cooled reactors Yankee-Rowe [5] and TRINO [6] attest to the same character of $Y_n(w)$ dependences for reactors of this type. Some discrepancy between our data and the data of [6], pertaining to the values of the neutron yields, the ratios of the partial contributions from the individual nuclides, and the shapes of the $Y_n(w)$ curves for cooled fuel, is apparently due mainly to the difference in the initial enrichments of the fuel and the energy spectra of neutrons of the reactor core for various reactors. The results of [5] are given in a form which does not allow them to be compared directly with our data. The use in that paper of incorrect values of the specific yields of (αn) neutrons for $^{242}CmO_2$ and $^{244}CmO_2$ resulted in a substantial overestimation of Y_n (up to 30-50% or more), especially at short cooling times and low burn-ups, when the ^{242}Cm contribution is large.

The data obtained in the present paper can be used to predict the expected level of neutron radiation from spent fuel elements and fuel assemblies of VVÉR reactors. It is necessary, naturally, to know the burn-up distribution over the height and diameter of the fuel elements and fuel assemblies. Account must also be taken of the neutron-multiplication effect which can appreciably increase the neutron yield, especially when use is made of containers constructed of hydrogen-containing materials or with water cooling as well as when fuel is stored in ponds. The $Y_n(w, t_{cool})$ relations established may also prove useful in the development of neutron methods of passive nondestructive analysis of spent nuclear fuel.

LITERATURE CITED

1. V. Ya. Gabeskiriya et al., At. Energ., 44, No. 5, 446 (1978).
2. T. P. Makarova et al., in: Zwei Tagung Nukleare Analysenverfahren (Dresden, 1979), Preprints der Vorträge und Posterbeiträge, Dresden (1979), p. 212.
3. N. S. Shimanskaya, "Nuclear constants of transactinide isotopes of the fuel cycle," Preprint No. RI-70, Leningrad (1978).
4. G. V. Gorshkov et al., Natural Neutron Background of Atmosphere and Earth [in Russian], Atomizdat, Moscow (1966).
5. H. Bailey et al., Nucl. Technol., 17, No. 3, 217 (1973).
6. S. Hsue, At. Energy Rev., 16, No. 1, 89 (1978).

STEAM ENTRAINMENT IN THE DOWNCOMING ZONE OF A CIRCULATION LOOP

L. N. Polyanin, A. L. Putov, and A. V. Efimov

UDC 621.039.52.44

In determining the hydraulic characteristics of the circulation loop of boiling-water-type reactors, the entrainment of steam in the downcoming branch of the loop is customarily referred to as the entrainment coefficient. It is defined as the ratio of the mass flow rate of steam through the downcoming inlet cross section $G_s^{dc.s}$ to the total flow rate of steam through the outlet cross section of the uptake (driving) section $G_s^{dr.s}$, i.e., $\Psi = G_s^{dc.s}/G_s^{dr.s} = X_{dc.s}/X_{dr.s}$, where $X_{dc.s}$ and $X_{dr.s}$ are the corresponding values of the steam mass flow rates.

Figure 1 shows a diagram of the loop with natural circulation of the heat carrier in a setup used for studying the entrainment of steam [1-3]. Depending on the operational regime of the setup, both the usual circulating entrainment (if the average velocity of the liquid phase in the entrainment zone is greater than the velocity of the steam bubbles toward the surface) as well as the "suspended" or "apparent" entrainment, which is related to the radial nonuniformity in the velocity of the liquid phase in the downcoming zone of the circulation loop, can occur.

Semiempirical relations for the velocity of individual gas bubbles toward the surface [4] cannot be used in the calculations, since in a two-phase flow, as a rule, bubbles of different sizes are present and their velocities turn out to be correlated [5]. For this reason, the velocity with which individual bubbles reach the surface is some characteristic bubble velocity of the vapor phase, decreased by a factor of $1/(1-\varphi)$ [6, 7] and determined, e.g., by the empirical relation [7]

$$a = \begin{cases} (0.65 - 0.0039p)\sqrt[4]{d_{dr.s}/63}, & d_{dr.s} < 200 \text{ mm} \\ 0.86 - 0.0052p, & d_{dr.s} \geqslant 200 \text{ mm}, \end{cases} \quad (1)$$

where a is the bubble velocity, m/sec; p is the pressure, kgf/cm^2 (1 kg/cm^2 = 98066.5 Pa); $d_{dr.s}$ is the diameter of the driving section, mm. It should be noted that expression (1) can be used in those cases when the true volume steam content of the flow φ does not exceed 0.5-0.6.

The trajectories of the steam bubbles rising above the edge of the overflow are determined by the radial w_r and axial w_z components of the bubble velocities. The velocity component along the z axis is

$$w_z(r, z) = W_{Tz}(r, z) + a/[1 - \varphi_T(r, z)], \quad (2)$$

where φ_T is the true volume steam content at an arbitrary point (r, z) above the driving section; w_{Tz} is the axial component of the true velocity of the liquid phase.

Assuming that the flow velocity of the liquid varies linearly with height above the driving section for small values of the mass flow rate of the steam content $X_{dr.s}$ we can write

Translated from Atomnaya Énergiya, Vol. 49, No. 5, pp. 317-319, November, 1980. Original article submitted February 19, 1980.

 0038-531X/80/4905-0770$07.50

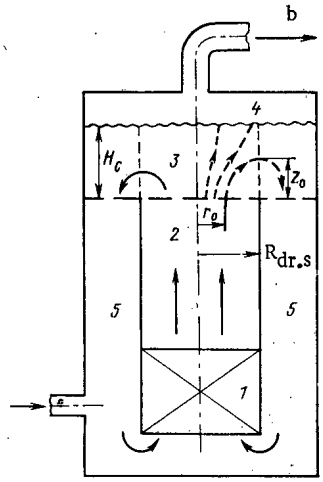

Fig. 1. Diagram of the circulation loop for the heat carrier: 1) heated section; 2) driving section; 3) separation layer; 4) steam volume; 5) entrainment section; a) feed water; b) steam.

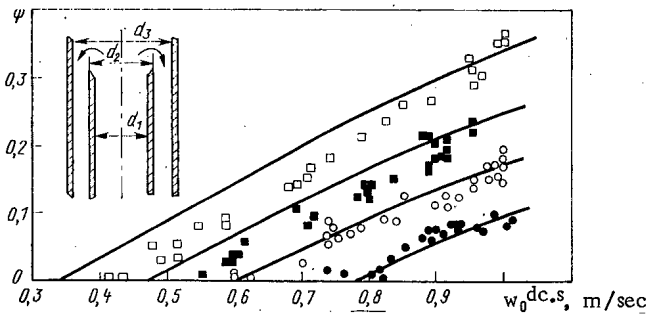

Fig. 2. The entrapment coefficient for steam as a function of the circulation rate in the downcoming zone with pressures of 100 (□); 75 (■); 50 (○), and 16 kgf/cm^2 (●); curves are calculation from (11); the dots are experimental points from [1, 2]; d_1, d_2, d_3 = 195, 237, and 269 mm.

$$w_{\tau z}(r, z) = w_0^{dr.s}(1 - z/H_c)/(1 - \varphi_\tau). \tag{3}$$

where $w_0^{dr.s}$ is the circulation rate in the driving section; H_C is the height of the liquid layer above the edge of the overflow. According to the equation of conservation of matter, the radial component of the true velocity of the liquid phase is given by

$$w_{\tau r}(r, z) = r w_0^{dr.s}/2H_c(1 - \varphi_\tau). \tag{4}$$

Thus, the equation for the trajectory of a steam bubble will have the parametric form

$$\frac{dz}{d\tau} = \frac{a}{1-\varphi_\tau} + \frac{w_0^{dr.s}(1 - z/H_c)}{1-\varphi_\tau};$$
$$\frac{dr}{d\tau} = \frac{r w_0^{dr.s}}{2H_c(1-\varphi_\tau)}. \tag{5}$$

Dividing the first of the equations in the system (5) by the second and integrating, we obtain an equation relating the coordinates of the initial motion of the bubble as a function of the driving section (r, 0) and its position ($R_{dr.s}$, z) after some time τ:

$$z = H_c \Omega_{dr.s}(1 - r^2/R^2_{dr.s}), \tag{6}$$

where $\Omega_{dr.s} = \omega_{dr.s} + X_{dr.s}(1 - \omega_{dr.s}) = 1 + a/w_0^{dr.s}$; $\omega_{dr.s}$ is the slipping coefficient.

Circulating entrainment of steam in the downcoming section of the loop will begin with the section $z = z_0$. Below it, the group velocity with which the vapor bubbles rise to the surface becomes less than the average downward velocity of water w_0. From the condition that $w_0(z_0) = a/[1 - \varphi_0(z_0)]$, where

$$w_0(z_0) = w_0^{dc.s}\ (1 - z_0/H_c)/[1 - \varphi_0(z_0)], \tag{7}$$

we obtain

$$z_0 = \Omega_{dc.s} H_c. \tag{8}$$

Here, $\Omega_{dc.s} = 1 - a/w_0^{dc.s}$, $w_0^{dc.s}$ is the rate of circulation in the downcoming section of the loop.

Substituting the value of z_0 from equality (8) into Eq. (6), we obtain

$$r_0 = R_{dr.s}\,(1 - \Omega_{dc.s}/\Omega_{dr.s})^{1/2}. \tag{9}$$

All of the steam that traverses the annular region of the driving section outlet $r_0 < r < R_{dr.s}$ will be trapped in the downcoming section of the circulation loop. When the vapor phase has a uniform distribution in the section $z = 0$ the entrainment coefficient is

$$\Psi = 1 - (r_0/R_{dr.s})^2 = \Omega_{dc.s}/\Omega_{dr.s}. \tag{10}$$

The experimental data obtained under laboratory conditions [1-3] and for a BWR-type reactor [8] agree satisfactorily with calculations based on formula (10) (Fig. 2).

We note that a consequence of the assumption that the velocity of the liquid phase varies linearly with height above the driving section is the equality of the true volume steam content above the downcoming and driving sections. This is easy to see by substituting the value of Ψ from expression (10) into the formula for the true volume steam content above the downcoming section of the circulation loop for $z = 0$:

$$\varphi_{dc.s} = \frac{1}{1 + \rho''/\rho'\,(\Omega_{dc.s}/\chi_{dr.s}\,\Psi - 1)}. \tag{11}$$

This equality is also verified by experiment [3] and justifies expression (3).

LITERATURE CITED

1. V. I. Abramov et. al., Teploenergetika, No. 8, 46 (1963).
2. M. N. Kemel'man et al., Izv. Vyssh. Ucheb. Zaved. Energ., No. 6, 35 (1965).
3. C. Princ, "Aspects of two-phase gas–liquid separation related to nuclear steam supply," Dissertation, Delft (1971).
4. F. Peebles and H. Garber, J. Chem. Eng. Prog., 49, 88 (1953).
5. S. M. Konstantinov, A. A. Kisurkin, and E. A. Neduzhko, Izv. Vyssh. Ucheb. Zaved. Energ., No. 2, 90 (1976).
6. G. B. Wallis, One-Dimensional Two-Phase Flows, McGraw–Hill, New York (1969).
7. L. N. Polyanin and A. L. Putov, At. Energ., 47, 56 (1979).
8. T. Uga, Nucl. Eng. Des., 22, 252 (1972).

NONSTATIONARY DIFFUSION OF NEUTRONS IN A SYSTEM CONSISTING OF TWO MEDIA SEPARATED BY A PLANAR BOUNDARY

A. V. Zhemerev, Yu. A. Medvedev, and E. V. Metelkin

UDC 621.039.512.4

The propagation of neutrons with energy $\lesssim 1$ MeV in matter, according to [1, 2], can be separated into two stages. In the first stage, the neutrons are moderated by elastic collisions with nuclei, and then, moderated to thermal energies, they diffuse without loss in energy until they vanish as a result of absorption processes. Nonstationary moderation of neutrons in uniform media has been studied in great detail [3, 4]. However, for the solution of a wide class of applied problems, it is necessary to calculate the nonstationary neutron distribution in a system consisting of several media with sharply differing neutron transport properties. Such problems arise, e.g., in the propagation of a neutron pulse in the atmosphere when one takes into account the influence of the Earth's surface (or water), in studying physical neutron parameters of moderators and breeding media consisting of different materials, etc.

Moderation of neutrons in a system consisting of two different media with a planar separation boundary, i.e., the first stage of neutron propagation, was examined in [5]. In the present work, we study the second stage of this process: nonstationary diffusion of thermal neutrons in a system consisting of two media with a planar separation boundary. The thermal neutron source is assumed to be a pulsed point source, i.e., it is defined by the Green's function for the diffusion equation. The distribution of thermal neutrons from fast neutron sources can be found by calculating the convolution of this Green's function with the moderated neutron distribution, determined from the investigation of the first stage of the propagation process.

The spatiotemporal distribution of thermal neutrons from a point source situated at the point $\mathbf{r}_0$ is described by the following equation [1]:

$$\frac{1}{v}\frac{\partial\Phi(\mathbf{r},\ t)}{\partial t}-\frac{l}{3(1+g-\mu)}\Delta\Phi(\mathbf{r},\ t)+\frac{1}{l_a}\Phi(\mathbf{r},\ t)=\delta(t)\,\delta(\mathbf{r}-\mathbf{r}_0), \tag{1}$$

where $\Phi(\mathbf{r}, t)$ is the flux of thermal neutrons; v is their velocity; l and l_a are the free path length of neutrons before scattering and absorption, respectively; $g = l/l_a$; μ is the average cosine of the scattering angle.

We will assume that the separation boundary between the media coincides with the surface $z = 0$, and the neutron source is located on the axis 0z at the point $z = z_0 > 0$. Transforming to dimensionless variables

$$t'=\frac{vt}{l_2};\ \{x',\ y',\ z'\}=\frac{\sqrt{3(1+g_2-\mu_2)}}{l_2}\{x,\ y,\ z\}, \tag{2}$$

Eq. (1) for each medium can be represented in the following form:

$$\text{for}\quad z<0\quad \frac{\partial\Phi_1}{\partial t}-a\delta^2\Delta\Phi_1+\frac{1}{a}g_1\Phi_1=0; \tag{3a}$$

$$\text{for}\quad z>0\quad \frac{\partial\Phi_2}{\partial t}-\Delta\Phi_2+g_2\Phi_2=s_T\delta(t)\,\delta(x)\,\delta(y)\,\delta(z-z_0), \tag{3b}$$

where $a = l_1/l_2$; $\delta^2 = (1 + g_2 - \mu_2)/(1 + g_1 - \mu_1)$: $g_i = l_i/l_{ai}$; $i = 1, 2$; $s_T = v[\sqrt{3(1 + g_2 - \mu_2)}/l_2]^3$. In what follows, we will omit for simplicity the prime notation for the variables and we will assume that the first medium is more dense than the second, i.e., $a < 1$. At the separation boundary ($z = 0$), the functions Φ_1 and Φ_2 must satisfy the following adjoining conditions:

$$\Phi_1=\Phi_2;\ a\delta^2(\partial\Phi_1/\partial z)=\partial\Phi_2/\partial z, \tag{4}$$

corresponding to the continuity of the flux and neutron current across the boundary.

Translated from Atomnaya Énergiya, Vol. 49, No. 5, pp. 319-321, November, 1980. Original article submitted February 19, 1980.

0038-531X/80/4905-0773$07.50

Using the Laplace transformation (variable p) in time and a Fourier transformation (variables k_x and k_y) in space with spatial variables x and y, as well as the adjoining conditions (4), it is easy to obtain an expression for the transformed solutions to the system (3):

$$\Phi_2 = \frac{s_T \exp[-\sqrt{p+k^2+g_2}\,|z-z_0|]}{2\sqrt{p+k^2+g_2}} - \frac{s_T \exp[-\sqrt{p+k^2+g_2}\,(z+z_0)]}{2\sqrt{p+k^2+g_2}} + \frac{s_T \exp[-\sqrt{p+k^2+g_2}\,(z+z_0)]}{\sqrt{p+k^2+g_2}+\delta\sqrt{ap+a^2\delta^2k^2+g_1}}; \quad (5)$$

$$\Phi_1 = \frac{s_T \exp[-\sqrt{p+k^2+g_2}\,z_0 + \sqrt{ap+a^2\delta^2k^2+g_1}\,(z/a\delta)]}{\sqrt{p+k^2+g_2}+\delta\sqrt{ap+a^2\delta^2k^2+g_1}}, \quad (6)$$

where $k^2 = k_x^2 = k_y^2$. It is also easy to determine the corresponding expression when the neutron source is located in a more dense medium (with $z = -z_0$):

$$\Phi_2 = \frac{s_T \exp[-\sqrt{ap+a^2\delta^2k^2+g_1}\,(z_0/\delta a) - \sqrt{p+k^2+g_2}\,z]}{\sqrt{p+k^2+g_2}+\delta\sqrt{ap+a^2\delta^2k^2+g_1}}; \quad (7)$$

$$\Phi_1 = \frac{s_T \exp[-\sqrt{ap+a^2\delta^2k^2+g_1}\,(|z+z_0|a\delta)]}{2\delta\sqrt{ap+a^2\delta^2k^2+g_1}} - \frac{s_T \exp\left[-\sqrt{ap+a^2\delta^2k^2+g_1}\,\frac{(z_0-z)}{a\delta}\right]}{2\delta\sqrt{ap+a^2\delta^2k^2+g_1}} + \frac{s_T \exp\left[-\sqrt{ap+a^2\delta^2k^2+g_1}\left(\frac{z_0-z}{a\delta}\right)\right]}{\sqrt{p+k^2+g_2}+\delta\sqrt{ap+a^2\delta^2k^2+g_1}}. \quad (8)$$

We note that each term in expressions (5) and (8) has a well-defined physical meaning. The first term is the solution to the diffusion equation for a uniform medium, in which the source is located, and the second term determines the leakage of neutrons and is a solution to an analogous problem with a "negative" source, while the third term determines the effect of the neighboring medium on the diffusion process in the given medium. Thus, the first two terms in expressions (5) and (8) represent the distribution function for neutrons diffusing only in the given medium. Expressions (5)-(8) are quite complicated, making it difficult to calculate the original functions. However, in one particular case of practical interest, they are significantly simplified: contact of two media with strongly differing densities.

Let us first examine a planar neutron source located in the less dense medium (the surface $z = z_0$). The solution to the diffusion equation in this case can be obtained from expressions (5) and (6) with $k = 0$. In the absence of absorption ($g_1 = g_2 = 0$), using the inverse Laplace transformation, we obtain

$$\Phi_2 = s_n \frac{\exp\left[-\frac{(z-z_0)^2}{4t}\right]}{\sqrt{4\pi t}} + \frac{(1-\delta\sqrt{a})}{(1+\delta\sqrt{a})} s_n \frac{\exp\left[-\frac{(z+z_0)^2}{4t}\right]}{\sqrt{4\pi t}}; \quad (9)$$

$$\Phi_1 = s_n \frac{\exp[-(z_0 - z/\delta\sqrt{a})^2/4t]}{(1+\delta\sqrt{a})\sqrt{\pi t}}, \quad (10)$$

where $s_n = (v/l_2)\sqrt{3(1+g_2-\mu_2)}$. If the first medium is much more dense than the second ($a \ll 1$), then it is possible to take $a = 0$ in expression (9), and this expression transforms into the solution of the problem with a zero neutron flux through the boundary. We would arrive at exactly the same result if in solving the system (3a) and (3b) we neglected in (3a) the derivative with respect to time, i.e., having determined the nonstationary solution to the diffusion equation in the second medium, we join it [see (4)] to the corresponding stationary solution for the first medium. The physical meaning of this approximation stems from the fact that the first medium is much more dense than the second ($l_1 \ll l_2$) and the neutrons diffuse much more rapidly in it, since $\langle z \rangle \sim \sqrt{vt/l}$. In this case, the solution to the diffusion equation in the first medium will be quasistationary. This can be obtained from expression (10) setting $z = 0$ and then $a = 0$. This solution will coincide with the value of the function Φ_2 at the separation boundary ($z = 0$). Evidently, this approximation is more exact for the second, less dense medium, while in the first, in the absence of absorption, it is valid for short distances from the separation boundary ($z \ll \delta\sqrt{a z_0}$), where there are many neutrons that were once located in the second medium.

In the presence of absorption, setting $a = 0$ in formula (5) and using the inverse Laplace transformation, we obtain

$$\Phi_2 = \frac{s_n \exp(-g_2 t)}{\sqrt{4\pi t}}\left\{\exp\left[-\frac{(z-z_0)^2}{4t}\right] + \exp\left[-\frac{(z+z_0)^2}{4t}\right]\right\} - s_n \exp(-g_2 t)\,\delta\sqrt{g_1}\exp[\delta\sqrt{g_1}\,(z+z_0) + \delta^2 g_1 t]\,\mathrm{Erfc}\left[\frac{z+z_0}{2\sqrt{t}} + \delta\sqrt{g_1 t}\right], \quad (11)$$

where Erfc (z) = 1 − Erf (z), and Erf (z) is the error function [6].

Using the asymptotic expression Erfc (z) ≈ $\exp(-z^2)/\sqrt{\pi}z$ (for $z \gtrsim 3$ [6]), the function (11) can be written in the form

$$\Phi_2 = \frac{s_n \exp(-g_2 t)}{\sqrt{4\pi t}} \left\{ \exp\left[-\frac{(z-z_0)^2}{4t} \right] + \frac{(z+z_0-2\delta\sqrt{g_1 t})}{(z+z_0+2\delta\sqrt{g_1 t})} \exp\left[-\frac{(z+z_0)^2}{4t} \right] \right\}. \quad (12)$$

It follows from here that initially [for $t < (z + z_0)/2\delta\sqrt{g_1}$] the distribution function (12) takes on larger values than the solution corresponding to the problem in the uniform medium (first term), while at later times [$t > (z + z_0)/2\delta\sqrt{g_1}$], it takes on smaller values. This behavior of the distribution function stems from the strong difference in the density of the media in contact [see (9)] and the presence of absorption in the first, more dense medium.

Setting k = 0 and $ap = 0$ in formula (6) and using the inverse Laplace transformation, we obtain

$$\Phi_1(z, t) = \exp[(\sqrt{g_1}/a\delta)z] \; \Phi_2(z=0, t), \quad (13)$$

where Φ_2 is determined by expression (11). From here it follows that the solution to the diffusion equation in the first, more dense medium ($a \ll 1$) is quasistationary. Since for $t \gtrsim 1$, $p \lesssim 1$ are characteristic, then the solution obtained (13) is a good approximation for $g_1 \gg a$, since it is in this case that it is possible to neglect the term ap in comparison with g_1 in formula (6). Here, it is necessary to keep in mind the fact that the diffusion approximation is valid for $g_1 \ll 1$. The two conditions noted above ($g_1 \gg a$, $g_1 \ll 1$) do not contradict each other, since we assume that the first medium is significantly more dense than the second, i.e., $a \ll 1$. (For the system ground−air, $a \approx 5 \cdot 10^{-4}$ [2]).

Let us now assume that the neutron source is situated in the more dense medium [see (7), (8)] and $a \ll 1$. Setting k = 0 in (7), neglecting the term ap and using the inverse Laplace transformation, we obtain

$$\Phi_2 = s_n \exp\left[-g_2 t - \frac{\sqrt{g_1}}{a\delta} z_0 \right] \left\{ \frac{\exp[-z^2/4t]}{\sqrt{\pi t}} - \delta\sqrt{g_1} \exp[z\delta\sqrt{g_1} + \delta^2 g_1 t] \operatorname{Erfc}\left[\frac{z}{2\sqrt{t}} + \delta\sqrt{g_1 t} \right] \right\}. \quad (14)$$

Expression (14) is, apparently, a good approximation to the solution of the diffusion equation, if $a \ll g_1 \ll 1$ (see above).

Setting k = 0 in (8), $ap = 0$ in the last term, and using the inverse Laplace transformation we obtain

$$\Phi_1 = \frac{s_n \exp[-g_1 t/a]}{\delta\sqrt{a}\sqrt{4\pi t}} \left\{ \exp\left[-\frac{(z+z_0)^2}{4a\delta^2 t} \right] - \exp\left[-\frac{(z-z_0)^2}{4a\delta^2 t} \right] \right\} + s_n \exp\left[-g_2 t - \right.$$

$$\left. - \frac{\sqrt{g_1}}{a\delta}(z_0 - z) \right] \left\{ \frac{1}{\sqrt{\pi t}} - \delta\sqrt{g_1} \exp(\delta^2 g_1 t) \operatorname{Erfc}(\delta\sqrt{g_1 t}) \right\}. \quad (15)$$

The first term in formula (15) describes the diffusion of neutrons that did not reach the second medium. The second term represents the distribution function of neutrons that were once in the second medium. This distribution function is quasistationary, and it can be represented in the form (13), where Φ_2 will be determined by (14).

Let us consider a point neutron source and assume that the first medium is significantly more dense than the second ($a \ll 1$). In this case, setting $a^2\delta^2 k^2 = 0$ in expressions (5)-(8), we obtain

$$\Phi_i = \frac{s_\tau}{s_n} \frac{\exp(-\rho^2/4t)}{4\pi t} \Phi_{i,\,\text{planar}} \quad (i = 1, 2),$$

where $\rho^2 = x^2 + y^2$; $\Phi_{i\,\text{planar}}$ is the solution to the corresponding problem with a planar source, obtained earlier [see (11), (13)-(15)].

The representation of the distribution function in the form (16) reflects the fact that the neutrons entering the more dense medium from the less dense medium emanate from the same point into which they enter, since in the more dense medium they have a significantly shorter free path length. In addition, the diffusion of neutrons in the more dense medium over significant distances is determined by the neutrons that enter it from the less dense medium.

LITERATURE CITED

1. A. Weinberg and E. Wigner, Physical Theory of Nuclear Reactors [Russian translation], IL, Moscow (1961).
2. P. A. Yampol'skii, Neutrons from an Atomic Explosion [in Russian], Atomizdat, Moscow (1961).
3. M. V. Kazarnovskii, Tr. Fiz. Inst. Akad. Nauk, 11, 176 (1959).
4. M. V. Kazarnovskii, in: Theoretical and Experimental Problems of Nonstationary Neutron Transport [in Russian], Atomizdat, Moscow (1972).
5. Yu. A. Medvedev and E. V. Metelkin, At. Energ., 48, 308 (1980).
6. I. S. Gradshtein and I. M. Ryzhik, Tables of Integrals, Sums, Series, and Products [in Russian], Nauka, Moscow (1971).

DISTORTION OF THE NEUTRON FIELD IN REACTORS WITH RANDOMLY DISTRIBUTED PERTURBATIONS OF THE MACROSCOPIC CROSS SECTIONS

V. K. Goryunov

UDC 621.039.564.2:621.039.512.45

In reconstructing the neutron field from the results of measurements in separate regions of the reactor, as well as in a physical calculation of the HRR power, there arises the question of the accuracy of the results obtained, in particular, of the relationship between the accuracy of the results and the error in the starting data: the macroscopic interaction cross sections. In a large number of problems, one can or must assume a random distribution of errors in the macroscopic cross sections over the elements in the active zone, e.g., over the HRR.

Changing the initial neutron field as a result of superimposing randomly distributed perturbations of the macroscopic cross sections for a large number of HRR is not a trivial repetition of the nature of the perturbations. The fine mosaic structure of piecewise constant perturbations, within the limits of each HRR, as it turned out, leads to global distortions in the neutron field encompassing up to half the active zone.

The repeated amplification of the amplitude of the fluctuations in the neutron field in comparison with the characteristic values of the perturbations is also important in practice. The mean-square fluctuations in the HRR power with a 1% mean-square perturbation of the macroscopic cross section are estimated in [1-3] by the method of statistical modeling. The results show a 2.5-11-fold amplification of the fluctuations in the HRR power for thermal neutron reactors with large active zones.

The previously proposed models [4] describing analytically the distortions in the neutron field and the energy distribution density can be viewed as a solution to the diffusion equation for the flux deviation from the initial flux in the presence of randomly distributed perturbations in the critical reactor. The results of the numerical experiments indicated describe this model satisfactorily [5]. It turned out that the fluctuations in the neutron field are determined by the following characteristics of the reactor and the perturbations: sensitivity of the material parameter to the given perturbation of the properties of the active zone; the law governing the distribution of perturbations and, in particular, for a Gaussian distribution, the degree of their correlation and mean-square value of the perturbation; properties of the reflector and the dimensions of the active zone.

In a reactor with radius R with boundary condition $(\Phi_0'/\Phi_0)|_{r=R} = -\lambda$, the variance of the relative fluctuations in the neutron field, according to [4], is expressed by a series consisting of products of radial–azimuthal harmonics $J_m[\mu_m^{(\gamma)}(r/R)]\exp[im(\varphi + \varphi_m)]$ – the characteristic functions of the unperturbed equation (φ_m is the random phase of the i-th harmonic):

Translated from Atomnaya Énergiya, Vol. 49, No. 5, pp. 321-323, November, 1980. Original article submitted March 6, 1980.

0038-531X/80/4905-0776$07.50

TABLE 1. Parameters of the Distortion in the Neutron Field as a Function of the Boundary Conditions $H = [-R/\Phi(r)]\,[\partial\Phi(r)/\partial r]\,|_{r=R}$

Statistical param. of contribution of harmonics	H	No. of harmonic "mγ" (m is azimuthal No., γ is radial No.)								
		«02»	«11»	«12»	«21»	«22»	«31»	«32»	«41»	«42»
Mean-square amplitude	100	0,0472	0,1399	0,0416	0,0620	0,0290	0,0370	0,0217	0,0251	0,0169
	1	0,0814	0,2912	0,0705	0,1432	0,0500	0,0928	0,0383	0,0675	0,0307
	0,01	0,0953	0,4783	0,0824	0,2312	0,0592	0,1478	0,0459	0,1066	0,0373
Correl. coef. between harmonic amplitudes "m1" and "m2"	100			0,278		0,283		0,285		0,285
	1			0,099		0,089		0,082		0,075
	0,01			0,001		0,001		0,001		0,001
Prob. for predominance of a harmonic on av. in reactor, %	100	8,3	60,7	5,3	16,3	1,6	4,2	0,5	1,0	2,1
	1	4,1	70,4	1,5	17,9	0,2	4,6	0,0	1,2	0,0
	0,01	2,7	72,9	1,0	17,8	0,2	4,3	0,0	1,1	0,0
Schematic diagram showing zero lines of harmonics		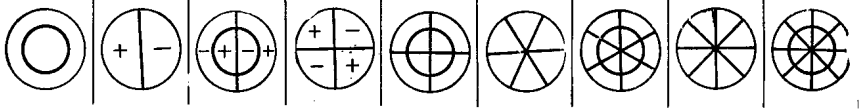								

$$\left\langle\left[\frac{\delta\Phi(r,\varphi)}{\Phi_0(r,\varphi)}\right]^2\right\rangle=\left(\frac{\partial\varkappa_0^2}{\partial x}\sigma_x\right)^2 R^2\int\limits_{S_{a.z}}\rho(r')\,dr'\sum_{m,\eta,\gamma}a_m^{\eta\gamma}(\lambda R)\,\frac{J_m\left(\mu_m^{(\eta)}\frac{r}{R}\right)J_m\left(\mu_m^{(\gamma)}\frac{r}{R}\right)}{\left[J_3\left(\mu_0^{(1)}\frac{r}{R}\right)\right]^2}. \tag{1}$$

Here, $\delta\Phi(r,\varphi)$ is the deviation of the neutron field at a point with coordinates (r,φ) relative to the unperturbed field $\Phi_0(r,\varphi)$; $(\partial\varkappa_0^2/\partial x)\,\sigma_x$ is the change in the material parameter with a deviation in the properties of the active zone x (macroscopic cross section for some process, enrichment, density, temperature, etc.) from the initial value by the mean-square perturbation σ_x (computed, e.g., according to the double-group criticality equation); $\rho(r)$ is the normalized correlation function for perturbations, and in the absence of correlations of perturbations between different HRR $\rho(r)$ is U-shaped within a single HRR, and its integral equals the area of the HRR in the plane of the active zone; $J_0(\mu_0^{(1)}\,r/R)=\Phi_0(r,\varphi)$ is the distribution function for the unperturbed neutron field; $a_m^{\eta\nu}(\lambda R)$ is the fractional contribution of the products of the harmonics to the variance of the field and depends on the albedo of the reflector.

In order to interpret the result obtained, let us examine the random function of the coordinates $\delta\Phi(r)$, which is the sum of radial–azimuthal harmonics $f_n(r)$ with random amplitude z_n:

$$\delta\Phi(r)=\sqrt{A}\sum_n z_n f_n(r). \tag{2}$$

The variance of this function in relative units for a Gaussian distribution of the random quantities z_n with variance σ_n^2 equals

$$\left\langle\left[\frac{\delta\Phi(r)}{f_0(r)}\right]^2\right\rangle=A\sum_{n,l}k_{nl}\sigma_n\sigma_l\,\frac{f_n(r)\,f_l(r)}{[f_0(r)]^2}, \tag{3}$$

where k_{nl} is the correlation coefficient between z_n and z_l. Comparison of (1) and (3) allows establishing the fact that $a_m^{\eta\eta}=\sigma_{m\eta}^2$ and some other relations.

Table 1 shows the results of calculations of the mean square values of the amplitudes and correlation coefficients between amplitudes of different harmonics. It should be noted that:

the contribution decreases sharply with increasing number of the radial harmonics and less sharply with increasing number of the azimuthal harmonics;

the degree of correlation of the contributions of radial harmonics decreases with decreasing λR (i.e., with the transition from the reactor without a reflector to a reactor with an ideal reflector) and there is no correlation between azimuthal harmonics;

the contribution increases with decreasing λR and the contributions of harmonics are simultaneously redistributed in magnitude with the exception of the first two ($\gamma = 1$; $m = 1, 2$).

Thus, a consequence of the randomly distributed perturbations in the properties of the active zone is the appearance of distortion in the neutron field. The distortion is described by the sum of several of the first radial–azimuthal harmonics with random amplitudes. The average value of each amplitude over the realiza-

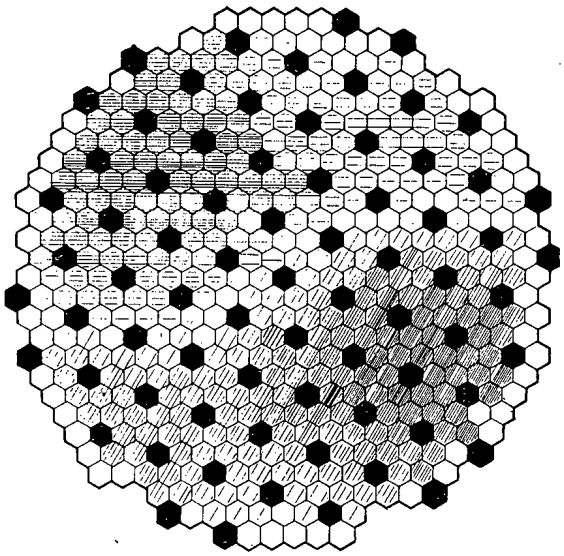

Fig. 1. A cartogram of the deviations in the neutron flux for typical realization of the random amplitudes z_n. Deviations with the same sign are indicated by shading in the same direction, and the number of lines corresponds to the percentage deviation. In each six HRR cells surrounding cells with control rods (black hexagons), the perturbation $\nu \Sigma_f^{(2)}$ is the same. The last series of peripheral channels was not considered.

tions equals zero, the variance (with a Gaussian perturbation) equals the product of the factor in front of the summation sign in (1) and $a_m^{\eta\eta}$. As the variance increases, the probability that a given amplitude differs from zero increases, and therefore the given harmonic gives the larger contribution to the field distortion. If, e.g., only two statistically independent harmonics are considered in the distortion, then the probability that one of them predominates on the average over the reactor is determined by the formula

$$P\left(\left|z_1\overline{\frac{f_1(\mathbf{r})}{f_0(\mathbf{r})}}\right|>\left|z_2\overline{\frac{f_2(\mathbf{r})}{f_0(\mathbf{r})}}\right|\right)=\frac{4}{\pi\sqrt{\overline{\sigma_1^2\sigma_2^2}}}\int_0^\infty dx\int_0^x dy\exp\left(-\frac{x^2}{\overline{\sigma_1^2}}-\frac{y^2}{\overline{\sigma_2^2}}\right)=$$

$$=\begin{cases}1-\frac{2}{\pi}\operatorname{arctg}\sqrt{\overline{\sigma_2^2/\sigma_1^2}}\,\overline{\sigma_1^2}\geqslant\overline{\sigma_2^2},\\ \frac{2}{\pi}\operatorname{arctg}\sqrt{\overline{\sigma_1^2/\sigma_2^2}}\,\overline{\sigma_1^2}\leqslant\overline{\sigma_2^2},\end{cases}$$

where $\overline{\sigma_i^2}$ is the over-the-reactor average variance of the contribution of the i-th harmonic:

$$\overline{\sigma_i^2}=\frac{\sigma_i^2}{S_{a.z.}}\int_{S_{a.z}}\left[\frac{f_i(\mathbf{r})}{f_0(\mathbf{r})}\right]^2 d\mathbf{r}.$$

The probabilities for the predominance of each harmonic over the others, corresponding to the mean-square contributions of the different harmonics averaged over the reactor, are shown in Table 1. We performed the calculation using a statistical modeling method [6] that takes into account the degree of correlation between separate harmonics.

The harmonic "11" (m = 1, γ = 1) is most likely to be manifested, which explains the paradoxical distortion in the distribution of the HRR power in two halves along the diameter in most numerical experiments. Figure 1 shows the results of the calculations of a typical realization of the relative deviation of the thermal neutron flux. We used the macroscopic constants from the thermal neutron reactor with radius 4.6 m from [3] with a 1% mean-square perturbation of the macroscopic cross section $\nu\Sigma_f^2$ for a block consisting of six HRR. The redistribution of the probabilities with a change in the reflector quality, in particular, the increase in the role of the harmonic "02" in reactors without reflectors, is interesting.

The data presented in the present work are sufficient to estimate the average dimension of the region with a distortion having a single sign and other characteristics for real reactors.

In conclusion, we note that the fluctuations of power in HRR are determined not only by the distortion in the neutron field, but also by the fluctuations in the fission cross sections and their interference with fluctuations in the neutron field. We can expect that the known probabilities and the fractional contributions of the harmonics will be used in positioning detectors for control systems and in methods for processing experimental data.

The author is grateful to Ya. V. Shevelev for the idea of applying the previously published model [4] to the disagreement between the computed and true fluxes in a real reactor.

LITERATURE CITED

1. V. A. Karpov, V. V. Postnikov, and V. G. Nazaryan, At. Energ., 40, 456 (1976).
2. V. A. Karpov, Preprint IAÉ-2758, Moscow (1976).
3. V. A. Karpov and A. N. Protsenko, Preprint IAÉ-2885, Moscow (1977).
4. V. K. Goryunov, At. Energ., 44, 357 (1978).
5. V. K. Goryunov, Preprint No. FÉI-851, Obninsk (1979).
6. S. M. Ermakov and G. A. Mikhailov, Course in Statistical Modeling [in Russian], Nauka, Moscow (1976).

FAST-RESPONSE REGULATOR IN THE SPATIAL DYNAMICS OF A REACTOR

A. M. Afanas'ev and B. Z. Torlin

UDC 621.039.515

In studies of automatic regulation of the spatial distribution of the neutron flux, the regulators are normally assumed to be fast-response devices, particularly when the suppression of xenon fluctuations is of interest [1-4]. As far as the formal aspect is concerned, this means that, in comparison with slow processes, the inertia of the electric drive and the sensors is insignificant and the gain K in the circuit transforming the signal from the sensor and transmitting the signal to the regulator component using the signal is infinite. The present work presents a quantitative estimate of the influence of the difference between a large and infinite K value upon the process for an astatic local regulator of the neutron field. The considerations involve the one-group diffusion approximation, in which one group of delayed neutrons and one link of internal feedback of the first order [4] with a positive reactivity coefficient α are included and the lifetimes of prompt neutrons are disregarded. After linearization and Laplace transformation, the initial equation system has the form

$$M^2\frac{d^2}{dz^2}\varphi+(k_0-1)\varphi-\beta\varphi+\lambda c+\Phi_0(\alpha x+\rho F)=0;$$
$$\omega c=\beta\varphi-\lambda c;\ \omega x=\varphi-x;\ \omega\rho=-K\varphi(z_*)/\Phi_0(z_*) \qquad (1)$$

with homogeneous boundary conditions on φ. The symbols φ, c, x, and ρ denote the Laplace transforms of the relative deviations from the stationary neutron flux values, the concentration of sources of delayed neutrons, the parameter of internal feedback, and reactivity, respectively; localization of a change in reactivity is described by the function F; z_* denotes the position coordinate of the sensor controlled by the regulator; and Φ_0 denotes the stationary neutron flux distribution. The rest of the notation is as usual. If an absorbing rod with its end at the point z_p is the final control element, then $F = H\delta(z - z_p)$. Both ω and λ are dimensionless (the time constant τ of the internal feedback is used as the unit in the measurements).

For $\Phi_0 = 1$ it is easy to obtain a transcendental equation relating the eigenvalues ω of system (1) to the reactor parameters:

$$\cos(B/n)\cos(B/\nu)=\varepsilon\omega B\sin B; \qquad (2)$$

$$b^2=\left(\frac{\alpha}{\omega+1}-\frac{\omega\beta}{\omega+\lambda}\right);$$
$$b=B(M/H);\ \varepsilon=(M/H)^2/K;\ n=H/z_p;\ \nu=H/(H-z_*) \qquad (3)$$
$$\text{for } z_*>z_p.$$

Translated from Atomnaya Énergiya, Vol. 49, No. 5, pp. 323-324, November, 1980. Original article submitted March 6, 1980.

0038-531X/80/4905-0779$07.50

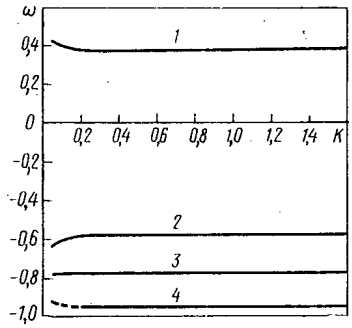

Fig. 1. Dependence of ω on K: 1) n = 5, ν = 5/4; 2) n = 5, ν = 5/3; 3) n = 5, ν = 2; 4) n = 5, ν = 10/3; – – –) Re ω for complex ω.

Under the condition $\varepsilon \ll 1$, which is applicable in a rather broad interval of possible K values, the solution to Eq. (2) for the greatest ω value can be represented rather accurately in the form $\omega = \omega_0 + \varepsilon\omega_1 = \omega_0 + \Delta\omega$, where ω_0 corresponds to the limit $\varepsilon = 0$. When only first-order terms in ε are kept, we obtain from Eq. (3):

$$\frac{\Delta\omega}{\omega_0} = -2\frac{B_1}{\omega_0 B_0}(\omega_0+1)\frac{\lambda+\omega_0}{\lambda+(1+2\omega_0)(1+\beta/b_0^2)-\alpha/b_0^2}; \tag{4}$$

wherein, according to Eq. (2), for $\nu > n$:

$$B_0 = \pi n/2; \tag{5}$$

$$\frac{B_1}{\omega_0 B_0} = -\varepsilon n\frac{\sin B_0}{\cos B_0/\nu}; \tag{6}$$

ω_0 is determined from Eq. (3) for $B = B_0$.

When the sensor is closer to the center than the end of the rod, i.e., if $n > \nu$, in Eqs. (5) and (6) n must be replaced by ν and ν by n, respectively. The case of symmetric position of the sensor and the end of the rod ($n = \nu$) requires special treatment. When, for $\varepsilon = 0$, ν tends to n, Eq. system (1) becomes degenerate and a second (multiple) root ω_0, i.e., a second-order pole, appears (a situation corresponding to a second-order Jordan box exists). This, in turn, means that in the description of the time dependence, there appear, in addition to terms of the form $\exp \omega t$, terms of the form $t \exp \omega t$. The degeneracy at $n = \nu$ vanishes when $\varepsilon \neq 0$. For small ε we have in place of Eq. (6)

$$\frac{B_1}{\omega_0 B_0} = \pm n\sqrt{\frac{\varepsilon}{\omega_0 B_0}\sin B_0}\,^{*}. \tag{7}$$

The formulas so far obtained can be used to estimate the error introduced into the parameter ω by substituting the real K value by an infinitely large K value. A comparison with calculated values has shown that though the formulas are very simple, they can be used not only for a qualitative evaluation of the effect but also for its quantitative estimation. Numerical calculations were made with a modified version of the FOSC program [5] which has been designed for determining ω in more complicated, yet one-dimensional reactor models. When Chebyshev polynomials were used in the program, it was possible to take into account the lifetime of the prompt neutrons and the inertia of the electric drive. Calculations were made with variations of various system parameters within wide ranges. The results were most significantly influenced by the positions of sensor and rod, the reactivity coefficient α, and the regulator amplification coefficient K. Figure 1 shows the dependence of ω on K in various versions of the sensor and rod positions. The stationary distribution Φ_0 was assumed as sinusoidal, $(M/H)^2 \approx 2 \cdot 10^{-3}$, $\lambda = 60$ (which corresponds to $\tau = 600$ sec), $\beta = 7.5 \cdot 10^{-3}$, and $\alpha = 10^{-2}$. The lifetime of the prompt neutrons was assumed as 10^{-3} sec; the time constant of the inertia of the motor was assumed as 1 sec, but these values were practically without influence on the function shown in Fig. 1. In ω, ε coordinates, curves 1-4 are transformed into clear straight lines, whereas the ratio $\Delta\omega/\omega_0$ calculated with Eqs. (4) and (6) differs from the results of the numerical calculations by approximately 1%.†

*When the expression under the root is negative, ω becomes complex.

† The ω_0 value in the case of a sinusoidal stationary neutron field is given with great accuracy by Eq. (3) with $b^2 = \left(\frac{M}{H}\right)^2 \pi^3 (n^2-1)/\left[4n \sin^2\left(\frac{\pi}{2n}\right)\left(1+\frac{1}{2}\frac{1}{4n^2-1}\right)\right]$.

Our investigations lead to the following important conclusions. The ω values hardly differ from ω_0 in a wide interval of K, i.e., at those K values the regulator can be considered a fast-response regulator. The greatest difference between ω and ω_0 ($\sim 17\%$) is noted at $K = 4.5 \cdot 10^{-2}$ (left end of curve 1). At this K value, $\tau = 30$ sec, and an imbalance $\Delta\Phi/\Phi_0 = 3 \cdot 10^{-2}$, the rate at which reactivity is introduced by the rod of the automatic regulator amounts to $6 \cdot 10^{-3}\beta$/sec, i.e., the rate is smaller by one order of magnitude than permitted by the rules of nuclear safety [6]. Depending upon the positions of the sensor and the rod, an increase in K can imply either an increase or a decrease in stability. Finally, it should be noted in analogy to the increase in stability upon spacing the sensor from the rod (known from previous publications [2-4, 7]), all the effects listed above are not described in the pointwise approximation.

LITERATURE CITED

1. A. Hitchcock, Stability of Nuclear Reactors [Russian translation], Gosatomizdat, Moscow (1963).
2. P. S. Postnikov and E. F. Sabaev, At. Energ., 26, No. 1, 56 (1969).
3. A. M. Afanas'ev and B. Z. Torlin, At. Energ., 43, No. 4, 243 (1977).
4. I. Ya. Emel'yanov et al., At. Energ., 46, No. 2, 82 (1979).
5. A. M. Afanas'ev, Preprint Inst. Theor. and Exp. Phys. ITÉF-83 [in Russian], Moscow (1979).
6. Rules of Nuclear Safety of Atomic Power Stations [in Russian] (PBYa-04-74), Atomizdat, Moscow (1976).
7. A. M. Afanas'ev and B. Z. Torlin, At. Energ., 44, No. 6, 530 (1978).

FAST RESPONSE OF THE REGULATOR IN A CYLINDRICAL REACTOR

B. Z. Torlin

UDC 621.039.515

The radial stability of a cylindrical reactor with a fast-response automatic central regulator was considered in [1]. The processes occurring in the reactor were considered slow enough so that the delay of the regulator could be disregarded.

Let us consider on a simple model the extent to which and the limits within which this ideal is correct. Disregarding prompt neutrons in a one-group diffusion approximation with feedback in the form of a simple inertial link [2] with a positive reactivity coefficient α we obtain after linearization and Laplace transformation:

$$\begin{aligned} &M^2\,\Delta\varphi + (k_0 - 1)\,\varphi - \beta\varphi + \lambda c + \alpha x\Phi_0 = 0;\\ &\omega c = \beta\varphi - \lambda c;\\ &\omega x = \varphi - x;\\ &\omega\gamma = -\varkappa\varphi\,(r_g)/\Phi_0\,(r_g) \end{aligned} \qquad (1)$$

with the following boundary conditions on φ:

$$R\varphi'\,(R) = \Gamma\varphi\,(R) \text{ and } r_c\varphi'\,(r_c) = \gamma\Phi_0\,(r_c).$$

The notation is interpreted as follows: φ, c, x, and γ denote the Laplace transforms of the relative deviations from the stationary levels of the neutron flux, the concentration of sources of delayed neutrons, the parameter of internal feedback, and the boundary condition on an absorbing rod of radius r_c, respectively; φ, c, and x are distributed over the interval $[r_c, R]$; R and r_g denote the radius of the core and of the circles on which the neutron flux measuring sensors of the regulating system are located; and $\varkappa$ denotes the amplification coefficient of the regulator.

The rest of the notation is as usual. The subscript 0 denotes the stationary quantities. We note that $\varkappa$ and λ, as well as the eigenfrequency ω, are dimensionless. The time constant τ of the internal feedback is chosen as the scale. The stability of the reactor is characterized by the real part of the eigenvalue ω at which the stability reaches its maximum.

In the case of a flat initial neutron distribution ($k_0 = 1$; $\Phi_0 = 1$ and $\Gamma = 0$), one can obtain for $r_c \ll R$

Translated from Atomnaya Énergiya, Vol. 49, No. 5, pp. 324-325, November, 1980. Original article submitted April 2, 1980.

0038-531X/80/4905-0781$07.50

from the system (1) a transcendental equation for the determination of ω:

$$N_1(B)\,J_0(B\chi_g) - N_0(B\chi_g)\,J_1(B) = \frac{2}{\pi}\,\varepsilon\omega J_1(B), \tag{2}$$

where

$$\chi_g = r_g/R; \quad \varepsilon = 1/\varkappa; \quad b = BM/R;$$

$$b^2 = \frac{\alpha}{1+\omega} - \frac{\omega\beta}{\lambda+\omega}; \tag{3}$$

J_n and N_n denote Bessel and Neumann functions of order n.

Since a small change Δk in reactivity is related to γ by $\Delta k = 4\gamma (M/R)^2$, we also have $\varepsilon = (4/K)(M/R)^2$, if the change is expressed via the effective amplification coefficient K, which relates the rate of introducing reactivity to the relative deviation of the neutron flux at the point of recording the flux with the sensors.

If ε is small enough, the solution to Eq. (2) can be written with high accuracy in the form $\omega = \omega_0 + \Delta\omega$, where

$$\frac{\Delta\omega}{\omega_0} = -2\,\frac{\Delta B}{B_0\omega_0}\,(\omega_0+1)\,\frac{\lambda+\omega_0}{\lambda+(1+2\omega_0)(1+\beta/b_0^2)-\alpha/b_0^2}; \tag{4}$$

$$\frac{\Delta B}{B_0\omega_0} = \frac{2\varepsilon}{\pi}\,\frac{J_n(B_0)}{B_0\psi(\chi_g)}; \tag{5}$$

$$\psi(\chi_g) = \psi_0(\chi_g) - \chi_g\psi_1(\chi_g);$$

$$\psi_i(\chi_g) = N_i(B_0)\,J_i(B_0\chi_g) - N_i(B_0\chi_g)\,J_i(B_0);$$

B_0 denotes the smallest root of the left side of Eq. (2); and ω_0 is determined from Eq. (3) for $b = b_0 = B_0M/R$. The dependence of B_0 upon χ_g has been analyzed in [1]. We recall that $B_0 \to 0$ for $\chi_g \to 0$ and $B_0 \to (\pi/2)\cdot\chi_g/(1-\chi_g)$ for $\chi_g \to 1$ [3].

The form of the function $\psi(\chi_g)$ must be established for analyzing the relations which have been obtained. Obviously, $\psi(\chi_g) \approx (2/\pi)\ln 1/\chi_g$ for $\chi_g \to 0$. When the asymptotic representation [3] of the functions J and N is employed, $\psi(\chi_g) \approx (2/\pi)(1-\chi_g)/B_0\sqrt{\chi_g}$ for $\chi_g \to 0$ is obtained. The function $\psi(\chi_g)$ is monotonic in the entire interval $0 < \chi_g < 1$. This means that the right side of Eq. (5) is small for $\chi_g \to 0$ and will oscillate with increasing amplitude when χ_g approaches 1. But this does not cause an increase in $\Delta\omega/\omega_0$ because the factor $1 + \omega_0 \approx \alpha/b_0^2$ entering into Eq. (4) decreases more rapidly for $\chi_g \to 1$.

With all these results, an upper limit of $\Delta\omega/\omega_0$ can be obtained for $\omega_0 < 0$. For $\lambda \gg 1$ the equation has the particularly simple form

$$\frac{\Delta\omega}{\omega_0} \leqslant 2\,\frac{\alpha}{K}. \tag{6}$$

When $\alpha = 10^{-2}$ and K = 0.5,* the ω_0 value obtained in the approximation of a fast-response regulator differs from the accurate solution by less than 4%. This calculation reveals that, for determining the stability of systems with a time constant of about 1 min in the feedback (or more than 1 min), the approximation of the fast-response regulator is quite satisfactory. The approximation is the better the smaller α and the greater the efficient amplification coefficient K of the regulator and also the greater the time constant τ, because K also increases with increasing time constant.

LITERATURE CITED

1. B. Z. Torlin, At. Energ., 45, No. 6, 457 (1978).
2. I. Ya. Emel'yanov et al., At. Energ., 46, No. 2, 82 (1979).
3. E. Jahnke, F. Emde, and F. Lösch, Special Functions [Russian translation], Nauka, Moscow (1964).
4. Rules of Nuclear Safety of Atomic Power Stations [in Russian], No. PBYa-04-74, Atomizdat, Moscow (1976).

*For the imbalance $\Delta\Phi/\Phi_0 = 3\cdot 10^{-2}$ and τ = 60 sec, this corresponds to a rate of 0.035 β/sec of introducing reactivity; this is two times smaller than the value allowed by the rules of nuclear safety [4].

CALCULATION OF THE OVERHEATING OF FUEL ELEMENTS, TAKING INTO ACCOUNT THE PROBABILITY OF DEVIATIONS OF THE CORE PARAMETERS

I. M. Kurbatov

UDC 621.039.517.5

In actual calculations of random deviations of the fuel element temperature, the sequential probabilistic approach has been increasingly used. The method deals with the nature of the deviations of the important core parameters and makes it possible to take into account the laws governing core parameter changes when the result of the common influence of numerous overheating factors is assessed [1-4].

But in such calculations the maximum deviations of the important parameters of a single fuel element are often used as factors of overheating for the technological channel or for a cell of the core; this is done by expanding the influence of each of the deviations over the entire group of fuel elements forming the channel.

Since the maximum deviations of some parameter will hardly occur in all fuel elements of the channel, the approach often leads to unjustifiably large results of the calculations. We consider in the present work a method of taking into consideration the influence of the "group effect" upon the overheating factors with which the random deviations of the fuel-element temperature in the core channel are calculated.

When the core channel consists of m homogeneous fuel elements with randomly changing parameters, the probability that all m elements which are assembled in the channel have unfavorable values of some important parameter $\mathcal{P}$ (condition of a hot channel resulting from a particular parameter) can be obtained from the following relation [5]:

$$P_M(m) = \frac{(pM)!\,(M-m)!}{M!\,(pM-m)}, \tag{1}$$

where M denotes the total number of fuel elements from which the core channels are composed by the random sampling method; and p denotes the probability of a certain fuel element parameter falling into the interval of unfavorable values (p depends on the probability distribution of the deviations of the parameter). Then $1-P$ defines the interval of admissible deviations of the parameter; pM denotes the total number of fuel elements having unfavorable values of the parameter in the set M.

For $M \gg m$ Eq. (1) is reduced to

$$P_M(m) \cong p^m. \tag{2}$$

When some value $P_M(m)$ is assumed (considering, e.g., requirements to the thermal reliability of the core), then we have

$$p = \sqrt[m]{P_M(m)}. \tag{3}$$

The P value obtained and the known probability distribution of the parameter under consideration can be used to determine the limit deviation of the parameter for a cell $(\Delta\mathcal{P})^*$, with the deviation to account for the given $P_M(m)$ value. Thus, for $P_M(3) = 0.00135$ (probability of a normal distribution of a random quantity going on one side beyond the 3σ limit; this probability is often assumed as a tolerable risk value in reliability calculations):

$$P = 0.111,$$

which corresponds almost to the deviation limit of a normal distribution of the parameter (factor of overheating for a cell):

$$(\Delta\mathcal{P})^* = 1.22\sigma.$$

Translated from Atomnaya Énergiya, Vol. 49, No. 5, pp. 325-326, November, 1980. Original article submitted March 19, 1980.

0038-531X/80/4905-0783$07.50

Usually $(\Delta\mathcal{F})^{\max} = 3\sigma$ is assumed for a fuel element, and this means that the factor of overheating is reduced about 2.5 times in the case under consideration. Accordingly, the fuel temperature deviation caused by this factor is reduced.

When the channel is composed of elements of two types (e.g., fuel elements and rotating substitutes), we obtain in analogy to Eq. (1):

$$P_{M_1M_2}(m_1,m_2)=\frac{(p_1M_1)!\,(M-m_1)!\cdot(p_2M_2)!\,(M_2-m_2)!}{M_1!\,(p_1M_1-m_1)!\cdot M_2!\,(p_2M_2-m_2)!}. \quad (4)$$

For $P_1 = P_2 = P$ the problem is reduced to the preceding problem. When $P_1 \neq P_2$, one can consider various combinations of the P_1 and P_2 values which lead to a given $P_{M_1M_2}(m_1, m_2)$ value.

LITERATURE CITED

1. A. Ya. Kramerov and Ya. V. Shevelev, Design Calculations of Nuclear Reactors [in Russian], Atomizdat, Moscow (1964).
2. A. I. Klemin, Probabilistic Design Calculations in Project Work on Nuclear Reactors [in Russian], Atomizdat, Moscow (1973).
3. Principles of Not-Channel Factor Calculations for Fast Reactors, IAEA-166, Vienna (1974).
4. V. A. Khranovskii and I. M. Kurbatov, At. Energ., 44, No. 3, 258 (1978).
5. I. V. Dunin-Barkovskii and N. V. Smirnov, Theory of Probability and Mathematical Statistics in Technology [in Russian], GITTL, Moscow (1955).

HOMOGENIZATION AND HETEROGENIZATION ERRORS IN THE CALCULATION OF RBMK

S. S. Gorodkov

UDC 621.039.51.12:539.125.52

The energy distribution in a channel reactor can be calculated with about equal success with a homogeneous grid or mesh program or a heterogeneous program (based on the source–sink method). As the differences in the results of these calculations are not small (up to 1–2% in k_{eff} and up to 10-20% in the neutron flux), the question of which of the algorithms is better arises. In order to obtain an answer, we made use of the fact that various small-group cell constants are used in each algorithm without considering that these constants were obtained from a one-cell multigroup kinetic calculation which is almost the same in both algorithms. Therefore the multigroup kinetic calculation of the reactor need not be necessarily used as a standard. Let us consider the model problem of a composite lattice in which the neutron transfer is described by the two-group diffusion equation

$$\hat{D}\Delta\Phi-\hat{\Sigma}\Phi=0, \quad (1)$$

where

$$\Phi=\begin{pmatrix}\Phi_f\\ \Phi_t\end{pmatrix},\ \hat{D}=\begin{pmatrix}D_f & 0\\ 0 & D_t\end{pmatrix},\ \hat{\Sigma}=\begin{pmatrix}\Sigma_a^f+\Sigma^{1\to2}-\nu\Sigma_f^f-\nu\Sigma_f^t\\ -\Sigma^{1\to2} \qquad\qquad \Sigma_a^t\end{pmatrix}.$$

The characteristics $\hat{D}$ and $\hat{\Sigma}$ are constant over the individual cells of the composite lattice and close to the characteristics used in the calculations of high-powered water-cooled channel reactors (RBMK). Thisproblem can be exactly solved with the homogeneous grid program having a step width of the grid much smaller than the step width of the lattice. When thereafter a solution with the heterogeneous program is obtained, the difference of the results provides an idea of the error which the heterogeneous approximation causes in the calculation of RMBK. For this purpose, we replace each cell of the composite lattice by a heterogeneous cell consisting of a homogeneous moderator with a filiform source–sink configuration on the axis [1]. The neutron field component which is of angular symmetry has in the cell the following form:

$$\phi(\mathbf{r})=\hat{Z}\,[\hat{I}_0(r)+\hat{K}_0(r)\,\hat{\alpha}]\,\varphi, \quad (2)$$

Translated from Atomnaya Énergiya, Vol. 49, No. 5, pp. 326-327, November, 1980.

0038-531X/80/4905-0784$07.50

TABLE 1. Some Results of a Comparison of the Calculation of Sublattices of RBMK

Approximation	Composite lattice	Δk_{eff}, %	$\delta\bar{\Phi}_t/\bar{\Phi}_t$, %			
			Maximum in cells R	Average in cells R	In cell P	In cell C
Exact solution - homogeneous						
Heterogeneous	I	0,29	—0,50	0,36	—2,84	7,84
	II	0,14	0,37	0,25	—2,20	8,95
Homogeneous grid, version A	I	1,47	—2,88	2,06	—14,43	6,17
	II	1,80	7,52	3,85	—7,57	18,27
Homogeneous grid, version B	I	—0,34	1,57	1,10	3,76	—8,85
	II	—0,59	0,74	0,35	5,86	—10,75
Exact solution - heterogeneous						
Homogeneous-grid, version A	I	1,18	—2,54	1,89	—11,59	—1,67
	II	1,66	7,25	3,55	—5,37	9,32
Homogeneous-grid, version B	I	—0,63	1,91	1,33	7,60	—16,69
	II	—0,73	—0,69	0,47	8,06	—19,70

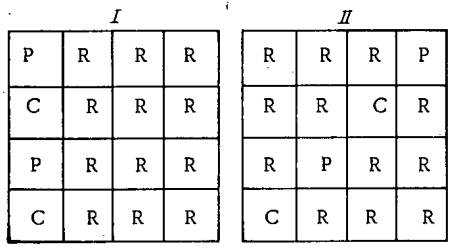

Fig. 1. Two types of composite lattices: R) technological channel; P and C) immersed and retracted absorbing rods, respectively.

where

$$\hat{z}=\begin{pmatrix}1 & 0\\ L^2/(\tau-L^2) & 1\end{pmatrix},\quad \varphi=\begin{pmatrix}\varphi_\tau\\ \varphi_L\end{pmatrix};$$

$$\hat{I}_0=\begin{pmatrix}I_0(r/\sqrt{\tau}) & 0\\ 0 & I_0(r/L)\end{pmatrix};\quad \hat{K}_0=\frac{1}{2\pi}\begin{pmatrix}K_0(r/\sqrt{\tau}) & 0\\ 0 & K_0(r/L)\end{pmatrix};$$

τ denotes the age of the neutrons; L denotes the diffusion length of the thermal neutrons in the moderator; φ_τ and φ_L denote free coefficients; and $\hat{\alpha}$ denotes a 2×2 matrix the elements of which are chosen so that the heterogeneous cell is equivalent to the initial cell. Among the several forms of equivalency we preferred the one which implies the simplest relation between the homogeneous and heterogeneous constants and requires that the ratio between the neutron leakage through the boundary and the average neutron flux over the cell ($\bar{\phi}=\hat{D}\bar{\Phi}$) is the same in the homogeneous and heterogeneous cells. This condition leads to the equation

$$\hat{\Sigma}\hat{D}^{-}=[\hat{Z}(\hat{I}_1-\hat{K}_1\hat{\alpha})]\,[\hat{Z}(\hat{I}+\hat{K}\hat{\alpha})]^{-}, \tag{3}$$

from which $\hat{\alpha}$ can be determined. In Eq. (3), I_1 and $\hat{K}_1$ denote the integrals of $(\partial/\partial n)\,I_0(r)$ and $(\partial/\partial n)\,\hat{K}_0(r)$; over the surface of the cells; and $\hat{I}$ and $\hat{K}$ denote the average values of $\hat{I}_0(r)$ and $\hat{K}_0(r)$, respectively, taken over the cell volume. The heterogeneous calculation renders the coefficients φ, whereupon $\bar{\phi}$ can be determined with the formula

$$\bar{\phi}=\hat{Z}(\hat{I}+\hat{K}\alpha)\,\varphi. \tag{4}$$

In addition to the comparison of the heterogeneous calculation with the exact calculation, the homogeneous calculation made with a single mesh point or cell was included in the comparison. The mesh points can be situated either at the centers (version A) or in the corners of the cells (version B). These schemes are used in the vast majority of reactor calculations, because a twofold reduction of the step width of a two-dimensional mesh causes an eightfold increase in the number of calculations.

The two types of composite lattices used in the calculations are shown in Fig. 1. The homogeneous characteristics of the cells are close to those used in the calculations of RBMK. Each solution was normalized to the thermal neutron flux average over active cells. The results of the comparison are shown in the first part of Table 1. The error of heterogenization is so small that it would be advantageous to use the heterogeneous calculation instead of a coarse mesh calculation in the solution of homogeneous problems of this type.

An interesting detail is that version B which is conceptually equivalent to version A is actually more accurate.

The problem may be considered from the opposite viewpoint by assuming that the heterogeneous calculation is the exact calculation. The homogenization errors of this problem are equal with an accuracy of the sign of the heterogenization errors of the preceding problem. A comparison of the coarse grid solution with the heterogeneous solution (in the case under consideration, with the exact solution) reveals that the advantage of version B over version A decreases. One can therefore say that accurately executed homogenization and heterogenization contribute very little to the overall error in the calculation of RBMK when compared with the other approximations such as the two-dimensional, the small-group, the coarse-grid approximations, etc.

LITERATURE CITED

1. S. S. Gorodkov, At. Energ., 48, No. 6, 370 (1980).

DETERMINATION OF THE FLUX PARAMETERS IN A VERTICALLY ADJUSTABLE RING CHANNEL OF A REACTOR

V. N. Oleinik

UDC 621.039.5:532.5

The distribution of the coolant over the core cross section in shell-type reactors depends on the features of the flow at the entry section of the inner-shell hydraulic system. One of these sections in a water-moderated water-cooled power reactor is the vertically adjustable ring channel between the reactor shell and its cut-out portion. The coolant is supplied to the vertically adjustable ring channel via one or several inlet nozzles, i.e., the coolant supply is centered. Vortex zones develop close to the inlet nozzles. The fields of velocity and hydrodynamic pressure over the circumference of the vertically adjustable ring channel are significantly nonuniform [1]. Farther from the inlet nozzles the distribution of the hydrodynamic parameters in the vertically adjustable ring channel becomes more uniform. However, a full equilibration of the flux in the exit cross section of a vertically adjustable ring channel may not occur. It is therefore of great importance in practice to determine by calculation the hydrodynamic flux parameters over the length and the circumference of the vertically adjustable ring channel for various numbers of operative inlet nozzles. Experiments have shown that the hydraulic flow losses are small beyond the limits of the vortex zones in a vertically adjustable ring channel. We therefore determine the hydrodynamic flow parameters under the assumption that the flow is related to a potential.

Assume that a flow of nonviscous liquid or fluid enters through the inlet nozzle in a vertically adjustable ring channel having internal radius R_1, external radius R_2, and an impenetrable flow separator. Since the width of the vertically adjustable ring channel is always much smaller than its average radius $R = 0.5 (R_1 + R_2)$, the changes of the flow parameters over the width of the vertically adjustable channel can be disregarded. Thus, we consider the flow of a nonviscous fluid on some cylindrical surface having radius R and height H.

We represent the inlet nozzle as a source with the output Q and the linear dimensions 2δ along the axis and $2R\varepsilon$ over the circumference (Fig. 1).

The equation for the velocity potential $U(z, \varphi)$ in the flow region under consideration is of the form

$$\frac{1}{R^2}\frac{\partial^2 U}{\partial \varphi^2}+\frac{\partial^2 U}{\partial^2 z}=\begin{cases} Q/4\delta\varepsilon R & z_0-\delta<z<z_0+\delta;\\ & \varphi_0-\varepsilon<\varphi<\varphi_0+\varepsilon;\\ 0 & z_0-\delta>z;\ z_0+\delta<z;\\ & \varphi_0-\varepsilon>\varphi;\ \varphi_0+\varepsilon<\varphi. \end{cases} \quad (1)$$

Translated from Atomnaya Énergiya, Vol. 49, No. 5, pp. 327-329, November, 1980. Original article submitted April 2, 1980.

 0038-531X/80/4905-0786$07.50

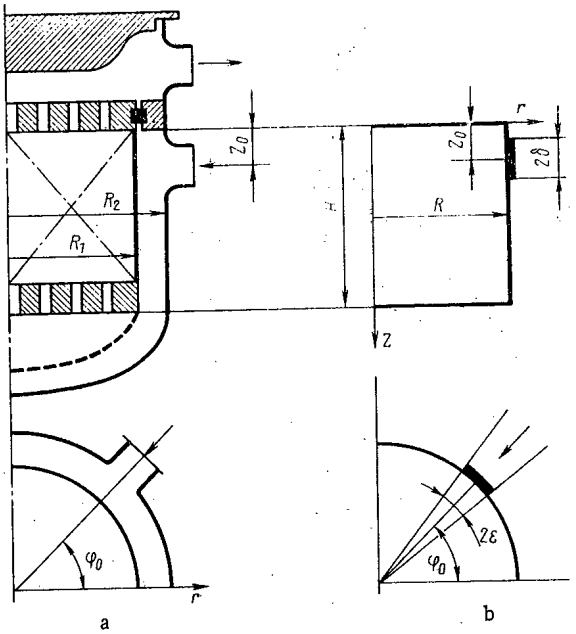

Fig. 1. Design (a) and calculated (b) scheme of the vertically adjustable ring channel of a water-moderated water-cooled power reactor.

The boundary conditions are

$$z = 0; \quad 0 < \varphi < 2\pi; \quad \partial U/\partial z = 0; \tag{2}$$

$$z = H; \quad 0 < \varphi < 2\pi; \quad \partial U/\partial z = \psi(\varphi); \tag{3}$$

$$0 < z < H; \quad \varphi = \varphi_0 + \pi; \quad \partial U/\partial \varphi = 0. \tag{4}$$

We use the method of separation of variables [2] for obtaining the solution to Eq. (1) at the boundary conditions (2)-(4):

$$U(z, \varphi) = \sum_{n=1}^{\infty} \left[\frac{a_n}{\lambda_n \operatorname{sh} \lambda_n H} \operatorname{ch} \lambda_n z - \frac{Q \cos \lambda_n R\varphi_0}{\pi R \lambda_n \operatorname{sh} \lambda_n H} \operatorname{ch} \lambda_n z_0 \operatorname{ch} \lambda_n (H - z) \right] \cos \lambda_n R\varphi, \tag{5}$$

where a_n denotes the coefficients of expanding the function $\psi(\varphi)$ in a Fourier series. The velocity components of the potential flow are obtained from Eq. (5):

$$v_z = \frac{\partial U}{\partial z} = \sum_{n=1}^{\infty} \left[\frac{a_n}{\operatorname{sh} \lambda_n H} \operatorname{sh} \lambda_n z + \frac{Q \cos \lambda_n R\varphi_0 \operatorname{ch} \lambda_n z_0}{\pi R \operatorname{sh} \lambda_n H} \operatorname{sh} \lambda_n (H - z) \right] \cos \lambda_n R\varphi; \tag{6}$$

$$v_\varphi = \frac{1}{R} \frac{\partial U}{\partial \varphi} = \sum_{n=1}^{\infty} \left[\frac{Q \cos \lambda_n R\varphi_0 \operatorname{ch} \lambda_n z_0}{\pi R \operatorname{sh} \lambda_n H} \operatorname{ch} \lambda_n (H - z) - \frac{a_n}{\operatorname{sh} \lambda_n H} \operatorname{ch} \lambda_n z \right] \sin \lambda_n R\varphi. \tag{7}$$

The eigenvalues λ_n are determined from Eq. (7) by using condition (4) in it:

$$\lambda_n = n\pi/R\,(\varphi_0 + \pi). \tag{8}$$

When the coolant arrives in a vertically adjustable ring channel through several inlet nozzles, the velocity components of the potential flow can be determined with the technique of flow superposition.

When the velocity values are known, the distribution of hydrodynamic pressure can be calculated with the Bernoulli equation, which applies to all points of the flow region under consideration:

$$\frac{p - p_N}{0.5\rho v_N^2} = 1 - \frac{v_z^2 + v_\varphi^2}{v_N^2}. \tag{9}$$

where v_N and p_N denote the velocity and hydrodynamic pressure of the flow in the inlet nozzle, respectively.

In order to check the resulting theoretical solution, the hydrodynamic flow characteristics in a vertically adjustable ring channel were experimentally checked on a sectional model. A 0.02-m-wide ring channel was formed by two 0.95-m-high coaxial cylinders. The inner cylinder was made from an aluminum alloy (radius

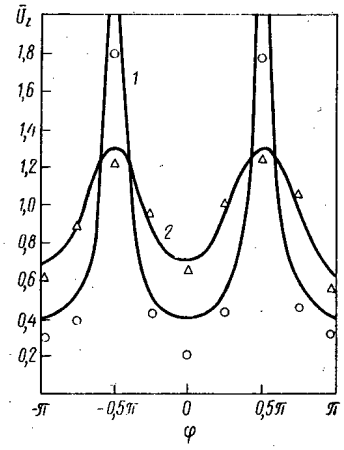

Fig. 2. Distribution of the axial velocity along the periphery of the ring channel during operation of two input nozzles. Calculated: 1, 2) $\bar{z}$ = 2.0 and 3.5; experimental: ○, △) $\bar{z}$ = 2.0 and 3.5, respectively.

of the outer surface 0.445 m) and imitated the cut-out reactor portion; the outer cylinder was made from Plexiglas (inner radius of the surface 0.465 m) and imitated the reactor shell. In order to supply air to the ring channel, the outer cylinder had two symmetrically arranged inlet nozzles with a diameter of 0.15 m. The end face close to the nozzle of the ring channel was covered with a metal end plate. The air left the ring channel through the other end face, which was free in one series of experiments and covered by a removable throttling-down grid with adjustable hydraulic drag in another series. The velocity of the air in the ring channel was measured with several movable Pitot–Prandtl tubes; the hydrodynamic pressure on the inner surface of the outer cylinder was measured with a U-shaped manometer filled with water.

It was established in tests that for a drag coefficient ≥ 5 for the porous grid placed at the outlet of the ring channel, the circular inhomogeneity in the distribution of the axial velocity component in the exit cross section disappeared. Therefore the velocity and the hydrodynamic pressure in the ring channel having the above geometry were calculated with boundary condition (3) in the form $\psi(\varphi) = \text{const}$. When the calculated distribution was compared with the experimental values of the axial velocity (Fig. 2), it was observed that substantial differences exist at small z values. The differences result from vortex zones near the inlet nozzles in the real flow. For larger z values, when the vortex zones are closed, the differences between the results of the calculations and the experimental values decrease, and for $\bar{z} = z/d_N = 3$, the calculated axial velocity values practically coincide with the experimental values. This point is confirmed by the corresponding comparison between calculated and experimental hydrodynamic pressure values.

Thus, with a known geometry of the vertically adjustable ring channel, the distribution of the hydrodynamic flow parameters in the channel outlet cross section can be obtained with the calculation scheme considered above, which is based on the assumption of a flow potential.

LITERATURE CITED

1. M. S. Fomichev, B. F. Berzina, and A. I. Emel'yanov, Problems of Atomic Science and Technology, Ser. Reactor Construction [in Russian], No. 2 (13), 29 (1976).
2. G. N. Polozhii, Equations of Mathematical Physics [in Russian], Vysshaya Shkola, Moscow (1964).

YIELDS OF ^{123}I, ^{124}I, ^{125}I, ^{126}I, ^{130}I, ^{131}I, AND ^{132}I UPON THE IRRADIATION OF TELLURIUM BY PROTONS, DEUTERONS, AND α PARTICLES AND ANTIMONY BY α PARTICLES

P. P. Dmitriev, M. V. Panarin, and Z. P. Dmitrieva

UDC 539.172.12

The half-life and energy of the γ quanta of ^{123}I are very suitable for use in medicine. The radioisotopic purity of ^{123}I, which is determined by the admixtures of other iodine radionuclides, is of principal significance in connection with its use in medicine. Therefore it is important to know which radionuclides are formed and in what amount in the method selected to obtain ^{123}I.

The yields of $^{123-126,130-132}I$ are measured in this paper for a thick target for the four most effective methods of obtaining ^{123}I: Te + p, Te + d, Te + α, and Sb + α. The yields of iodine nuclides are measured at a maximum particle energy of ~22 MeV (protons and deuterons) and ~44 MeV (α particles) and at five values of the particle energy less than the maximum value. The nuclides are formed mainly in reactions of the type (αxn) with x = 1, 2, and 3 and (αpxn) with x = 1 and 2.

We irradiated metal samples of tellurium and antimony in the deflected beam of the FÉI cyclotron (Obninsk), and we varied the particle energy with aluminum retarding foils. We identified the radionuclides from their γ emission and half-life, and we measured the activity of a nuclide from the number of pulses in the photopeak of a selected γ line. The following values of the half-life of the nuclides and the energy and quantum yields of the γ lines from [1] are used: ^{123}I (13.3 h; γ 159.0 keV; 82.9%), ^{124}I (4.18 days; γ 602.7 keV; 62.8%), ^{125}I (59.9 days; KX 28.03 keV + γ 35.48 keV; 146%), ^{126}I (12.9 days; γ 666.4 keV; 33%), ^{130}I (12.4 days; γ 536.1 keV; 100%), ^{131}I (8.04 days; γ 364.5 keV; 82%), and ^{132}I (2.3 h; γ 772.6 keV; 76%). The procedure for measuring the activity of the nuclides (except for ^{125}I) and the integrated irradiation current of the samples is similar to that described in [2].

We radiochemically separated ^{125}I from the samples 4 months after the irradiation, and we measured the activity of dry sources of ^{125}I similarly to the measurement of the activity of ^{28}Mg from the 30.6-keV γ line in [3]. The results of the measurements of the yields of $^{123-126,130-132}I$ are given in Table 1. The error in measurement of the yields is 12-13% (16-18% for ^{125}I) and is produced mainly by systematic errors in the measurement of nuclide activity and integrated current.

Upon the irradiation of tellurium, ^{120}I ($T_{1/2}$ = 1.35 h), ^{121}I ($T_{1/2}$ = 2.12 h), and ^{133}I ($T_{1/2}$ = 20.8 h) are also formed. The admixture of $^{120,121}I$ is negligibly small 10-20 h after irradiation; however, ^{121}I decays into ^{121}Te ($T_{1/2}$ = 17 days), and purification to free ^{123}I of ^{121}Te may be necessary. The yield of the reaction ^{130}Te (αp) ^{133}I at E_α = 44 MeV is estimated to be $\lesssim 20\ \mu Ci/\mu A \cdot h$.

Upon the irradiation of tellurium by α particles the radionuclides $^{120,121,123,125,131,132}I$ are also accordingly obtained through the isobaric nuclides: ^{120}Xe ($T_{1/2}$ = 40 min), ^{121}Xe ($T_{1/2}$ = 40.1 min), ^{123}Xe ($T_{1/2}$ = 2.08 h), ^{125}Xe ($T_{1/2}$ = 17.04 h), $^{131m,g}Te$ ($T^m_{1/2}$ = 30 h, $T^g_{1/2}$ = 25.0 min), and ^{132}Te ($T_{1/2}$ = 78.2 h). In this paper we measured the activity of $^{123,125,131}I$ after the decay of $^{123,125}Xe$ and $^{131m,g}Te$, and we calculated the yield for the end of irradiation. The activity of ^{132}I, which is formed as a result of the decay of ^{132}Te, is small due to the comparatively long half-life of ^{132}Te and the low yield of the reaction ^{130}Te (α2p) ^{132}Te. According to published data, the cross sections of (αxn) reactions are approximately 8-10 times greater than the cross sections of (αpxn) reactions in the region of nuclei with mass number A ≈ 120-130, and when tellurium is irradiated by α particles, ~80-90% $^{123,125}I$ is formed through $^{123,125}Xe$.

As is evident from Table 1, when thick targets made out of natural tellurium and antimony are irradiated, ^{123}I is obtained with large admixtures of other radionuclides of iodine. We will point out some ways to

Translated from Atomnaya Énergiya, Vol. 49, No. 5, pp. 329-330, November, 1980. Original article submitted April 18, 1980.

0038-531X/80/4905-0789$07.50

TABLE 1. Yields of Iodine Nuclides for Different Methods of Obtaining ^{123}I, $\mu Ci/\mu A \cdot h$*

Particle energy, MeV	^{123}I	^{124}I	^{125}I	^{126}I	^{130}I	^{131}I	^{132}I
			Te + p				
22,2±0,3	1127	264	31,4	97,0	1100		
21,0±0,3	910	195	26,0	72,5	1095		
20,0±0,3	720	148	21,6	72,0	1090		
17,1±0,4	334	91	15,2	55,0	972		
14,3±0,4	143	52	6,9	34,5	760		
9,8±0,5	35	15	1,2	9,2	320		
			Te + d				
22,1±0,3	400	127	8,5	91	3350	105	
21,0±0,3	288	109	6,9	86	3170	101	
18,4±0,4	194	68	3,7	71	2750	84	
17,1±0,4	163	51	2,6	62	2380	75	
12,3±0,5	69	8	0,6	23	1150	38	
9,5±0,5	24	1,1	0,2	9	440	14	
			Te + α				
43,4±0,5	39,2	1,23	0,83	0,94	37,4	3,9	224
38,6±0,5	11,8	0,65	0,41	0,42	20,4	1,8	170
33,2±0,5	1,8	0,30	0,22	0,15	7,3	0,85	69
31,0±0,6	1,2	0,25	0,15	0,08	4,3	0,58	43
26,6±0,7	0,6	0,12	0,09	0,03	1,8	0,3	13
19,2±0,8	0,2	0,02	0,02	0,01	0,5	0,1	2
			Sb + α				
43,9±0,5	1360	161	5,2	4,60			
38,8±0,5	1227	111	5,1	4,55			
33,4±0,6	950	46	4,5	4,35			
27,0±0,7	450	13	2,7	3,65			
19,6±0,8	65	7	0,25	1,85			
16,5±0,9	15	5	0,05	0,85			

*1 Ci = $3.700 \cdot 10^{10}$ Bq.

obtain ^{123}I of high purity through ^{123}Xe:

1) the reactions ^{122}Te (α3n) ^{123}Xe and ^{122}Te (^{3}He 2n) ^{123}Xe, enriched in ^{122}Te; the use of a thin target lowers the admixture of ^{125}I. A very large yield of ^{123}I is obtained from the reactions ^{127}I (p5n) ^{123}Xe (threshold 37 MeV) and ^{127}I (d6n) ^{123}Xe (threshold 39.6 MeV);

2) the reaction ^{122}Te (dn) ^{123}I, enriched in ^{122}Te;

3) the reaction ^{124}Te (p2n) ^{123}I, enriched in ^{124}Te, thin target;

4) the reaction ^{121}Sb (α2n) ^{123}I, thin target, and $E_\alpha \approx 28$ MeV. Enrichment of ^{121}Sb to about 99% increases the yield of ^{123}I by approximately two orders of magnitude and sharply reduces the admixtures of $^{125,126}I$.

It is possible to construct from the data of Table 1 the dependences of the yield of $^{123-126,130-132}I$ on the energy of the bombarding particles, which one can use to determine the target thickness and the particle energy for obtaining ^{123}I of high purity. The data of Table 1 also permit selecting the optimal means for obtaining other radionuclides of iodine.

A large number of publications have been devoted to the obtaining of ^{123}I. There are bibliographical citations in [4] to practically all the papers on obtaining ^{123}I published up to 1976. Yield curves of the radionuclides of iodine are lacking, and some particular problems in obtaining ^{123}I are usually discussed. The excitation functions of the reactions ^{121}Sb (α2n) ^{123}I and $^{121,123}Sb$ (α, n, 2n) ^{124}I are measured in [5, 6], and those of the reactions ^{124}Te (p2n) ^{123}I and ^{124}Te (pn) ^{124}I in [7]. The yield curves of $^{123,124}I$ are obtained by means of the integration of the excitation functions, and satisfactory agreement of the data of [6, 7] with the results of this paper is observed. Obtaining ^{123}I through ^{123}Xe has been investigated in [8].

LITERATURE CITED

1. N. G. Gusev and P. P. Dmitriev, Quantum Emission of Radioactive Nuclides [in Russian], Atomizdat, Moscow (1977).
2. P. P. Dmitriev and G. A. Molin, At. Energ., 48, No. 2, 122 (1980).
3. P. P. Dmitriev and G. A. Molin, At. Energ., 46, No. 3, 185 (1979).
4. R. Weinreich, in: Proc. Conf. Panel Discussion Iodine-123 in Western Europe, KFA-Jülich (1976), p. 49.
5. Y. Murakami et al., in: New Development Radiopharm. Labelled Composition, Vol. 1, IAEA, Vienna (1973), p. 257.
6. I. Watson et al., J. Inorg. Nucl. Chem., 35, 3047 (1973).
7. K. Kondo et al., Int. J. Appl. Rad. Isotopes, 28, 395 (1977).
8. D. Syme et al., ibid., 29, 29 (1978); V. Sodd et al., ibid., 24, 171 (1973); M. Guillaume et al., ibid., 26, 703 (1975); R. Weinreich et al., ibid., 25, 535 (1974); H. Lundqvist et al., ibid., 30, 39 (1979).

THE γ CONSTANT OF A RADIOACTIVE NUCLIDE IN THE INTERNATIONAL SYSTEM OF UNITS

N. G. Gusev and V. P. Mashkovich

UDC 539.166.2

Starting on January 1, 1980 the International System of Units (SI) has been introduced in the Soviet Union as obligatory for use in the national economy of the country [1, 2]. It is necessary in this connection to discuss the peculiarities of the usage of some widely employed units of physical quantities in the SI units.

One of these is the γ constant of a radionuclide, which is the dosage characteristic of the γ emission field of a point isotropic nuclide with fixed values of the activity Q of the nuclide and the distance r to the point of detection. The γ constant is widely used in our country and abroad in connection with the solution of problems of radiation physics, technology, dosimetry, and shielding from ionizing radiations [2-7]. Physicists have usually defined this quantity in non-SI units of the strength of the exposure dose, namely $R \cdot cm^2/h \cdot mCi$ for Q = 1 mCi and r = 1 cm [3-8].

For a point nuclide with activity Q (mCi) isotropically emitting γ quanta of m different energy groups with an energy E_{0i} (MeV) of the i-th group and a quantum yield n_i (γ quanta/disintegration), physicists have calculated the γ constant in non-SI units [$R \cdot cm^2/h \cdot mCi$] from the formula

$$\Gamma = \frac{3.7 \cdot 10^7 \frac{\text{disint.}}{\text{sec} \cdot \text{mCi}} \sum_{i=1}^{m} E_{0,i} \frac{\text{MeV}}{\text{quanta}} n_i \frac{\text{quanta}}{\text{disint.}} \bar{\gamma}_i \frac{\text{cm}^2}{\text{g}} 1.602 \cdot 10^{-6} \frac{\text{erg}}{\text{MeV}} 3600 \frac{\text{sec}}{\text{h}}}{4\pi\, 87.3\ \text{erg/g} \cdot \text{R}} = 194.5 \sum_{i=1}^{m} E_{0,i} n_i \bar{\gamma}_i \left[\frac{\text{R} \cdot \text{cm}^2}{\text{h} \cdot \text{mCi}}\right], \quad (1)$$

where $\bar{\gamma}_i$ is the mass coefficient of the energy absorption of γ quanta of the i-th energy group in air and 87.3 is the energy equivalent of 1 R in air.

In SI units the use of the unit of Kl/kg for the exposure dose is inconvenient and inadvisable in connection with the solution of practical problems. The values of the exposure (in roentgens) and absorbed (in rads) doses differ in non-SI units by only a factor of 1.14 in all, whereas in SI units the discrepancy reaches several orders of magnitude, and there is no simple integral relationship between them (1 Kl/kg = $3.88 \cdot 10^3$ R). In addition the concept of an exposure dose is only valid for one kind of radiation – γ quanta usually with energy $E_0 \lesssim 3$ MeV.

The most suitable characteristic of a γ-radiation field in connection with the definition of the γ constant in SI units is the absorbed dose in air. It is valid for all kinds of ionizing radiation, does not introduce ambiguous parameters into the calculations, is applicable for determining the fields in any dosage range, is convenient for the solution of many problems, and its unit of measurement has a simple integral relationship with the non-SI unit (1 Gy = 100 rd).

Translated from Atomnaya Énergiya, Vol. 49, No. 5, pp. 330-332, November, 1980. Original article submitted April 24, 1980.

0038-531X/80/4905-0791 $07.50

TABLE 1. The Values of Γ and Γ_{SI} of Some of the Most Widely Used Radionuclides

Nuclide	$T_{1/2}$	Γ, $\frac{R \cdot cm^2}{h \cdot mCi}$ [6]	Γ_{SI}, $\frac{aGy \cdot m^2}{sec \cdot Bq}$ †	Nuclide	$T_{1/2}$	Γ, $\frac{R \cdot cm^2}{h \cdot mCi}$ [6]	Γ_{SI}, $\frac{aGy \cdot m^2}{sec \cdot Bq}$ †
$^{24}_{11}Na$	15,005 h	18,14	119,4	$^{141}_{58}Ce$	32,50 days	0,433	2,851
$^{56}_{25}Mn$	2,578 h	8,468	55,75	$^{192}_{77}Ir$	74,02 days	4,605	30,32
$^{60}_{27}Co$	5,272 yr	12,85	84,60	$^{198}_{79}Au$	2,6946 days	2,305	15,18
$^{64}_{29}Cu$	12,71 h	1,127	7,420	$^{203}_{80}Hg$	46,76 days	1,292	8,506
$^{134}_{55}Cs$	2,062 yr	8,724	57,44	$^{226}_{88}Ra$ ‡	1600 yr	9,031	59,46
$^{137}_{55}Cs + ^{137}_{56}Ba^m$	30,174 yr	3,242	21,34	$^{226}_{88}Ra$ **	1600 yr	8,4	55,3

*The values of Γ are defined in [6] with the use of the energy equivalent of the roentgen, W = 87.7 ergs/g · R.

† The values of Γ_{SI} are calculated from the data of [6] with a correction to W = 87.3 ergs/g · R.

‡ Radium in equilibrium with the main daughter products of disintegration through RaD.

**Radium in equilibrium with the main daughter products of disintegration through RaD with an initial platinum filter 0.5 mm in thickness.

Therefore one should define the γ constant as follows in SI units. The strength of the absorbed dose in air produced by the γ emission of a point isotropic nuclide with an activity of 1 Bq at a distance of 1 m from it without initial filtering of the radiation is called the γ constant. The γ constant is expressed in aGy · m^2/sec · Bq.* We will denote this quantity as Γ_{SI}. In contrast to the γ constant in non-SI units, Γ_{SI} is calculated for a distance to the point of detection (r = 1 m) and a source activity (Q = 1 Bq) expressed in fundamental and derived SI units.

It is necessary to calculate Γ_{SI} from the formula

$$\Gamma_{CH} = \frac{1\frac{\text{disint.}}{\text{sec} \cdot \text{Bq}} \sum_{i=1}^{m} E_{0,i}\frac{\text{MeV}}{\text{quanta}} n_i \frac{\text{quanta}}{\text{disint.}} \bar{\gamma}_i \frac{m^2}{kg} 1{,}602 \cdot 10^{-13} \frac{J}{\text{MeV}} 10^{18} \frac{aGy}{Gy}}{4\pi \cdot 1 \frac{J}{kg \cdot Gy}} = 12747 \sum_{i=1}^{m} E_{0,i} n_i \bar{\gamma}_i \left[\frac{aGy \cdot m^2}{sec \cdot Bq}\right]. \quad (2)$$

The coefficients in Eqs. (1) and (2) are obvious from the cited dimensions.

It is easy to determine from Eqs. (1) and (2) the link between the γ constants:

$$\Gamma_{SI}\left(\frac{aGy \cdot m^2}{sec \cdot Bq}\right) = 6.554\Gamma\left(\frac{R \cdot cm^2}{h \cdot mCi}\right). \quad (3)$$

The values of the γ constants of widely used radionuclides are given in Table 1. We must make several important remarks with regard to the practical use of the γ constants.

1. The value of Γ_{SI} is numerically equal to the absorbed dose in air, expressed in aGy, produced by the γ emission of a point nuclide for one disintegration event at a distance r = 1 m from an isotropic source.

2. The strength of the absorbed dose in air P (aGy/sec) for a point nuclide with activity Q (Bq) at a distance r (m) from an isotropic source can be readily calculated from the formula

$$P = Q\Gamma_{SI}/r^2. \quad (4)$$

3. In converting from the strength of the absorbed dose in air P (aGy/sec) calculated from Eq. (4) to the strength of the equivalent dose P_{eq} (aZv/sec) for γ radiation,† one can use the relationship

$$\frac{P_{eq}}{P} = \frac{\bar{\gamma}_t}{\bar{\gamma}}, \quad (5)$$

where $\bar{\gamma}_t$ and $\bar{\gamma}$ are the mass coefficients of the energy absorption of γ quanta in tissue and air, respectively. We note that the quality coefficient is taken equal to unity in Eq. (5).

For soft biological tissue (ρ = 1 g/cm^3, $\bar{\gamma}_t = \bar{\gamma}_{H_2O}$) and for γ-quanta energy E_0 = 0.08–10 MeV, we get $\bar{\gamma}_t/\bar{\gamma}$ = 1.09 ± 0.02. Consequently,

$$P_{eq} = 1.09P = 1.09Q\Gamma_{SI}/r^2. \quad (6)$$

*1 aGy = 10^{-18} Gy.

†Zv = 100 rem.

erally adopted meaning of this quantity [8] with the use of the γ constant Γ_{Si} from the formula

$$m = Q\Gamma_{SI}/(3.7 \cdot 10^7 \cdot 55.3), \tag{7}$$

where $3.7 \cdot 10^7$ is the number of disintegrations per second of the activity in becquerels of a sample with a γ equivalent of 1 mg·equiv. Ra and 55.3 is the γ constant of radium in equilibrium with the main daughter products of disintegration through RaD with an initial platinum filter 0.5 mm thick (see Table 1).

One can find the strength of the absorbed dose in air P (aGy/sec) of a point isotropic sample with γ equivalent m (mg·equiv. Ra) at a distance r(m) from it by using the formula

$$P = 3.7 \cdot 10^7 m 55.3/r^2. \tag{8}$$

In conclusion, we note that when it is necessary to calculate the exposure dose in SI units one can, similarly to Γ_{SI}[aGy·m^2/sec·Bq], determine the γ constant from the exposure dose Γ_{SI}[aA·m^2/kg·Bq], whereupon Γ_{SI}[aA·m^2/kg·Bq] = 0.1939 Γ[R·cm^2/h·mCi].

LITERATURE CITED

1. COMECON Standard ST SEV 1052-78, "Metrology. Units of physical quantities," Standartov, Moscow (1978).
2. Procedural Pointers, the Introduction and Use of ST SEV 1952-78, "Metrology. Units of Physical Quantities" [in Russian], RD 50-160-79, Standartov, Moscow (1979).
3. N. G. Gusev, Handbook on Radioactive Emissions and Shielding [in Russian], Medgiz, Moscow (1956).
4. N. G. Gusev, V. P. Mashkovich, and G. V. Obvintsev, Gamma Radiation of Radioactive Isotopes and Fission Products [in Russian], Fizmatgiz, Moscow (1958).
5. N. G. Gusev, V. P. Mashkovich, and B. V. Verbitskii, Radioactive Isotopes as Gamma Emitters [in Russian], Atomizdat, Moscow (1964).
6. N. G. Gusev and P. P. Dmitriev, Quantum Radiation of Radioactive Nuclides. Handbook [in Russian], Atomizdat, Moscow (1977).
7. N. G. Gusev and P. P. Dmitriev, Quantum Radiation of Radioactive Nuclides, Data Handbook, Pergamon Press, Oxford (1979).
8. N. G. Gusev et al., Shielding from Ionizing Radiation, Vol. 1, Physical Principles of Radiation Shielding [in Russian], Atomizdat, Moscow (1969).

THICK TARGET YIELDS OF THE $^{12}C(p, \gamma)^{13}N$ REACTION

Yu. P. Antuf'ev, V. M. Mishchenko,
A. I. Popov, V. E. Storizhko,
and N. A. Shlyakhov

UDC 539.144.6;539.172.12

Work [1] described methods of diagnosing very powerful pulsed ion beams using nuclear reactions. During an examination of the possibility of using the $^{12}C(p, \gamma)^{13}N$ reaction for this purpose, it was shown that the data in [2, 3] concerning the yield of the $^{12}C(p, \gamma)^{13}N$ reaction, measured at $E_p = 1.0$ MeV, are uncertain by more than 30%. An earlier publication [4] presented the yield of the $^{12}C(p, \gamma)^{13}N$ reaction ($Y = 7.3 \cdot 10^{-10}$ ^{13}N/proton) measured by the instantaneous radiation of γ quanta at 2.365 MeV. However, this work did not present the proton energy at which the yield of the reaction was measured and did not calculate the fraction of the $^{13}C(p, \gamma)^{14}N$ reaction which yields γ quanta at 2.312 MeV.

Since the use of the $^{12}C(p, \gamma)^{13}N$ reaction for analytical applications is increasing, we decided to measure its yield by the β^+ decay of the ^{13}N radionuclides with the goal of obtaining additional data.

Set-Up for Measuring the Reaction Yield and Data Analysis

The work was conducted on the electrostatic accelerator KhFTI. The measurements were performed by the following methods. A current from the integrator opened a shutter at the starting signal, and a beam of protons began to bombard the carbontarget. Simultaneously, clocks started up, measuring the irradiation time of the target by protons. After an accumulation of a given charge Q, the integrator produced a signal at which the shutter stopped the proton beam, the clocks stopped, and the accumulator AI-4096-3M began to work according to a program of "slow time analysis." After this, the target moved from the position of "irradiation" into the position of "measurement" and the group of time spectra began. The time of the spectrum group was $\sim 3\tau$ (2400 seconds). The γ quanta of energy 511 keV were recorded by a NaI(Tl) crystal with dimensions 150 × 100 mm. The calculated coincidence efficiency was ~95% for a time window 50 nsec wide. The targets were prepared from reactor-grade graphite of a natural isotopic composition (containing 98.9% ^{12}C).

The lifetime τ of the nucleus ^{13}N and the initial number of counts per unit time of the detecting system N_1 were obtained by a computer fitting of the experimental time spectra by an exponential of the form $N = N_1 \exp(t/\tau)$, describing the decay of radioactive nuclei. To find the lifetime of the ^{13}N nucleus with minimal error, all of the measured time spectra were summed by channels to obtain the time spectrum used for work on the computer.

The reaction yield is calculated according to the formula

$$Y = \frac{N_1 \tau}{\varepsilon q} \left(\frac{t_{rad}/\tau}{1 - \exp(-t_{rad}/\tau)} \right),$$

where N_1 is the initial number of counts per unit of time registered in the system, τ is the lifetime of the nucleus ^{13}N obtained from analysis of the time spectra on the computer, q is the total number of protons incident on the target, ε is the efficiency of the detecting system, determined by the ^{22}Na source from the OSGI collection whose activity was defined with an error of ± 5%, and t_{rad} is the time of irradiation of the target by protons. Thus, as was seen in [2], the irradiation time of the sample was (0.1-0.2) τ, so that we can decrease the error associated with possible variation of the beam current during the irradiation time.

To determine the detection efficiency ε we introduced a correction for the dead time of the recording apparatus and for the coincidence of γ quanta with energies 1.28 and 0.511 MeV. With the goal of decreasing such corrections, the distance of the source from the surface of the NaI(Tl) crystal was chosen to be 120 mm. In this arrangement the fraction of coincidences of γ quanta of energies 1.28-0.511 MeV was less than 1%. The

Translated from Atomnaya Énergiya, Vol. 49, No. 5, pp. 332-333, November, 1980. Original article submitted May 13, 1980.

0038-531X/80/4905-0794$07.50

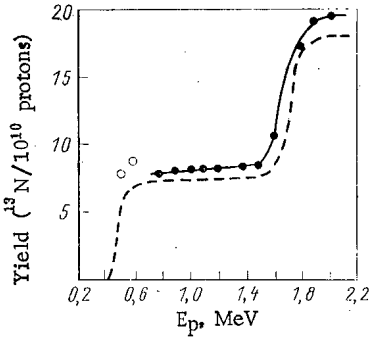

Fig. 1. Thick target yield of $^{12}C(p, \gamma)^{13}N$ reaction: ---) data [2]; ●) our data; —) yield function by points; ○) reaction yield measured with an H_2^+ beam.

yield of the $^{12}C(p, \gamma)^{13}N$ reaction was measured with an error of ± 7%.

Results of the Measurements

Our investigation determined the yield of the $^{12}C(p, \gamma)^{13}N$ reaction for eleven proton energies using H_1^+ ions and for two proton energies (541 keV and 592 keV) using H_2^+ ions. The data obtained concerning the yield of the $^{12}C(p, \gamma)^{13}N$ reaction are shown in Fig. 1. Here we can see the dependence of the yield of the $^{12}C(p, \gamma)^{13}N$ reaction on proton energy taken from [2]. It is evident that the reaction yield measured at proton energies of 541 and 592 keV significantly exceeds the data of [2]; this can be explained by a fraction of the $^{12}C(d, n)^{13}N$ reaction, conditioned by an absence of deuterium D_1^+ ions in the H_2^+ beam. It follows that due to the peculiarities of the operation of hf ion sources, the H_2^+ beams are enriched by D_1^+ ions in comparison with the natural isotopic composition of hydrogen. The estimates show that during the use of hydrogen ion beams of natural isotopic composition, the fraction of the $^{12}C(d, n)^{13}N$ reaction will not exceed 2-3% at hydrogen ion energies up to 600 keV.

The reaction yield we measured at $E_p = 1.0$ MeV, $Y = 8.14 \pm 0.64 \cdot 10^{-10}$ ^{13}N/proton, and the ratio of the reaction yields $Y(2.0\ \text{MeV})/Y(1.0\ \text{MeV}) = 2.41 \pm 0.05$ are in good agreement with the data in [2]. With the data of this work, we can adopt the value of the yield of the $^{12}C(p, \gamma)^{13}N$ reaction at a proton energy $E_p = 1.0$ MeV as

$$Y = (7.92 \pm 0.50) \cdot 10^{-10}\ ^{13}\text{N/proton}.$$

The value obtained for the lifetime of the ^{13}N nucleus is $\tau = 862.76 \pm 0.88$ sec, in good agreement with the lifetime $\tau = 862.24 \pm 0.24$ sec corresponding to the accepted value of the ^{13}N half-life, 9.961 ± 0.004 min [5].

LITERATURE CITED

1. F. Young, J. Golden, and C. Kapetanakos, Rev. Sci. Instrum., 48, No. 4, 432 (1977).
2. J. Seagrave, Phys. Rev., 84, 1219 (1951).
3. F. Riess, et al., Phys. Rev., 176, 1140 (1968).
4. W. Fowler and C. Lauritsen, Phys. Rev., 76, 314 (1949).
5. F. Ajzenberg-Selove, Nucl. Phys., A152, 31 (1970).

NEW RUSSIAN JOURNALS

IN ENGLISH TRANSLATION

BIOLOGY BULLETIN

Izvestiya Akademii Nauk SSSR, Seriya Biologicheskaya

The biological proceedings of the Academy of Sciences of the USSR, this prestigious new bimonthly presents the work of the leading academicians on every aspect of the life sciences—from micro- and molecular biology to zoology, physiology, and space medicine.

Volume 8, 1981 (6 issues) $225.00

SOVIET JOURNAL OF MARINE BIOLOGY

Biologiya Morya

Devoted solely to research on marine organisms and their activity, practical considerations for their preservation, and reproduction of the biological resources of the seas and oceans.

Volume 7, 1981 (6 issues) $145.00

WATER RESOURCES

Vodnye Resursy

Evaluates the water resources of specific geographical areas throughout the world and reviews regularities of water resources formation as well as scientific principles of their optimal use.

Volume 8, 1981 (6 issues) $250.00

HUMAN PHYSIOLOGY

Fiziologiya Cheloveka

A new, innovative journal concerned *exclusively* with theoretical and applied aspects of the expanding field of human physiology.

Volume 7, 1981 (6 issues) $225.00

SOVIET JOURNAL OF BIOORGANIC CHEMISTRY

Bioorganicheskaya Khimiya

Features articles on isolation and purification of naturally occurring, biologically active compounds; the establishment of their structure, methods of synthesis, and determination of the relation between structure and biological function.

Volume 7, 1981 (12 issues) $275.00

SOVIET JOURNAL OF COORDINATION CHEMISTRY

Koordinatsionnaya Khimiya

Describes the achievements of modern theoretical and applied coordination chemistry. Topics include the synthesis and properties of new coordination compounds; reactions involving intraspheral substitution and transformation of ligands; complexes with polyfunctional and macromolecular ligands; complexing in solutions; and kinetics and mechanisms of reactions involving the participation of coordination compounds.

Volume 7, 1981 (12 issues) $285.00

THE SOVIET JOURNAL OF GLASS PHYSICS AND CHEMISTRY

Fizika i Khimiya Stekla

Devoted to current theoretical and applied research on three interlinked problems in glass technology; the nature of the chemical bonds in a vitrifying melt and in glass; the structure-statistical principle; and the macroscopic properties of glass.

Volume 7, 1981 (12 issues) $175.00

LITHUANIAN MATHEMATICAL JOURNAL

Litovskii Matematicheskii Sbornik

An international medium for the rapid publication of the latest developments in mathematics, this quarterly keeps western scientists abreast of both practical and theoretical configurations. Among the many areas reported on in depth are the generalized Green's function, the Monte Carlo method, the "innovation theorem," and the Martingale problem.

Volume 21, 1981 (4 issues) $175.00

PROGRAMMING AND COMPUTER SOFTWARE

Programmirovanie

Reports on current progress in programming and the use of computers. Topics covered include logical problems of programming; applied theory of algorithms; control of computational processes; program organization; programming methods connected with the idiosyncracies of input languages, hardware, and problem classes; parallel programming; operating systems; programming systems; programmer aids; software systems; data-control systems; IO systems; and subroutine libraries.

Volume 7, 1981 (6 issues) $115.00

SOVIET MICROELECTRONICS

Mikroelektronika

Reports on the latest advances in solutions of fundamental problems of microelectronics. Discusses new physical principles, materials, and methods for creating components, especially in large systems.

Volume 10, 1981 (6 issues) $195.00

Send for Your Free Examination Copy

PLENUM PUBLISHING CORPORATION, 233 Spring St., New York, N.Y. 10013
In United Kingdom: 88/90 Middlesex St., London E1 7EZ, England
Prices slightly higher outside the U.S. Prices subject to change without notice.